



Measurements of inclusive and differential fiducial cross-sections of $t\bar{t}\gamma$ production in leptonic final states at $\sqrt{s} = 13$ TeV in ATLAS

ATLAS Collaboration*

CERN, 1211 Geneva 23, Switzerland

Received: 6 December 2018 / Accepted: 1 April 2019 / Published online: 3 May 2019
© CERN for the benefit of the ATLAS collaboration 2019

Abstract Inclusive and differential cross-sections for the production of a top-quark pair in association with a photon are measured with proton-proton collision data corresponding to an integrated luminosity of 36.1 fb^{-1} , collected by the ATLAS detector at the LHC in 2015 and 2016 at a centre-of-mass energy of 13 TeV. The measurements are performed in single-lepton and dilepton final states in a fiducial volume. Events with exactly one photon, one or two leptons, a channel-dependent minimum number of jets, and at least one b -jet are selected. Neural network algorithms are used to separate the signal from the backgrounds. The fiducial cross-sections are measured to be $521 \pm 9(\text{stat.}) \pm 41(\text{sys.}) \text{ fb}$ and $69 \pm 3(\text{stat.}) \pm 4(\text{sys.}) \text{ fb}$ for the single-lepton and dilepton channels, respectively. The differential cross-sections are measured as a function of photon transverse momentum, photon absolute pseudorapidity, and angular distance between the photon and its closest lepton in both channels, as well as azimuthal opening angle and absolute pseudorapidity difference between the two leptons in the dilepton channel. All measurements are in agreement with the theoretical predictions.

1 Introduction

Measurements of top-quark properties play an important role in testing the Standard Model (SM) and its possible extensions. Studies of the production and kinematic properties of a top-quark pair in association with a photon ($t\bar{t}\gamma$) probe the $t\gamma$ electroweak coupling. For instance, deviations in the transverse momentum (p_T) spectrum of the photon from the SM prediction could point to new physics through anomalous dipole moments of the top quark [1–3]. A precision measurement of the $t\bar{t}\gamma$ production cross-section could effectively constrain some of the Wilson coefficients in top-quark effective field theories [4]. Furthermore, differential distributions of photon production in $t\bar{t}$ events could provide insight on

the $t\bar{t}$ production mechanism, in particular about the $t\bar{t}$ spin correlation and the charge asymmetry [5].

Evidence for the production of a top-quark pair in association with an energetic, isolated photon was found in proton-antiproton ($p\bar{p}$) collisions at the Tevatron collider at a centre-of-mass energy of $\sqrt{s} = 1.96$ TeV by the CDF Collaboration [6]. Observation of the $t\bar{t}\gamma$ process was reported by the ATLAS Collaboration in proton-proton (pp) collisions at $\sqrt{s} = 7$ TeV [7]. Recently, both the ATLAS and CMS Collaborations measured the $t\bar{t}\gamma$ cross-section at $\sqrt{s} = 8$ TeV [8, 9]. In the ATLAS measurement, the differential cross-sections with respect to the transverse momentum p_T and absolute pseudorapidity $|\eta|^1$ of the photon were reported. In the CMS measurement, the ratio of the $t\bar{t}\gamma$ fiducial cross-section to the $t\bar{t}$ total cross-section was measured.

This paper describes a measurement of the $t\bar{t}\gamma$ production cross-section in final states with one or two leptons, electron or muons, referred to as the single-lepton or dilepton channel, based on a data set recorded at the LHC in 2015 and 2016 at a centre-of-mass energy of $\sqrt{s} = 13$ TeV and corresponding to an integrated luminosity of 36.1 fb^{-1} . The photon can originate not only from a top quark, but also from its charged decay products, including a charged fermion (quark or lepton) from the decay of the W -boson. In addition, it can be radiated from an incoming charged parton. In this analysis, no attempt is made to separate these different sources of photons, but criteria are applied to suppress those radiated from top-quark decay products: e.g. by requiring the photon to have a large angular distance from the lepton(s). In each channel, the fiducial inclusive cross-section, referred to as fiducial cross-section in the following for simplicity, is measured with a likelihood fit to the output of a neural network trained to

¹ ATLAS uses a right-handed coordinate system with its origin at the nominal interaction point (IP) in the centre of the detector and the z -axis along the beam pipe. The x -axis points from the IP to the centre of the LHC ring, and the y -axis points upward. Cylindrical coordinates (r, ϕ) are used in the transverse plane, ϕ being the azimuthal angle around the z -axis. The pseudorapidity is defined in terms of the polar angle θ as $\eta = -\ln \tan(\theta/2)$.

* e-mail: atlas.publications@cern.ch

differentiate between signal and background events. In both channels, differential cross-sections, normalized to unity, are measured in the same fiducial region without performing the likelihood fit, as a function of the photon p_T , the photon $|\eta|$, and the distance ΔR between the photon and its closest lepton. The distance ΔR between two objects is defined as the quadratic sum of their pseudorapidity difference $\Delta\eta$ and azimuthal opening angle $\Delta\phi$. In the dilepton channel, the normalized differential cross-sections are also measured as a function of the absolute pseudorapidity difference $|\Delta\eta|$ and $\Delta\phi$ between the two leptons, the latter being sensitive to the spin correlation of the $t\bar{t}$ pair. The measured cross-sections are compared to predictions from leading order (LO) generators. The predictions for the inclusive cross-sections are corrected by next-to-leading order (NLO) k -factors [10] in the strong interaction, calculated at parton level.

This paper is organized as follows. The ATLAS detector is briefly introduced in Sect. 2. The data and simulation samples used are listed in Sect. 3. The derivation of the NLO correction to the LO cross section is described in Sect. 4. The object and event selection, and the neural-network algorithms are presented in Sect. 5. The estimation of the backgrounds are introduced in Sect. 6. The definition of the fiducial region and the strategies to extract the fiducial and differential cross-sections are described in Sect. 7. The evaluation of the systematic uncertainties are discussed in Sect. 8. Section 9 gives the final results, and Sect. 10 presents the conclusion.

2 ATLAS detector

The ATLAS detector [11] consists of three main components. The innermost component is the Inner Detector (ID), which is used for tracking charged particles. It surrounds the beam pipe and is located inside a superconducting solenoid, operating with a magnetic field of 2 T. An additional silicon pixel layer, the insertable B-layer, was added between 3 and 4 cm from the beam line to improve b -hadron tagging [12, 13] for Run 2. The calorimeter outside the ID is divided into two subsystems. The inner subsystem is the electromagnetic calorimeter (ECAL) and the second is the hadronic calorimeter (HCAL). The outermost layer is the third main component of the ATLAS detector: the muon spectrometer (MS), which is within a magnetic field provided by air-core toroid magnets with a bending integral of about 2.5 Tm in the barrel and up to 6 Tm in the end-caps. The ID provides tracking information from silicon pixel and silicon microstrip detectors in the pseudorapidity range $|\eta| < 2.5$ and from a transition radiation tracker (TRT) covering $|\eta| < 2.0$. The magnetic field of the superconducting solenoid bends charged particles for the momentum measurement. The ECAL uses lead absorbers and liquid argon (LAr) as active medium and is divided into barrel ($|\eta| < 1.475$)

and end-cap ($1.375 < |\eta| < 3.2$) regions. The HCAL is composed of a steel/scintillating-tile calorimeter, segmented into three barrel structures within $|\eta| < 1.7$, and two copper/LAr hadronic endcap calorimeters, that cover the region $1.5 < |\eta| < 3.2$. The solid angle coverage is completed with forward copper/LAr and tungsten/LAr calorimeter modules, optimised for electromagnetic and hadronic measurements respectively, and covering the region $3.1 < |\eta| < 4.9$. The MS measures the deflection of muon tracks within $|\eta| < 2.7$ using multiple layers of high-precision tracking chambers in toroidal fields of approximately 0.5 T and 1 T in the central and end-cap regions, respectively. The MS is instrumented with separate trigger chambers covering $|\eta| < 2.4$.

Data are selected from inclusive pp interactions using a two-level trigger system [14]. A hardware-based trigger uses custom hardware and coarser-granularity detector data to initially reduce the trigger rate to approximately 100 kHz from the original 40 MHz LHC proton bunch crossing rate. Next, a software-based high-level trigger, which has access to the full detector granularity, is applied to further reduce the event rate to 1 kHz.

3 Data and simulation samples

The data used for this analysis were recorded by the ATLAS detector in 2015 and 2016 at a centre-of-mass energy of 13 TeV, corresponding to an integrated luminosity of 36.1 fb^{-1} . Only the data-taking periods in which all detector systems were operating normally are considered. Candidate events were collected using single-lepton triggers, designed to select events with at least one isolated high- p_T electron or muon.

The signal and background processes were modelled using Monte Carlo (MC) generators and passed through a detector simulation using GEANT 4 [15, 16]. The simulated events were reconstructed with the same software algorithms as data. To account for overlapping pp collisions (pile-up), multiple interactions were simulated with the soft QCD processes of PYTHIA v8.186 [17] using the set of tuned parameters called A2 [18] and the MSTW2008LO parton distribution functions (PDF) set [19].

The $t\bar{t}\gamma$ signal sample was simulated as a $2 \rightarrow 7$ process for the semileptonic and dileptonic decay channels of the $t\bar{t}$ system at LO by MADGRAPH5_aMC@NLO v2.33 [20] (denoted as MG5_AMC in the following) interfaced with PYTHIA v8.212 [21], using the A14 set of tuned parameters [22] and the NNPDF2.3LO PDF set [23]. The photon could be radiated from an initial charged parton, an intermediate top quark, or any of the charged final state particles. The top-quark mass, top-quark decay width, W -boson decay width, and fine structure constant were set to 172.5 GeV, 1.320 GeV, 2.085 GeV, and $1/137$, respectively. The five-flavour scheme

was used where all the quark masses are set to zero, except for the top quark. The renormalization and the factorization scales were set to $0.5 \times \sum_i \sqrt{m_i^2 + p_{T,i}^2}$, where the sum runs over all the particles generated from the matrix element calculation. The photon was requested to have $p_T > 15$ GeV and $|\eta| < 5.0$. At least one lepton with $p_T > 15$ GeV was required, with all the leptons satisfying $|\eta| < 5.0$. The ΔR between the photon and any of the charged particles among the seven final-state particles were required to be greater than 0.2. The resulting total cross-section of the sample was calculated to be 4.62 pb. The NLO k -factors, introduced in Sect. 4, were applied to correct the fiducial cross-sections and acceptances to NLO.

The inclusive $t\bar{t}$ sample [24] was generated with POWHEG-BOX v2 [25] using the NNPDF3.0NLO PDF set [26], and interfaced with PYTHIA v8.210 using the A14 tune set and the NNPDF2.3LO PDF set. The h_{damp} parameter, which controls the p_T of the first additional parton emission beyond Born level in POWHEG, was set to 1.5 times the top-quark mass. The production of a vector boson ($V = W, Z$) in association with a photon ($V\gamma$) was simulated with SHERPA v2.2.2 [27], and the inclusive production of V +jets [28] was simulated with SHERPA v2.2.1, both using the NNPDF3.0NLO PDF set. The s -channel single top quark and tW samples [24] were produced with POWHEG-BOX v1 using the CT10 (NLO) PDF set [29], interfaced with PYTHIA v6.428 using the Perugia 2012 tune set [30] and the CTEQ6L1 PDF set [23]. The t -channel single top quark was produced with the same generator and parton shower, with the four-flavour scheme and the corresponding CT104fs PDF set [23]. The diboson samples of WW, WZ and ZZ [31] were generated by SHERPA v2.1, using the CT10 (NLO) PDF set. The $t\bar{t}V$ samples [32] were generated with MG5_AMC v2.2 using the NNPDF3.0NLO PDF set, interfaced with PYTHIA v8.210 using the NNPDF2.3LO PDF set. For all samples without photon radiation in the matrix element calculation, the radiation was simulated by the corresponding parton shower. The EvtGen program [33] was used to simulate the decay of bottom and charm hadrons, except for the SHERPA samples. All these samples were generated with NLO precision in QCD and, in the case of SHERPA samples, the NLO calculations were performed for up to one or two additional partons.

To assess the effects of initial- and final-state radiation (ISR and FSR), alternative signal samples were produced with the relevant PYTHIA 8 A14 Var3c tune parameters [22] varied to increase or decrease the parton radiation. The effect of the choice of parton shower algorithm for the signal is evaluated with a sample generated using Herwig v7.0.1 [34] instead of PYTHIA v8.212. An alternative $t\bar{t}$ sample was generated to enhance the parton shower radiation, with the renormalization and factorization scales varied down by a factor of two, the high radiation variation of the A14 Var3c tune

parameter and the h_{damp} value increased by a factor of two. A corresponding $t\bar{t}$ sample with reduced parton shower radiation was generated with the renormalization and factorization scales multiplied by a factor of two and the low radiation variation of the A14 Var3c tune parameter. The uncertainty arising from the choice of $t\bar{t}$ generator is evaluated using a SHERPA v2.2 sample. An alternative $Z\gamma$ sample, generated by MG5_AMC v2.33 interfaced with PYTHIA v8.212, is used to evaluate the modelling uncertainty of the $Z\gamma$ background estimate.

The $t\bar{t}$ and V +jets samples contain events already accounted for by the $t\bar{t}\gamma$ and $V\gamma$ samples. Based on truth information, the overlap is removed by vetoing the events where the selected photon originates from the hard interaction in the $t\bar{t}$ and V +jets samples.

4 Next-to-leading order k -factor for $t\bar{t}\gamma$

Calculations at NLO precision in QCD are available for the $t\bar{t}\gamma$ process at a centre-of-mass energy of $\sqrt{s} = 14$ TeV [10], extending results performed using the approximation of stable top quarks [35]. A dedicated calculation at $\sqrt{s} = 13$ TeV has been performed for both single-lepton and dilepton channels, by the authors of Ref. [10]. The renormalization and factorization scales are both set to the top-quark mass, while the rest of the parameters are set to the same values used by the MG5_AMC $t\bar{t}\gamma$ MC sample, as described in Sect. 3. These calculations are used to derive corrections at parton level to the normalization of the LO $t\bar{t}\gamma$ MC sample.

The NLO calculation is performed at parton level in a phase space very close to the fiducial region defined in Sect. 7.1. The lepton (at least one lepton) is required to have $p_T > 25$ GeV for the single-lepton (dilepton) channel, and all leptons must have $|\eta| < 2.5$. The photon is required to have $p_T > 20$ GeV and $|\eta| < 2.37$. Jets are reconstructed from quarks and gluons using the anti- k_r algorithm [36] with a radius parameter of $R = 0.4$, and they are required to have $p_T > 25$ GeV and $|\eta| < 2.5$. At least four (two) jets are required for the single-lepton (dilepton) channel. All jets are required to be separated from the photon by $\Delta R(\gamma, \text{jet}) > 0.4$. Leptons are required to be separated from the photon by $\Delta R(\gamma, \ell) > 1.0$. The leptons in the dilepton channel are required to be separated from the jets by $\Delta R(\text{jet}, \ell) > 0.4$.

The LO cross-sections are calculated using the MG5_AMC LO sample at particle level in the same phase space as above to derive the NLO k -factors for the single-lepton and dilepton channels. Since the kinematic properties of all the objects used in the NLO theoretical calculation are taken from parton level, the photons, leptons, and jets of the LO MC sample must be defined carefully to correspond to those at the parton level. This is achieved by requiring the photon and the leptons to be produced from the matrix element rather than

from the parton shower and adding the QED radiation simulated by the parton shower back to the leptons. The anti- k_t algorithm with $R = 0.4$ is used for jet clustering, using all the final state particles, excluding the above photon, leptons, and their corresponding neutrinos.

The calculated NLO cross-sections are 120 fb and 31 fb for the e +jets and $e\mu$ channels, while the calculated LO cross-sections are 92 fb and 21 fb for the same channels, respectively, resulting in NLO k -factors of 1.30 and 1.44. These k -factors are applied to other single-lepton or dilepton channels. Statistical uncertainties are negligible. Systematic uncertainties of the k -factors receive contributions from two sources. For the NLO theoretical cross-section, the relative uncertainty due to the QCD scale and PDF choices are 14% (13%) for the single-lepton (dilepton) channel, with the QCD scale uncertainty dominating. For the LO MC cross-section, the non-perturbative effects in the parton shower model are studied by turning off the multiple parton interaction and hadronization of PYTHIA 8 separately, resulting in an uncertainty of 8% (4%) for the single-lepton (dilepton) channel. In addition, the jet cone size is varied from 0.4 to 0.3 or 0.5 separately to evaluate the impact of additional QCD radiation on the reconstruction of the particle-level jet. The resulting uncertainties are 11% (6%) for the single-lepton (dilepton) channel. Summing up the components in quadrature, the total relative uncertainty on the k -factor is 20% (15%) for the single-lepton (dilepton) channel.

5 Object and event selection

The object and event selection at the detector level are introduced in Sects. 5.1 and 5.2 respectively. The neural-network algorithms used in the analysis are described in Sect. 5.3. In Sect. 7.1, the fiducial region at particle level is defined.

5.1 Object selection

Electron candidates are reconstructed from energy deposits in the central region of the ECAL associated with reconstructed tracks from the ID [37] and are required to have a $p_T > 25$ GeV and an absolute calorimeter cluster pseudorapidity $|\eta_{\text{cluster}}| < 2.47$, excluding the transition region between the barrel and endcap calorimeters ($|\eta_{\text{cluster}}| \notin [1.37, 1.52]$). “Tight” likelihood-based identification criteria are applied, which correspond to an efficiency between 80% and 90% for electrons in different p_T and η ranges measured in $Z \rightarrow ee$ events [37]. Muon candidates are reconstructed by an algorithm that combines the track segments in the various layers of the MS with the tracks in the ID [38] and are required to have a $p_T > 25$ GeV and $|\eta| < 2.5$. “Medium” cut-based identification criteria are required, which correspond to an average efficiency around 96% in $t\bar{t}$ events for muons in dif-

ferent p_T and η ranges [38]. Isolation criteria are applied to both the electron and muon candidates using calorimeter- and track-based information to obtain 90% efficiency for leptons with $p_T = 25$ GeV, rising to 99% efficiency at $p_T = 60$ GeV in $Z \rightarrow \ell\ell$ events. The transverse impact parameter divided by its estimated uncertainty $|d_0|/\sigma(d_0)$ is required to be lower than five for electron candidates and three for muon candidates. The longitudinal impact parameter must satisfy $|z_0 \sin(\theta)| < 0.5$ mm for both. The lepton reconstruction and identification efficiencies in simulation are corrected to match the corresponding values in data [37, 38].

A photon could convert into an electron positron pair when it traverses the material before entering the active volume of the ECAL. Photon candidates are reconstructed from energy deposits in the central region of the ECAL [39] and classified as unconverted if there is no matching track or reconstructed conversion vertex or as converted if there is a matching reconstructed conversion vertex or a matching track consistent with originating from a photon conversion. They must have a $p_T > 20$ GeV and $|\eta_{\text{cluster}}| < 2.37$, excluding the transition region between the barrel and endcap. “Tight” cut-based identification criteria, based on discriminating variables and corresponding to an efficiency around 85% at 40 GeV, are applied [39]. Cut-based p_T -dependent isolation criteria are applied using calorimeter- and track-based information and correspond to an efficiency between 75% and 90% for prompt photons (photons not from hadron decays) in $Z \rightarrow \ell\ell\gamma$ events. The photon reconstruction and identification efficiencies in simulation are corrected to match the corresponding values in data [39].

Jets are reconstructed using the anti- k_t algorithm with a radius parameter of $R = 0.4$ from topological clusters of energy deposits in the calorimeter [40]. The jet energy scale and jet energy resolution are calibrated using energy- and η -dependent calibration schemes resulting from simulation and *in situ* corrections based on data [41]. The jets are required to have a $p_T > 25$ GeV and $|\eta| < 2.5$. Jets likely to originate from pile-up are suppressed by using the output of a multivariate jet-vertex-tagger (JVT) [42]. Scale factors are used to correct the selection efficiency in simulation to match data. Jets containing b -hadrons (b -jets) are identified with a b -tagging algorithm using a multivariate discriminant that combines information about secondary vertices and track impact parameters (MV2c10) [43, 44]. The operating point used corresponds to an overall 77% b -tagging efficiency in $t\bar{t}$ events, with a corresponding rejection of c -jets (light-jets) by a factor of 6 (134). Efficiencies to tag b -, c -, and light-jets in the simulation are scaled by p_T - and η -dependent factors [43] to match the efficiencies in data.

The transverse energy carried by the neutrinos is accounted for in the reconstructed missing transverse momentum E_T^{miss} [45], which is computed as the transverse component of the negative vector sum of all the selected electrons, muons, pho-

Table 1 Summary of the event selection. “OS” means the charges of the two leptons must have opposite signs

e +jets	μ +jets	ee	$\mu\mu$	$e\mu$
Primary vertex				
1 e	1 μ	2 e , OS	2 μ , OS	1 e + 1 μ , OS
Trigger match				
≥ 4 jets		≥ 2 jets		
≥ 1 b -jet				
1 γ				
$ m(e, \gamma) - m(Z) > 5$ GeV	-			
-	$m(\ell, \ell) \notin [85,95]$ GeV		-	
-	$m(\ell, \ell, \gamma) \notin [85,95]$ GeV		-	
-	$E_T^{\text{miss}} > 30$ GeV		-	
-	$m(\ell, \ell) > 15$ GeV			
$\Delta R(\gamma, \ell) > 1.0$				

tons, and jets, as well as ID tracks associated with the primary vertex but not with any of the above objects, which is called track-based soft term.

An overlap removal procedure is applied to avoid the same calorimeter energy deposit or the same track being reconstructed as two different objects. Electrons sharing their track with a muon candidate are removed. Jets within a $\Delta R = 0.2$ cone of an electron are removed. After that, electrons within a $\Delta R = 0.4$ cone of a remaining jet are removed. When a muon and a jet are close, the jet is removed if it has no more than two associated tracks and is within $\Delta R < 0.2$ of the muon, otherwise the muon is removed if it is within $\Delta R < 0.4$ of the jet and the jet has more than two associated tracks. Photons within a $\Delta R = 0.4$ cone of a remaining electron or muon are removed. Finally, the jets within a $\Delta R = 0.4$ cone of a remaining photon are removed.

5.2 Event selection

The events must have at least one primary vertex with at least two associated tracks, each with $p_T > 400$ MeV. Primary vertices are formed from reconstructed tracks spatially compatible with the interaction region. The primary vertex with the highest sum of p_T^2 over all associated tracks is chosen. Events are categorized into the single-lepton channel if their final state contains exactly one lepton (electron or muon), and into the dilepton channel if they contain two electrons, two muons, or one electron and one muon, with each pair required to be of opposite charge. The lepton (at least one of the leptons) must be matched to a fired single-lepton trigger for the single-lepton (dilepton) channel. The p_T of the electron (muon) that fired the trigger has to be larger than 27 (27.5) GeV in order to match the higher lepton p_T trigger threshold in 2016. The selected events must have at least four (two) jets in the single-lepton (dilepton) channel, at least one of which is b -tagged, and exactly one photon. A Z -boson veto

is applied in the single electron channel by excluding events with invariant mass of the system of the electron and the photon around the Z -boson mass ($|m(e, \gamma) - m(Z)| < 5$ GeV), where $m(Z) = 91.188$ GeV. In the dilepton channel when the two leptons have the same flavour, events are excluded if the dilepton invariant mass or the invariant mass of the system of the two leptons and the photon is between 85 and 95 GeV, and E_T^{miss} is required to be larger than 30 GeV. The dilepton invariant mass is required to be higher than 15 GeV to suppress events from J/ψ , Υ and γ^* decays. Finally, to suppress photons radiated from lepton(s), the ΔR between the selected photon and lepton(s) must be greater than 1.0. The event selection is summarized in Table 1.

There are four types of backgrounds to the selected $t\bar{t}\gamma$ candidates, three of which are events with a misidentified object. The contribution from events in which the selected photon candidate originates from a jet or a non-prompt photon from hadron decays, referred to as hadronic-fake background, is estimated following the method outlined in Sect. 6.1. The contribution from events in which the selected photon candidate originates from an electron, referred to as electron-fake background, is estimated following the method outlined in Sect. 6.2. The contribution from events in which the selected lepton candidate originates from a jet or a non-prompt lepton from heavy-flavour decays, referred to as fake-lepton background, is estimated following the method outlined in Sect. 6.3. Finally, the contribution from events with a prompt photon (excluding the $t\bar{t}\gamma$ signal and the fake-lepton background with prompt photon radiation), referred to as prompt-photon background, is estimated following the method outlined in Sect. 6.4. In the single-lepton channel, the main backgrounds are from events with a hadronic-fake or electron-fake photon and $W\gamma$ production, while in the dilepton channel, $Z\gamma$ production and events with a hadronic-fake photon are the dominant backgrounds.

Table 2 The observed data and the expected event yields for the signal and backgrounds in the single-lepton and dilepton channels. All data-driven corrections and systematic uncertainties are included. The signals are scaled by the NLO k -factors. The fake-lepton background in the dilepton channel is negligible, represented by a “-”. The $Z\gamma$ ($W\gamma$) background in the single-lepton (dilepton) channel is included in “Other prompt”. The uncertainty of the $W\gamma$ background in the single-lepton channel is not given since the normalization of this background is a free parameter in the likelihood fit

Channel	Single lepton	Dilepton
$t\bar{t}\gamma$	6490 ± 420	720 ± 34
Hadronic-fake	1440 ± 290	49 ± 27
Electron-fake	1650 ± 170	2 ± 1
Fake lepton	360 ± 200	-
$W\gamma$	1130	
$Z\gamma$		75 ± 52
Other prompt	690 ± 260	18 ± 7
Total	11750 ± 710	863 ± 78
Data	11662	902

A total number of 11 662 and 902 candidate events are selected for the single-lepton and dilepton channels, respectively, with expected numbers of 6490 ± 420 and 720 ± 34 signal events, where the corresponding NLO k -factors are applied and the uncertainties include the simulation statistical uncertainty and all systematic uncertainties introduced in Sect. 8. Table 2 summarizes the observed data and the expected event yields for the signal and background processes. Figures 1 and 2 show comparisons of the data with the expected simulated distributions. The simulation is corrected with data-driven corrections. The statistical uncertainty of data and systematic uncertainties are included. The signals are scaled by the NLO k -factors.

5.3 Multivariate analysis

To discriminate the $t\bar{t}\gamma$ signal from backgrounds, a neural-network algorithm, called the event-level discriminator (ELD), is trained separately for the single-lepton and dilepton channels. Given the significant contribution of hadronic-fake photons in the single-lepton channel, a dedicated neural network, referred to as the prompt-photon tagger (PPT) in the following, is trained to discriminate between prompt photons and hadronic-fake photons. The PPT is used as one of the inputs to the ELD in the single-lepton channel.

Both neural-network algorithms are feedforward binary classifiers that have been trained using Keras [46] and evaluated using LWTNN [47]. Theano [48] is used as backend. The input variables are normalized to have a standard deviation of 1 and a mean of 0. To reduce the risk of over-training, regularization methods such as *dropout* [49] and *batch nor-*

malization [50] layers are used. Additionally, k -fold cross-validation is performed.

Five variables which characterize the photon candidate shower shape in the transverse and lateral directions utilizing the energy deposits in the first and second layer of the ECAL, R_η , R_ϕ , w_{η_2} , w_{s3} , and F_{side} , and one variable which characterizes the energy leakage fraction into the HCAL, R_{had} , are used in the PPT. These are the standard discriminating variables used in ATLAS for photon identification [39] and their definitions are given in the Appendix. Prompt photons from simulated QCD-Compton processes and hadronic-fake photons from simulated dijet events are used as signal and background photons in the training and testing of the PPT. Photons are required to pass the Tight identification and have $p_T > 25$ GeV and $|\eta_{\text{clu}}| < 2.37$, excluding the calorimeter transition region. The PPT shape of the prompt photons in simulation is corrected to match data in photon p_T - η bins. The correction factors for each bin are extracted from the ratio between the PPT output distribution in data and that of simulation, using photons in a $Z \rightarrow \ell\ell\gamma$ control region. The control region is defined by requiring exactly one photon and two opposite-sign leptons, with the invariant mass of the lepton pair between 60 and 100 GeV. The resulting correction factors range from 0.5 to 2.0 and are in general around unity. PPT systematic uncertainties are evaluated separately for prompt photons and fake photons and are discussed in Sect. 8.3. The PPT output distribution after event selection in the single-lepton channel is shown in Fig. 3. The shape difference between data and prediction of the PPT is caused by the shape difference between data and simulation of the input discriminating variables and is covered by the assigned systematic uncertainties.

Simulated signal and background events passing the event selection are used for the training and testing of the ELD, except for the fake-lepton background in the single-lepton channel which is taken from data as described in Sect. 6.3. In the dilepton channel, the selection criteria on the E_T^{miss} , the invariant masses, and the jet multiplicity are removed to increase the sample size for training. The training takes 15 (7) variables as input for the single-lepton (dilepton) channel, which are summarized in Table 3. The b -tagging related variables are important for the ELD training in both channels, because of their discriminating power against background without real heavy flavour jets, which have significant contributions. The use of the PPT as input to ELD improves the discrimination power against hadronic-fake background.

Variables like the dilepton invariant mass and missing transverse energy are useful for the ELD training in the dilepton channel, due to the dominant background of $Z\gamma$. The distributions of the ELD after event selection are shown in Fig. 4 for the single-lepton and dilepton channels. The shapes of the ELD are compared between signal and total background in Fig. 5 for the single-lepton and dilepton channels.

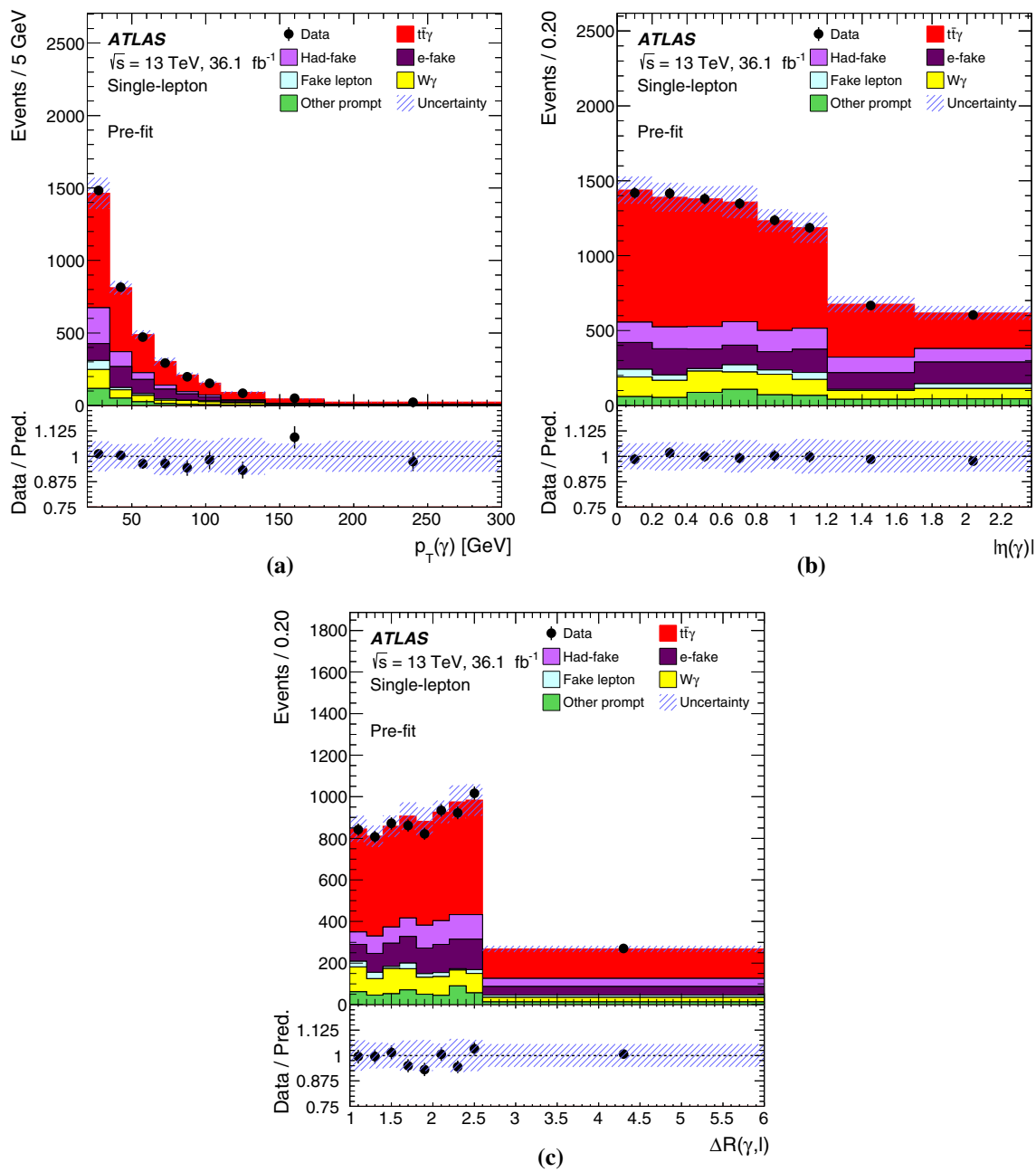


Fig. 1 Distributions of the **a** photon p_T , **b** photon $|\eta|$, and **c** $\Delta R(\gamma, \ell)$ in the single-lepton channel after event selection and before likelihood fit. All data-driven corrections and systematic uncertainties are included. Overflow events are included in the last bin

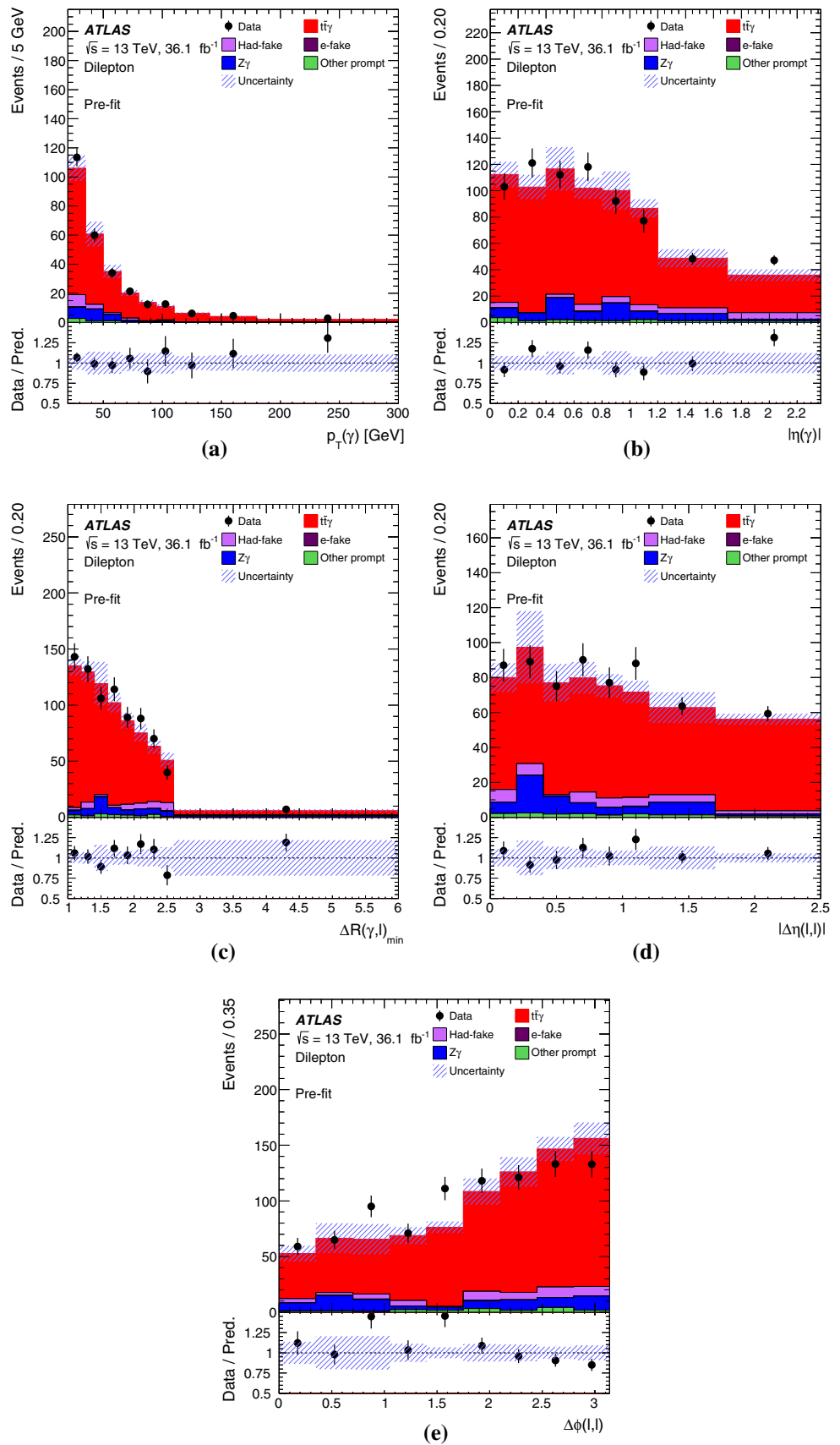
In the single-lepton channel, the kinematic properties and jet flavour compositions are similar between the $t\bar{t}\gamma$ signal and the dominating background, which is $t\bar{t}$ production with a hadronic-fake or electron-fake photon. In the dilepton channel, this is not the case since $Z\gamma$ production is dominant. Thus the ELD is more discriminating in the dilepton channel than in the single-lepton channel. The ELD is used in the likelihood fit to data to extract the fiducial cross-sections.

6 Background estimation

6.1 Hadronic-fake background

The hadronic-fake background is an important background in this analysis. Its main source is the $t\bar{t}$ process, where one of the final state jets is reconstructed and identified as a photon. In addition, there are small contributions from W +jets and single top processes to the single-lepton channel and from Z +jets events to the dilepton channel.

Fig. 2 Distributions of the **a** photon p_T , **b** photon $|\eta|$, **c** minimum $\Delta R(\gamma, \ell)$, **d** $|\Delta\eta(\ell, \ell)|$, and **e** $\Delta\phi(\ell, \ell)$ in the dilepton channel after event selection and before likelihood fit. All data-driven corrections and systematic uncertainties are included. Overflow events are included in the last bin. In particular, events with $|\Delta\eta(\ell, \ell)| > 2.5$ are included in the last bin of **d**



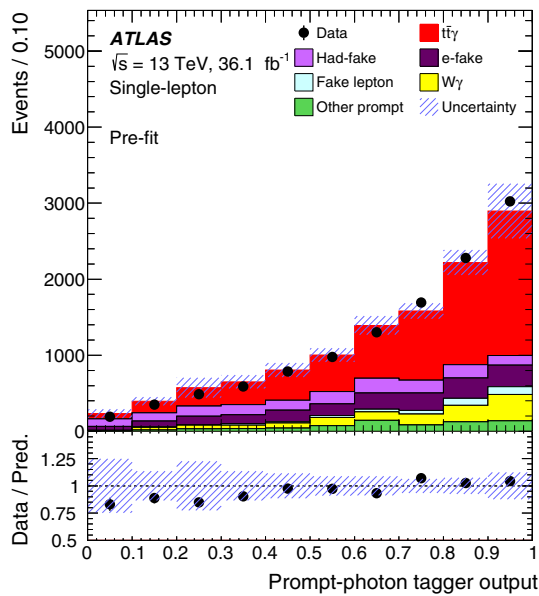


Fig. 3 Distributions of the output of the prompt-photon tagger in the single-lepton channel after event selection and before likelihood fit. All data-driven corrections and systematic uncertainties are included

The hadronic-fake background is estimated using all the simulation samples by requiring that the selected photon is a hadron or from a hadronic decay at generator level. A data-driven method, called the ABCD method, is applied to derive a set of scale factors, based on the ratio of hadronic-fake back-

ground estimated by the method over the one from simulation. This set of scale factors is derived in the single-lepton channel and applied to both the single-lepton and dilepton channels to calibrate the simulation to match data.

In the ABCD method, the isolation selection and part of the Tight identification criteria of the photon, which are assumed to be uncorrelated, are inverted to define three regions enriched with hadronic-fake photons. These regions are orthogonal to one another, and to the signal region. Region A uses photons that pass the isolation selection defined in Sect. 5.1 but fail at least two out of the four identification requirements on the discriminating variables F_{side} , w_{s3} , ΔE , and E_{ratio} (defined in the Appendix), while passing all other Tight identification criteria. These four variables describe the shower shape in the first layer of ECAL and are chosen for their small correlation with the photon isolation but strong discrimination power between prompt and hadronic-fake photons. Region B uses photons that fail the identification criteria as in region A and do not pass the isolation selection. Additionally, the sum of the p_T of all tracks within $\Delta R = 0.2$ around the photon is required to be larger than 3 GeV to further suppress the prompt-photon contribution. Region C selects photons that fail the isolation requirements as in region B but pass the Tight identification. Region D is the signal region.

The hadronic-fake background in the signal region can be expressed as:

Table 3 Input variables for the event-level discriminator for the single-lepton and dilepton channels. For events without the 5th jet, the $p_T(j_5)$ is set to zero

Variable	Description	Single lepton	Dilepton
PPT	Prompt-photon tagger output	✓	
H_T	Scalar sum of the p_T of the leptons and jets	✓	
$m(\gamma, \ell)$	Invariant mass of the system of the photon and the lepton	✓	
E_T^{miss}	Missing transverse energy	✓	✓
m_W^T	Reconstructed transverse mass of the leptonically decaying W -boson $= \sqrt{2 \times p_T(\ell) \times E_T^{miss} \times (1 - \cos(\Delta\phi(\ell, E_T^{miss}))}$	✓	
N_{jets}	Jet multiplicity	✓	
$p_T(j_1)$	p_T of the leading jet (ordered in p_T)	✓	✓
$p_T(j_2)$	p_T of the sub-leading jet	✓	✓
$p_T(j_3)$	p_T of the third jet	✓	
$p_T(j_4)$	p_T of the fourth jet	✓	
$p_T(j_5)$	p_T of the fifth jet	✓	
N_{b-jets}	b -jet multiplicity	✓	✓
$b_1(j)$	highest b -tagging score of all jets	✓	✓
$b_2(j)$	second highest b -tagging score of all jets	✓	✓
$b_3(j)$	third highest b -tagging score of all jets	✓	
$m(\ell, \ell)$	Invariant mass of the system of the two leptons		✓

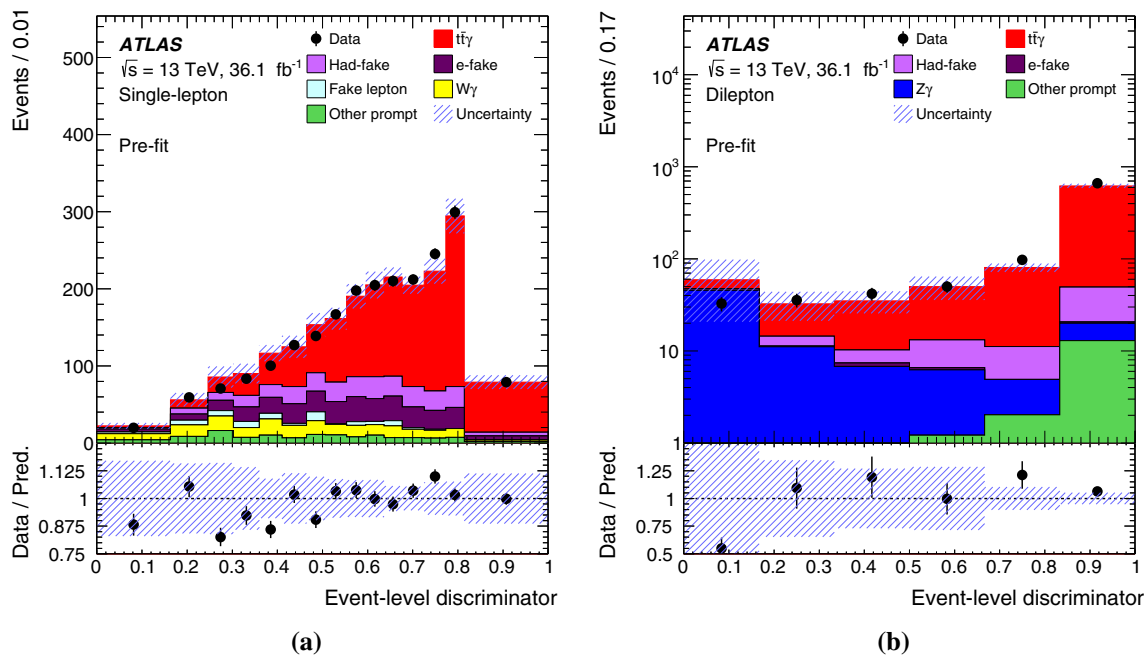


Fig. 4 Distributions of the ELD for the **a** single-lepton and **b** dilepton channels after event selection and before likelihood fit. All data-driven corrections and systematic uncertainties are included

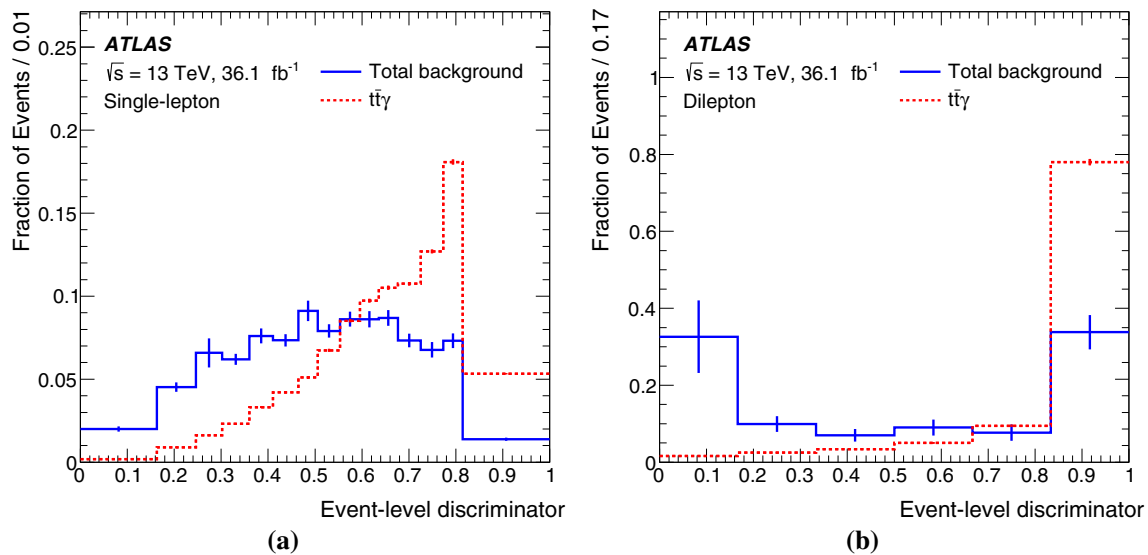


Fig. 5 Comparison of the shape of the ELD between signal and total background in the **a** single-lepton and **b** dilepton channels after event selection. All data-driven corrections are included

$$N_{D, est.}^{h-fake} = \frac{N_{A, data}^{h-fake} \times N_{C, data}^{h-fake}}{N_{B, data}^{h-fake}} \times \theta_{MC},$$

$$\theta_{MC} = \frac{N_{D, MC}^{h-fake} / N_{C, MC}^{h-fake}}{N_{A, MC}^{h-fake} / N_{B, MC}^{h-fake}},$$

where $N_{A, data}^{h-fake}$, $N_{B, data}^{h-fake}$ and $N_{C, data}^{h-fake}$ are the numbers of hadronic-fake events in regions A, B, and C, estimated by subtracting the events with prompt photons and other back-

grounds from the number of data events in these regions, and $N_{A, MC}^{h-fake}$, $N_{B, MC}^{h-fake}$, $N_{C, MC}^{h-fake}$ and $N_{D, MC}^{h-fake}$ are the numbers of hadronic-fake events predicted by simulation in regions A, B, C, and D. The factor θ_{MC} corrects for possible bias caused by residual correlation between the isolation variables and the four discriminating variables used to define the regions.

The ABCD method is applied to photons in different p_T - η bins, separately for converted and unconverted photons. The resulting scale factors range from 0.8 to 3.2, with typical

values around 1.5 and large statistical and systematic uncertainties of more than 0.5. These scale factors are applied to the MC-based hadronic-fake background prediction.

6.2 Electron-fake background

Dilepton events where an electron is mis-identified as a photon contribute to the electron-fake background in the single-lepton channel. Its main source is the $t\bar{t}$ dileptonic decay process. When the lepton is an electron, there is also some contribution from the $Z \rightarrow ee$ process. A data-driven method is applied to derive a set of scale factors to correct the electron-to-photon fake rate in simulation to match data.

The electron-to-photon fake rate is measured with a tag-and-probe method using two control regions (CR), exploiting the $Z \rightarrow ee$ process. For the first CR, $Z \rightarrow ee$ event candidates are selected in which one of the electrons fulfills the photon selection criteria, i.e. contributes to the electron-fake background, and the electron-photon pair should have an invariant mass in the range [40, 140] GeV and an opening angle greater than 2.62 rad. The electron is called the tag electron and the electron-fake photon candidate is referred to as probe photon. Non- Z -boson backgrounds are subtracted with a sideband fit of the invariant mass distribution. The fitted signal contains $Z \rightarrow ee\gamma$ contributions with one of the electrons not reconstructed or identified which is subtracted using simulation. For the second CR, events with an electron-positron pair satisfying the same requirements as in the first CR are selected and the same procedure is applied. The fake rate is calculated as the ratio of the number of probe photons over the number of probe electrons. To avoid a trigger bias, the tag electron in both CRs must match the single-lepton trigger. A set of p_T - η binned fake-rate scale factors is determined by taking the ratio between the fake rate in data and in the simulation. The values of the scale factors range from 0.8 to 2.1 and are in general consistent with unity within their uncertainties.

The electron-fake background in the single-lepton channel is validated in a control region selected by replacing the photon in the signal region event selection with an electron. This region is dominated by $t\bar{t}$ events and Z +jets events in the single electron channel with negligible contribution from other processes. The ratio of data over prediction in this region is 0.98 ± 0.01 , where the uncertainty is due to the sample size. This overall correction is applied to the electron-fake background predicted by simulation in the single-lepton channel signal region, in addition to the fake-rate scale factors.

The electron-fake background in the dilepton channel is very small. Simulation is used to predict its contribution. No dedicated control region is selected to validate this background.

6.3 Fake-lepton background

In the single-lepton channel, the fake-lepton background is dominated by multi-jet processes with an additional photon which could either be a prompt or a fake photon. It is estimated directly from data by using a matrix method [51]. The number of background events in the signal region is evaluated by applying efficiency factors (fake lepton and real lepton efficiencies) to the number of events satisfying a tight (identical to the signal selection) as well as a looser lepton selection. The fake-lepton efficiency is measured using data in control regions dominated by multi-jet background with the real lepton contribution subtracted using simulation. The real lepton efficiency is extracted from a tag-and-probe technique using leptons from Z boson decays. The efficiencies are parametrized as a function of the lepton η and m_W^T (the lepton p_T and m_W^T) when the lepton is an electron (muon).

In the dilepton channel, the contamination of background processes with at least one fake lepton is estimated by selecting same-sign dilepton events in data, after subtracting events with two same-sign prompt leptons, using simulation. The fake-lepton background in the dilepton channel is found to be negligible.

6.4 Prompt-photon background

All background processes to $t\bar{t}$ production are also background to $t\bar{t}\gamma$ production when accompanied by prompt-photon radiation. These processes include $W\gamma$, $Z\gamma$, and associated production of a photon in single top, diboson, and $t\bar{t}V$ productions. In the single-lepton channel, $W\gamma$ is the dominant prompt-photon background, and $Z\gamma$ and the others are grouped together as ‘‘Other prompt’’. In the dilepton channel, $Z\gamma$ is dominant, with all others grouped as ‘‘Other prompt’’. Background from $t\bar{t}$ production with a photon produced in an additional pp interaction in the same bunch crossing has been studied and is found to be negligible.

Validation regions are selected to check the modelling of $W\gamma$ in the single-lepton channel and $Z\gamma$ in the dilepton channel. The $Z\gamma$ validation region is selected by requiring exactly one b -tagged jet and the invariant mass of the system of the two leptons in a mass window of [60, 100] GeV. The $W\gamma$ validation region is selected with the same event selection as for the signal region of the single-lepton channel, with the following modifications: the number of jets must be either two or three; exactly one b -jet is required; the E_T^{miss} is required to be larger than 40 GeV; the ELD value must be smaller than 0.04; and the invariant mass of the system of the lepton and photon is required to be smaller than 80 GeV if the lepton is an electron. The modelling of $W\gamma$ is also checked in a light-flavour validation region requiring zero b -jet and without the ELD cut.

The normalization of the $W\gamma$ background is treated as a free parameter of the likelihood fit in the single-lepton channel, since this background is well separated from the $t\bar{t}\gamma$ signal by the ELD and the uncertainty of its theoretical prediction is large. The shape of $W\gamma$ is taken from simulation and checked in the validation region to ensure good modelling. The normalization and shape of the $Z\gamma$ background in the dilepton channel as well as other prompt backgrounds in both channels are predicted by simulation.

7 Analysis strategy

The analysis is performed in two parts, one being the measurement of the fiducial cross-section and the other the measurement of normalized differential cross-sections in the same fiducial region. Both parts share the same strategy for the estimation of backgrounds and systematic uncertainties. In the fiducial cross-section measurement, the ELD is fitted and the post-fit background yields and systematic uncertainties are used. In the normalized differential cross-section measurements, no fit is performed, except for the determination of the $W\gamma$ contribution in the single-lepton channel, where a systematics-free ELD fit is performed.

7.1 Fiducial region definition

The fiducial region of the analysis is defined at particle level in a way that mimics the event selection in Sect. 5.2. Leptons must have $p_T > 25$ GeV and $|\eta| < 2.5$ and must not originate from hadron decays. Photons not from hadron decays and in a $\Delta R = 0.1$ cone around a lepton are added to the lepton before the lepton selection. Photons are required to have $p_T > 20$ GeV and $|\eta| < 2.37$ and must not originate from hadron decays or be used for lepton dressing. The photon isolation computed from the ratio of the scalar sum of the transverse momentum of all stable² charged particles around the photon over its transverse momentum must be smaller than 0.1. Jets are clustered using the anti- k_r algorithm with $R = 0.4$ using all final state particles excluding non-interacting particles and muons that are not from hadron decays. Jets must have $p_T > 25$ GeV and $|\eta| < 2.5$. A ghost matching method [52] is used to determine the flavour of the jets, with those matched to b -hadrons tagged as b -jets. A simple overlap removal is performed: jets within $\Delta R < 0.4$ of a selected lepton or photon are removed. For events in the single-lepton (dilepton) channel, exactly one photon and exactly one lepton (two leptons) are required. At least four (two) jets are required with at least one of them b -tagged. Events are rejected if there is any lepton and photon pair sat-

isfying $\Delta R(\gamma, \ell) < 1.0$. The acceptance for the generated signal events to pass the fiducial selection of the single-lepton (dilepton) channel is 8.2% (0.96%).

7.2 Fiducial cross-section

The fiducial cross-section is extracted using a profile likelihood fit to the ELD distribution. The parameter of interest, the fiducial cross-section σ_{fid} , is related to the number of signal events in bin i of the ELD as

$$N_i^s = L \times \sigma_{\text{fid}} \times C \times f_i^{\text{ELD}},$$

where L is the integrated luminosity, C is the correction factor for the signal efficiency and for migration into the fiducial region, and f_i^{ELD} is the fraction of signal events falling into bin i of the ELD. The correction factor C is defined as $N_{\text{MC}}^{s,\text{sel}}/N_{\text{MC}}^{s,\text{fid}}$, where $N_{\text{MC}}^{s,\text{sel}}$ is the simulated number of signal events passing the event selection described in Sect. 5.2 and $N_{\text{MC}}^{s,\text{fid}}$ is the corresponding number of signal events generated in the fiducial region defined in Sect. 7.1. The value of C is 0.36 (0.30) for the single-lepton (dilepton) channel, with negligible statistical uncertainty.

A likelihood function is defined from the product over all bins of the ELD distribution:

$$\mathcal{L} = \prod_i P \left(N_i^{\text{obs}} | N_i^s(\theta) + \sum_b N_i^b(\theta) \right) \times \prod_t G(0 | \theta_t, 1),$$

where N_i^{obs} , N_i^s , and N_i^b are the observed number of events in data, the predicted number of signal events, and the estimated number of background events in bin i of the ELD, which form a Poisson term P in that bin. Nuisance parameter θ_t is to parameterize a systematic uncertainty t , which is constrained by a Gaussian $G(0 | \theta_t, 1)$, so that when it changes from zero to ± 1 , the quantities affected by this systematics in the likelihood change by ± 1 standard deviation. The collection of all the systematic uncertainties is denoted as θ . For systematic uncertainties related to the finite number of MC events, the Gaussian terms in the likelihood are replaced by Poisson terms. Each systematic uncertainty affects N_i^s and N_i^b in each bin of the ELD. The cross-section is measured by profiling the nuisance parameters and maximizing this likelihood.

7.3 Normalized differential cross-sections

An unfolding procedure is applied to the observed detector-level distribution of a given observable, with backgrounds subtracted, to derive the true distribution of the signal at particle level, from which the differential cross-section as a function of the observable is calculated. The differential cross-section is normalized to unity.

² A stable particle is a particle with $c \times \tau > 10$ mm, where c is the speed of light and τ is the lifetime of the particle.

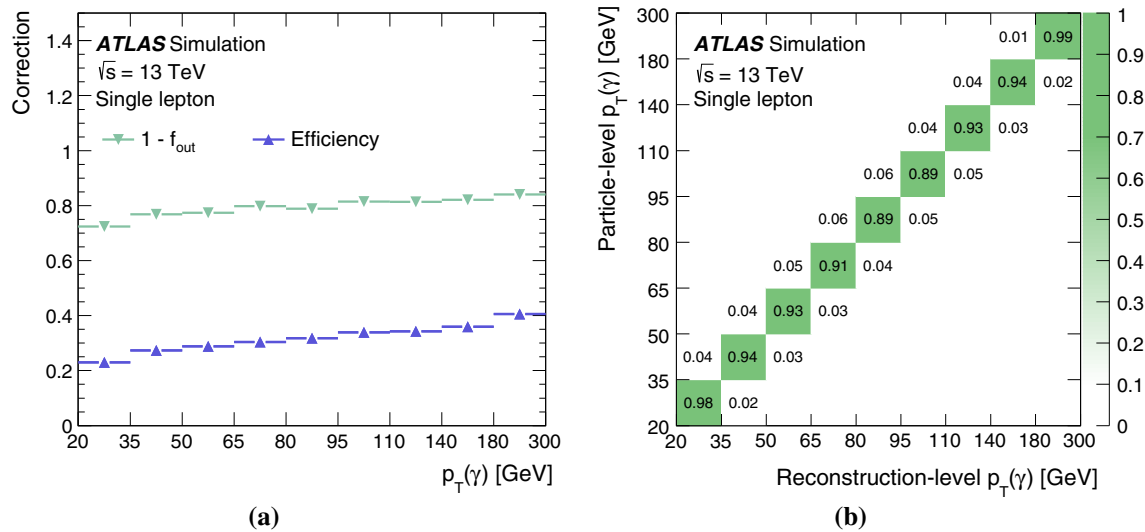


Fig. 6 The **a** efficiency and outside fraction and **b** migration matrix for the photon p_T in the single-lepton channel

The differential cross-section is given by

$$\sigma_k = \frac{1}{L} \times \frac{1}{\epsilon_k} \times \sum_j M_{jk}^{-1} \times (N_j^{obs} - N_j^b) \times (1 - f_{out,j}).$$

The indices j and k indicate the bin of the observable at detector and particle levels, respectively. The variables N_j^{obs} and N_j^b are the number of observed events and of estimated background events in bin j at detector level, respectively. The efficiency ϵ_k is the fraction of signal events generated at particle level in bin k of the fiducial region to be reconstructed and selected at detector level and have the objects, that are used to define the observable to be unfolded, matched between reconstruction and particle-levels with $\Delta R < 0.1$. The migration matrix M_{kj} expresses the probability for an event in bin k at particle level to end up in bin j at detector level, calculated from events passing both the fiducial region selection and the event selection, as well as the above matching procedure. The outside-migration fraction $f_{out,j}$ is the fraction of signal events generated outside the fiducial region but reconstructed and selected in bin j at detector level or events failing the above matching. The signal MC sample is used to determine ϵ_k , $f_{out,j}$, and M_{kj} , the values of which are illustrated in Fig. 6, using the photon p_T in the single-lepton channel as an example. The normalization and the corresponding uncertainty of the $W\gamma$ contribution in the single-lepton channel are taken from the likelihood fit introduced in Sect. 7.2 but without systematic uncertainties included. The normalized differential cross-section is

$$\sigma_k^{norm} = \frac{\sigma_k}{\sum_k \sigma_k},$$

where the sum is over all the bins of the observable.

The inversion of the migration matrix M_{kj} is approximated using the iterative Bayesian method [53] implemented in the ROOUNFOLD package [54]. The method relies on the Bayesian probability formula to invert the migration matrix, starting from a given prior of the particle-level distribution and iteratively updating it with the posterior distribution. The binning choices of the unfolded observables take into account the detector resolution and the expected statistical uncertainty, with the latter being the dominating factor. Three iterations are chosen which give a good convergence of the unfolded distribution and a statistically stable result. Tests are performed, using simulation, to verify that the unfolding procedure does not bias the results while the estimated uncertainties are still reasonable. The results are cross-checked with other unfolding methods, which give consistent results.

The chosen observables to unfold are the photon p_T and $|\eta|$ and the ΔR between the photon and the closest lepton for both single-lepton and dilepton channels and the $\Delta\phi$ and $|\Delta\eta|$ between the two leptons for the dilepton channel. These are all lepton or photon observables, therefore the migration matrices are almost diagonal, making the unfolding simple and converging fast. The kinematic properties of the photon are sensitive to the $t\gamma$ coupling, while the dilepton $\Delta\phi$ is sensitive to the $t\bar{t}$ spin correlation. The normalized differential cross-sections are measured, since the overall signal normalization is given by the measured fiducial cross-section.

8 Systematic uncertainties

Signal and background modelling and experimental uncertainties in the analysis are described in this section, as well as the PPT systematic uncertainty. They affect the normaliza-

tion of signal and background and/or the shape of their corresponding distributions, such as the ELD and the observables to be unfolded. Each of the signal and background modelling uncertainties is correlated between different channels for the relevant signal or background process. Each of the experimental uncertainties is correlated between signal and simulated backgrounds and between different channels. The PPT systematic uncertainty is separately studied for the prompt, electron-fake, and hadronic-fake photons. Table 5 gives a summary of these uncertainties and their impact to the fiducial cross-section measurements.

8.1 Signal modelling uncertainties

The signal modelling uncertainties include the uncertainties due to the choice of the QCD scales, the parton shower, the amount of ISR and FSR, and the PDF set. Their effects on the corrections defined in Sect. 7 (both for the fiducial and normalized differential cross-section measurements) as well as on the shape of the ELD distributions are evaluated.

To study the QCD scale uncertainty, the renormalization and factorization scales are varied up and down by a factor of two from their nominal choices independently or simultaneously. The largest variation of the corrections or the shapes is assigned as the uncertainty. To evaluate the parton shower uncertainty, PYTHIA 8 and HERWIG 7 both interfaced to MG5_AMC are compared. The ISR/FSR uncertainty is studied by comparing the variations of the A14 tune parameters of PYTHIA 8 with its nominal values. The PDF uncertainty is evaluated using the standard deviation of the distribution formed by the 100 eigenvector set of the NNPDF set [23].

8.2 Background modelling uncertainties

The systematic uncertainties on the hadronic-fake background due to background subtraction in the hadronic-fake control regions A, B, and C are estimated by varying up and down the signal by 100%, the other MC-based backgrounds by 50%, and the other data-driven backgrounds by their estimated uncertainties, separately. The statistical uncertainties in the three data control regions are also considered. Systematic uncertainties arising from the correction factor θ_{MC} , the extrapolation of the hadronic-fake scale factors, and the shapes of the distributions of the ELD and the observables to be unfolded are estimated using $t\bar{t}$ samples rather than all of the simulated hadronic-fake samples, since $t\bar{t}$ is the dominant source of the hadronic-fake background. The uncertainty due to the rate of additional QCD radiation is estimated by comparing the samples with enhanced/reduced parton shower radiation as described in Sect. 3 with the nominal sample, and the uncertainty due to the modelling of the generator and

parton shower is estimated by comparing POWHEG+PYTHIA 8 with SHERPA.

The systematic uncertainties on the electron-fake background mainly come from the sideband fit when measuring the fake rate, which is estimated by varying the fit parameters within their uncertainties. The uncertainty due to $Z \rightarrow ee\gamma$ subtraction is also considered by replacing the $Z\gamma$ MC sample by the Z +jets sample, where the photon radiation is described by the parton shower. Uncertainties of the shapes of the distributions are evaluated using $t\bar{t}$ systematic variations MC samples as for the hadronic-fake background. In the dilepton channel where the electron-fake background is very small, a 50% uncertainty is assumed to cover a possible mis-modelling in the estimate.

For evaluating the systematic uncertainty of the fake-lepton background in the single-lepton channel, several alternative parameterizations of the real and fake efficiencies of the matrix method are studied and two predicting larger and smaller yields are selected as up and down variations. The lepton η , b -jet multiplicity, and m_W^T (the lepton η , minimum ΔR between the lepton and the closest jet, and the jet p_T) parameterization is used as up (down) variation when the lepton is an electron. The jet p_T and b -jet multiplicity (the lepton p_T , η , and minimum ΔR between the lepton and the closest jet) parameterization is used as up (down) variation when the lepton is a muon. The resulting uncertainties are around 50%, and given that this background contribution is relatively small, no additional systematic uncertainties are considered.

The uncertainty on the $V\gamma$ background shape is studied by varying the renormalization and factorization scales up and down by a factor of two from their nominal values independently or simultaneously and then choosing the maximum shape distortions as the QCD scale uncertainties. For the $Z\gamma$ background in the dilepton channel, SHERPA is compared with MG5_AMC+PYTHIA 8 to evaluate the shape uncertainty due to the choice of generator and parton shower. No shape modelling uncertainty is assigned to the other small prompt backgrounds. Apart from the $W\gamma$ background in the single-lepton channel whose normalization is a free parameter in the likelihood fit, a normalization uncertainty of 50% is assigned to each source of the prompt-photon background, included in Table 2 as “ $Z\gamma$ ” and “Other prompt”.

8.3 Experimental uncertainties

Experimental systematic uncertainties affect the normalization and shape of the simulated signal and background samples. For MC-based backgrounds calibrated to data using data-driven techniques, only the shape variations are considered.

The photon identification and isolation efficiencies as well as the efficiencies of the lepton reconstruction, identification,

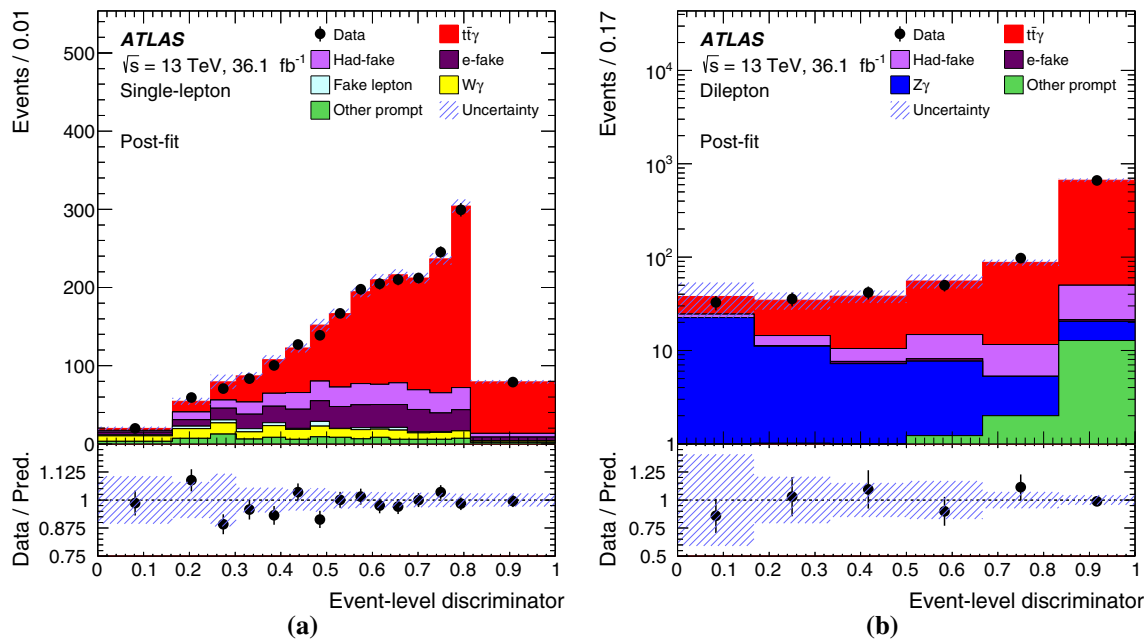


Fig. 7 The post-fit ELD distributions for the **a** single-lepton and **b** dilepton channels. All the systematic uncertainties are included

isolation, and trigger in the MC samples are all corrected as mentioned in Sect. 5.1. These corrections, which are p_T and η dependent, are varied to study their impact on the final results. Similarly, the corrections to the lepton and photon momentum scale and resolution in simulation are varied within their uncertainties [38,55].

The PPT systematic uncertainty is evaluated separately for prompt photons and hadronic-fake photons. The data-driven PPT scale factors as mentioned in Sect. 5.1 are turned on and off to assign a PPT systematic uncertainty for the prompt photon. The resulting uncertainty is also assigned to the electron-fake photon PPT output distribution, since its shape and shape difference between data and simulation are similar to that of the prompt photons. The maximum PPT shape difference between data and prediction in the hadronic-fake control region C of Sect. 6.1, with the expected signal contamination in this region varied by $\pm 50\%$, is used to estimate the hadronic-fake PPT uncertainty. The hadronic-fake photons in region C are non-isolated while those of the signal region are isolated. To account for a possible underestimation of the systematic uncertainty caused by this difference, the shape differences between data and prediction in the isolated hadronic-fake control region A of Sect. 6.1 are considered as an additional PPT systematic uncertainty. The PPT shape uncertainties are estimated in photon p_T and η bins.

The jet energy scale (JES) uncertainty is derived using a combination of simulations, test beam data and *in situ* measurements [56–58]. Additional contributions from jet flavour composition, η -intercalibration, punch-through, single-particle response, calorimeter response to different jet

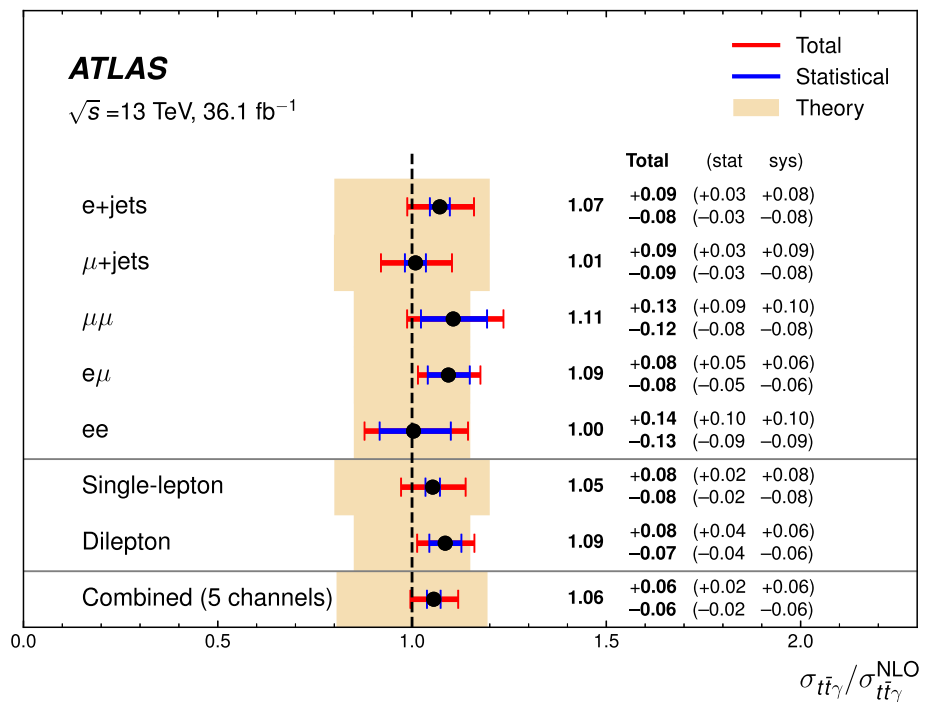
Table 4 The observed data and post-fit event yields for the signal and backgrounds in the single-lepton and dilepton channels. All data-driven corrections and systematic uncertainties are included. The fake-lepton background in the dilepton channel is negligible, represented by a “-”. The $Z\gamma$ ($W\gamma$) background in the single-lepton (dilepton) channel is included in “Other prompt”

Channel	Single lepton	Dilepton
$t\bar{t}\gamma$	$7\,040 \pm 350$	780 ± 44
Hadronic-fake	$1\,470 \pm 180$	49 ± 26
Electron-fake	$1\,620 \pm 160$	2 ± 1
Fake lepton	186 ± 68	–
$W\gamma$	900 ± 370	
$Z\gamma$		55 ± 29
Other prompt	570 ± 180	18 ± 7
Total	$11\,790 \pm 180$	906 ± 38
Data	11 662	902

flavours, and pile-up are taken into account, resulting in 21 uncorrelated JES uncertainty subcomponents. The jet energy resolution (JER) in simulation is smeared up by the measured JER uncertainty [59]. The uncertainty associated with the JVT cut is obtained by varying the efficiency correction factors. The b -tagging weights used for jet flavour tagging are corrected by data, separately for b -jets, c -jets, and light-flavour jets [44,60]. The corrections are varied by their measured uncertainties.

The uncertainties associated with energy scales and resolutions of photons, leptons and jets are propagated to the

Fig. 8 The measured fiducial cross-sections normalized to their corresponding NLO SM predictions [10] for the five individual channels and for the single-lepton and dilepton channels, as well as the combination of all channels. The statistical uncertainties are the inner error bars, while the total uncertainties are the outer error bars. The NLO prediction for the inclusive fiducial cross-section is represented by the dashed vertical line, and the theoretical uncertainties are represented by the shaded bands



E_T^{miss} . Additional uncertainties originate from the modelling of its soft term [61].

The uncertainty in the combined 2015+2016 integrated luminosity is 2.1%. It is derived, following a methodology similar to that detailed in Ref. [62], and using the LUCID-2 detector for the baseline luminosity measurements [63], from calibration of the luminosity scale using x-y beam-separation scans.

The uncertainty associated to the modelling of pile-up in the simulation is assessed by varying the reweighting of the pile-up in the simulation within its uncertainties.

8.4 Systematic uncertainties of the measured differential cross-section

Systematic uncertainties for unfolding arise from the detector response description, signal modelling, and background modelling. The systematic uncertainties due to background modelling and the detector response are evaluated by varying the input detector-level pre-fit distributions, unfolding them with corrections based on the nominal signal sample, and calculating the difference of the resulting unfolded distributions with respect to the nominal one. The systematic uncertainties due to signal modelling are evaluated by varying the signal corrections, i.e. the migration matrix M_{kj} , the efficiency ϵ_k and the fraction $f_{\text{out},j}$ as defined in Sect. 7.3, with which the nominal input detector-level pre-fit distributions are unfolded, and calculating the difference of the resulting unfolded distributions with respect to the nominal one. The statistical uncertainties of the signal and background MC

Table 5 Summary of the effects of the groups of systematic uncertainties on the fiducial cross-section in the single-lepton and dilepton channels. Due to rounding effects and small correlations between the different sources of uncertainty, the total systematic uncertainty is different from the sum in quadrature of the individual sources

Source	Single lepton (%)	Dilepton (%)
Signal modelling	± 1.6	± 2.9
Background modelling	± 4.8	± 2.9
Photon	± 1.1	± 1.1
Prompt-photon tagger	± 4.0	–
Leptons	± 0.3	± 1.3
Jets	± 5.4	± 2.0
b-tagging	± 0.9	± 0.4
Pile-up	± 2.0	± 2.3
Luminosity	± 2.3	± 2.3
MC sample size	± 1.9	± 1.7
Total systematic uncertainty	± 7.9	± 5.8
Data sample size	± 1.5	± 3.8
Total uncertainty	± 8.1	± 7.0

samples are also considered. The covariance matrix C_{ij} for each of these systematic uncertainties is estimated as $\sigma_i \times \sigma_j$, where σ_i and σ_j are the symmetrized uncertainties for bin i and bin j of the unfolded distribution. The covariance matrix for the statistical uncertainty of data is calculated by the unfolding algorithm [54].

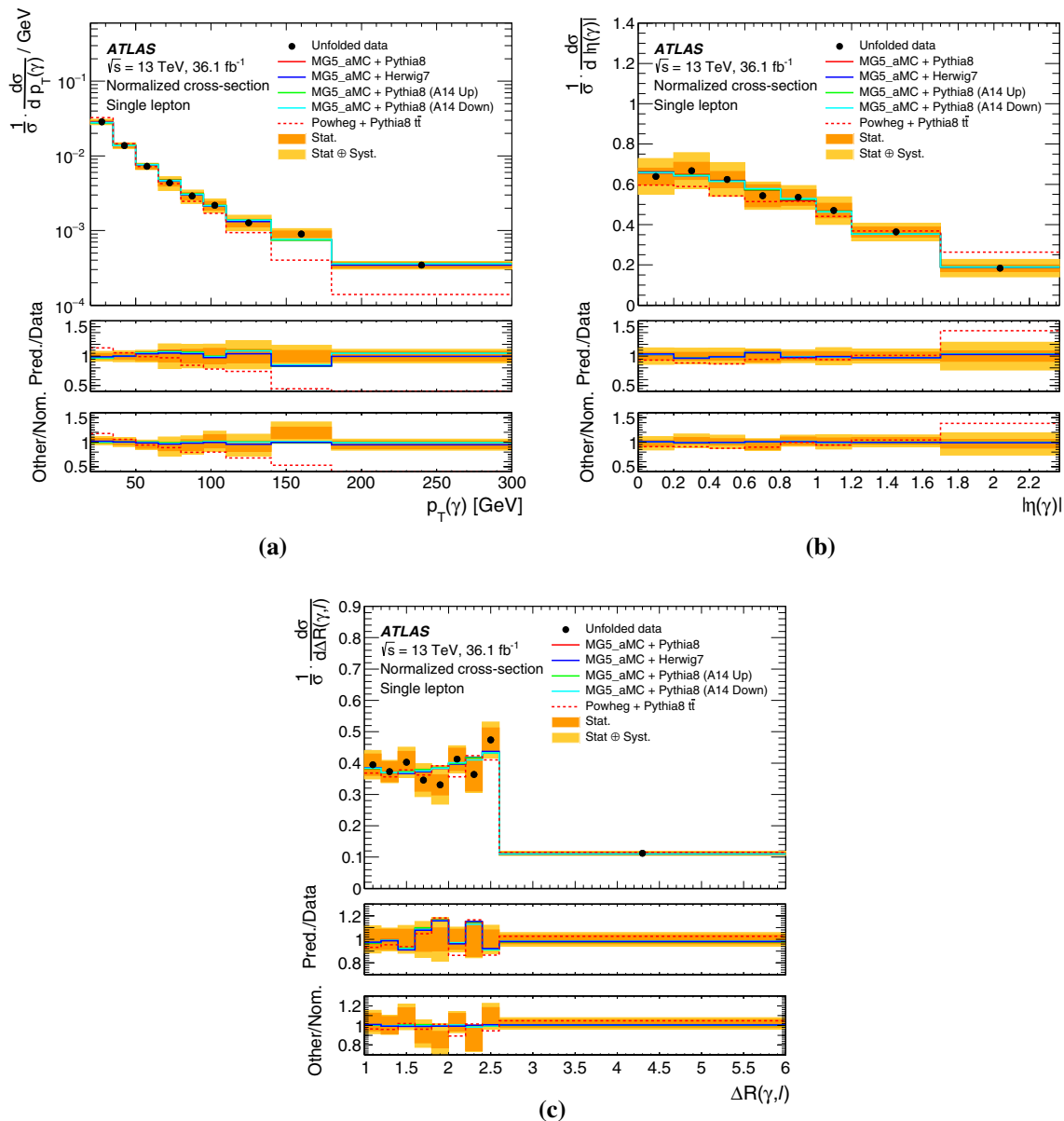


Fig. 9 The normalized differential cross-sections as a function of the **a** photon p_T , **b** photon $|\eta|$, and **c** $\Delta R(\gamma, \ell)$ in the single-lepton channel. The unfolded distributions are compared to the predictions of the MG5_AMC+PYTHIA 8 together with the up and down variations of the PYTHIA 8 A14 tune parameters, the MG5_AMC+Herwig 7, and the

POWHEG+PYTHIA 8 $t\bar{t}$ where photon radiation is modelled in the parton shower. The top ratio-panel shows the ratios of all the predictions over data. The bottom ratio-panel shows the ratios of the alternative predictions and data over the nominal prediction. Overflows are included in the last bin

9 Results

9.1 Fiducial cross-sections

The fiducial cross-section is extracted via a binned maximum likelihood fit to the ELD distribution in data as described in Sect. 7.2. The measured cross-sections are

$$\sigma_{fid}^{SL} = 521 \pm 9(\text{stat.}) \pm 41(\text{sys.}) \text{ fb and}$$

$$\sigma_{fid}^{DL} = 69 \pm 3(\text{stat.}) \pm 4(\text{sys.}) \text{ fb,}$$

for the single-lepton and dilepton channels, respectively, and agree well within uncertainties with the corresponding predicted cross-sections of $495 \pm 99 \text{ fb}$ and $63 \pm 9 \text{ fb}$. The ELD distributions after the fit (post-fit) are shown in Fig. 7 for the single-lepton and dilepton channels. The corresponding event yields are summarized in Table 4, including all the

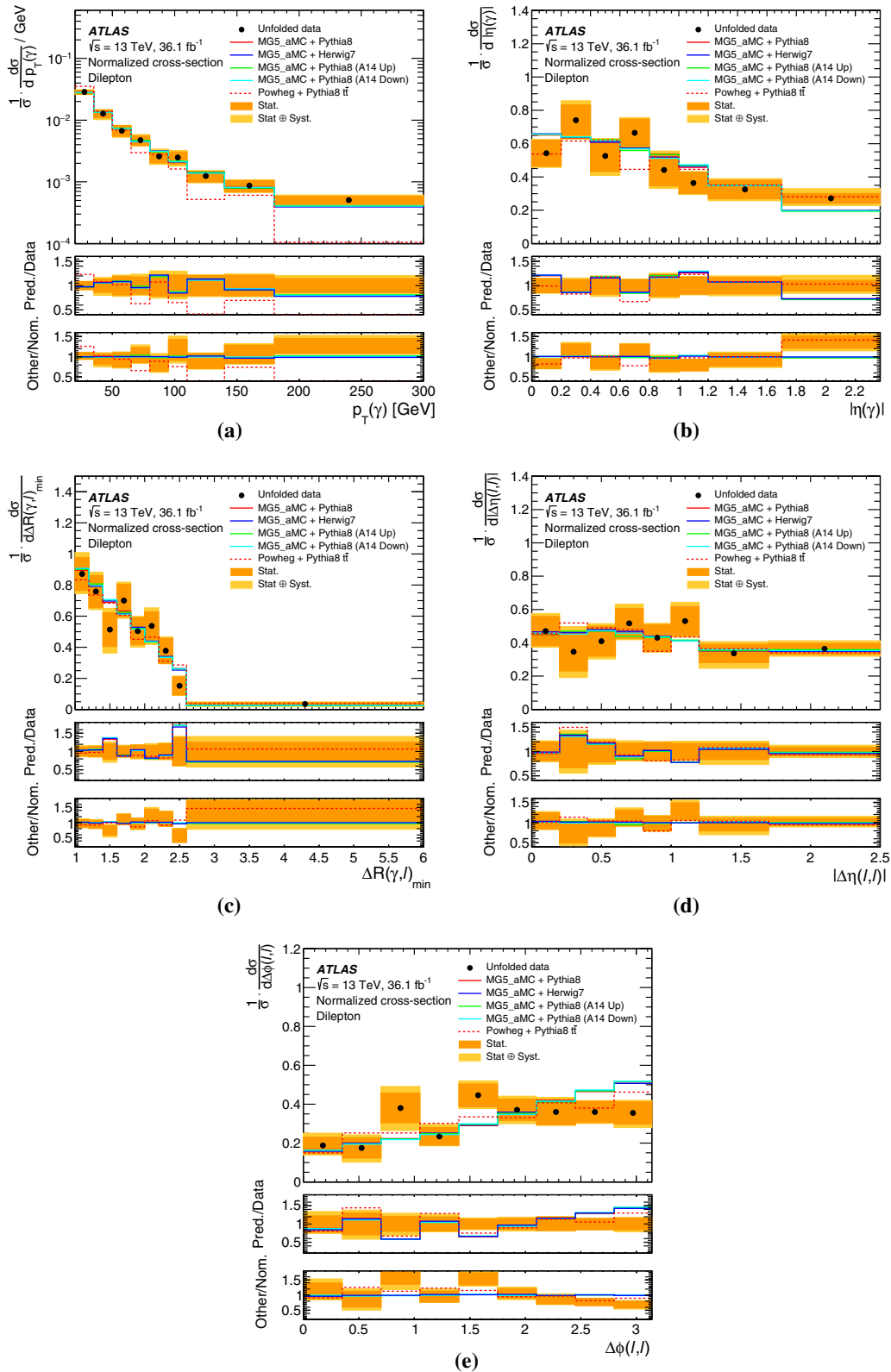


Fig. 10 The normalized differential cross-sections as a function of the **a** photon p_T , **b** photon $|\eta|$, **c** minimum $\Delta R(\gamma, \ell)$, **d** $|\Delta\eta(\ell, \ell)|$, and **e** $|\Delta\phi(\ell, \ell)|$ in the dilepton channel. The unfolded distributions are compared to the predictions of the MG5_AMC+PYTHIA 8 together with the up and down variations of the PYTHIA 8 A14 tune parameters, the

MG5_AMC+Herwig 7, and the POWHEG+PYTHIA 8 $t\bar{t}$ where photon radiation is modelled in the parton shower. The top ratio-panel shows the ratios of all the predictions over data. The bottom ratio-panel shows the ratios of the alternative predictions and data over the nominal prediction. Overflows are included in the last bin

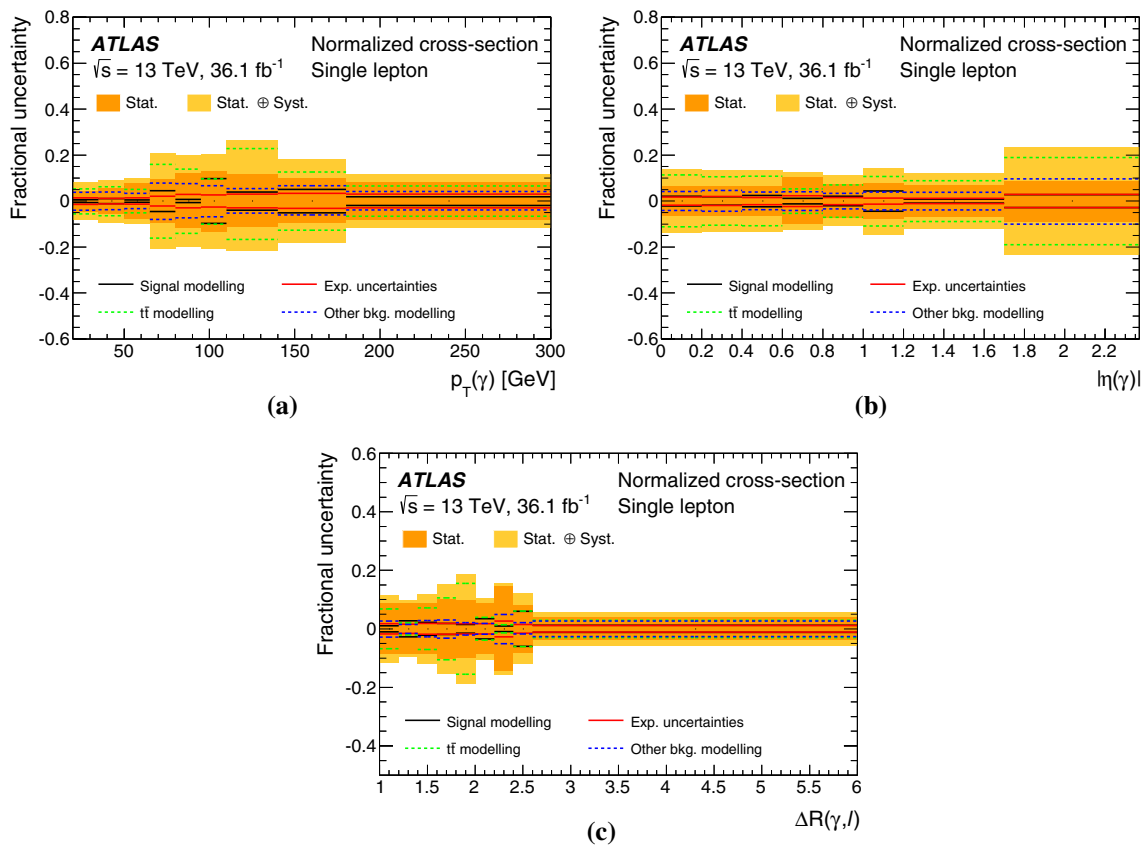


Fig. 11 The decomposed systematic uncertainties for the normalized differential cross-sections as a function of the **a** photon p_T , **b** photon $|\eta|$, and **c** $\Delta R(\gamma, \ell)$ in the single-lepton channel

systematic uncertainties. Compared to pre-fit (Table 2), the signal event yields are higher, while some of the background event yields are lower. Some of the systematic uncertainties are moderately constrained, e.g. the parton shower uncertainty of the $t\bar{t}\gamma$ and $t\bar{t}$ modelling and the PPT shape uncertainty of prompt photons.

The fiducial cross-sections in each of the individual channels (e +jets, μ +jets, ee , $e\mu$, and $\mu\mu$) as well as a combined single-lepton and dilepton cross-section are also measured. The former are measured by fitting the ELD distribution in each individual channel separately, while the latter is measured by fitting them simultaneously, sharing the same signal strength parameter $\mu = \sigma_{t\bar{t}\gamma} / \sigma_{t\bar{t}\gamma}^{NLO}$, which scales coherently the fiducial cross-sections of each channel. A comparison of all measurements with the predictions is shown in Fig. 8.

All the systematic uncertainties introduced in Sect. 8 are grouped into a smaller set of classes and summarized in Table 5 for the single-lepton and dilepton channels. The effect of each group of uncertainties is calculated from the quadratic difference between the relative uncertainty in the measured fiducial cross-section with this group of uncertainties included or excluded from the fit with corresponding nuisance parameters fixed to their fitted values. In the single-

lepton channel, the jet-related and background modelling systematic uncertainties are dominant, followed by the PPT and signal modelling systematic uncertainties. In the dilepton channel, the data statistical uncertainty is the leading contribution, followed by the signal and background modelling systematic uncertainties. The luminosity and pile-up uncertainties are also important in this channel.

9.2 Normalized differential cross-sections

The normalized differential cross-sections are shown in Figs. 9 and 10, for the single-lepton and dilepton channels, respectively. They are compared to the nominal $t\bar{t}\gamma$ sample (MG5_AMC+PYTHIA 8) and the samples with variations of the PYTHIA 8 A14 tune parameters and the alternative parton shower model of MG5_AMC+Herwig 7. In addition, a comparison with the nominal $t\bar{t}$ POWHEG+PYTHIA 8 MC sample where prompt-photon radiation is modelled in the parton shower is included. All $t\bar{t}\gamma$ samples predict very similar shapes and describe the data well. A small deviation from the prediction is observed in the dilepton $\Delta\phi$ distribution, where the leptons in the prediction are more back-to-back than in data. The deviation of data from the prediction is 1.5 standard

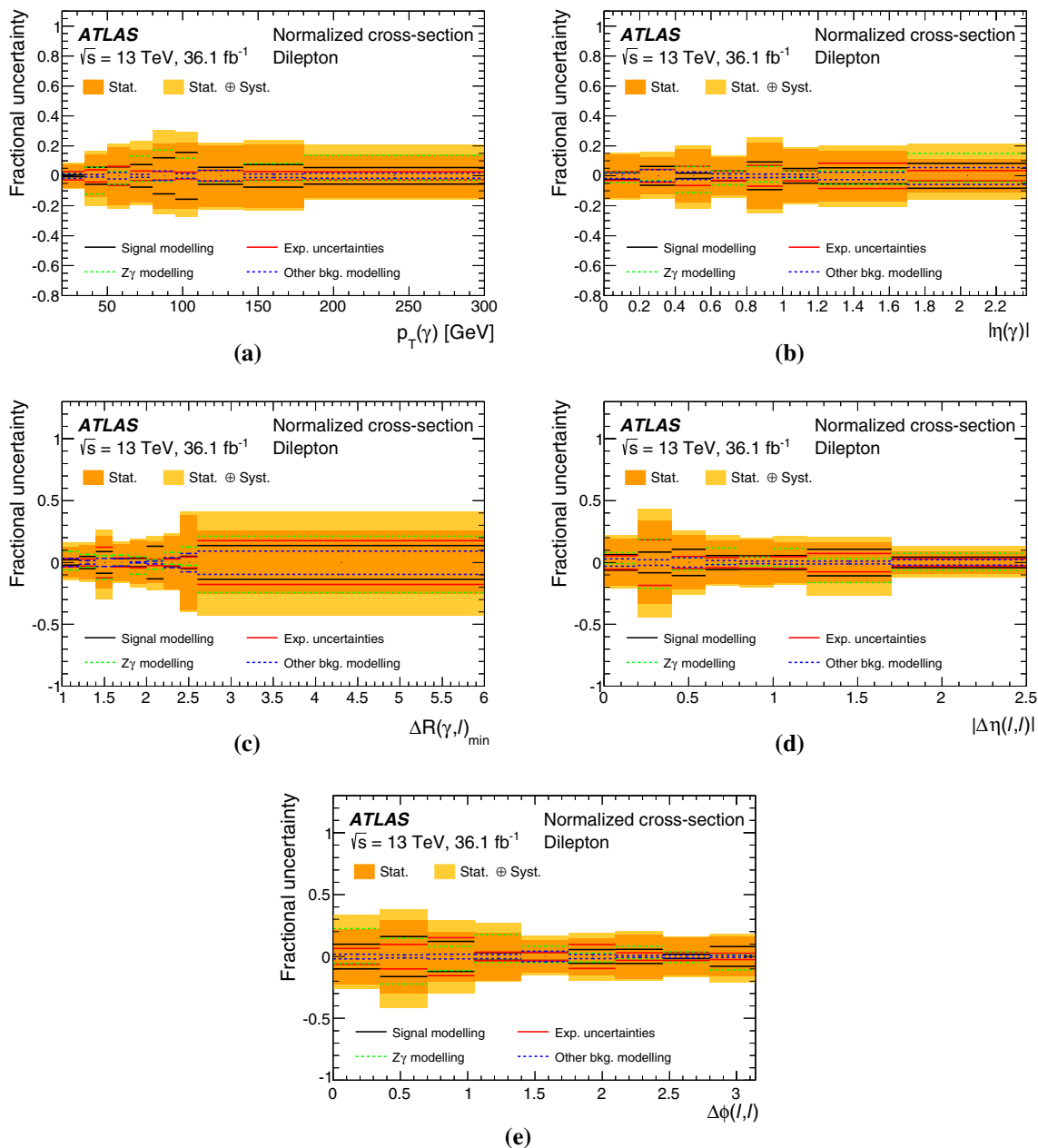


Fig. 12 The decomposed systematic uncertainties for the normalized differential cross-sections as a function of the **a** photon p_T , **b** photon $|\eta|$, **c** minimum $\Delta R(\gamma, \ell)$, **d** $|\Delta\eta(\ell, \ell)|$, and **e** $\Delta\phi(\ell, \ell)$ in the dilepton channel

deviations, based on the χ^2 calculated according to the procedure described in what follows. The POWHEG+PYTHIA 8 $t\bar{t}$ sample gives an improved agreement with data compared to the nominal and varied $t\bar{t}\gamma$ samples, although the overall agreement is still poor. It can also be seen from Figs. 9(a) and 10(a) that the photons generated by PYTHIA 8 have a softer p_T spectrum than in data.

The systematic uncertainties of the unfolded distributions are decomposed into the signal modelling uncertainty, experimental uncertainty, and background modelling uncertainty in both channels. In the single-lepton (dilepton) channel, the

background modelling uncertainty is split into $t\bar{t}$ ($Z\gamma$) and the others. These decomposed uncertainties are illustrated in Figs. 11 and 12 for the single-lepton and dilepton channels, respectively. For the single-lepton channel, the systematic uncertainty is dominated by the $t\bar{t}$ modelling, which is used to model the shapes of the hadronic-fake and electron-fake backgrounds. For the dilepton channel, the systematic uncertainty is dominated by the $Z\gamma$ modelling, mostly from the comparison between SHERPA and MG5_AMC+PYTHIA 8 generators. Because the unfolding is performed with the distributions before the fit, the background modelling uncertain-

Table 6 The correlation matrix for the normalized differential cross-section as a function of $\Delta\phi(\ell, \ell)$ in the dilepton channel, accounting for the statistical and systematic uncertainties

Bin	0.0–0.35	0.35–0.7	0.7–1.05	1.05–1.4	1.4–1.75	1.75–2.1	2.1–2.45	2.45–2.8	2.8–3.14
0.0–0.35	1.00	−0.07	0.05	−0.36	−0.18	−0.08	−0.19	−0.13	−0.24
0.35–0.7		1.00	0.29	0.21	0.09	0.11	0.21	0.02	0.32
0.7–1.05			1.00	0.12	0.05	0.10	0.14	0.05	0.23
1.05–1.4				1.00	0.26	0.18	0.29	0.20	0.41
1.4–1.75					1.00	0.15	0.16	0.14	0.21
1.75–2.1						1.00	0.17	0.15	0.23
2.1–2.45							1.00	0.12	0.33
2.45–2.8								1.00	0.18
2.8–3.14									1.00

Table 7 χ^2/ndf values and p -values between the measured normalized differential cross-sections and predictions from several generators in the single-lepton channel

Predictions	$p_T(\gamma)$		$ \eta(\gamma) $		$\Delta R(\gamma, \ell)$	
	χ^2/ndf	p -value	χ^2/ndf	p -value	χ^2/ndf	p -value
MG5_AMC + PYTHIA8	3.2/8	0.92	0.7/7	1.0	5.0/8	0.76
MG5_AMC + HERWIG7	2.3/8	0.97	0.9/7	1.0	4.8/8	0.78
MG5_AMC + PYTHIA8 (A14 Up)	3.3/8	0.91	0.8/7	1.0	4.9/8	0.77
MG5_AMC + PYTHIA8 (A14 Down)	2.6/8	0.96	0.9/7	1.0	4.6/8	0.80
POWHEG + PYTHIA8 $t\bar{t}$	25.4/8	< 0.01	2.8/7	0.9	8.7/8	0.37

Table 8 χ^2/ndf values and p -values between the measured normalized differential cross-sections and predictions from several generators in the dilepton channel

Predictions	$p_T(\gamma)$		$\eta(\gamma)$		$\Delta R(\gamma, \ell)$		$ \Delta\eta(\ell, \ell) $		$\Delta\phi(\ell, \ell)$	
	χ^2/ndf	p -value	χ^2/ndf	p -value	χ^2/ndf	p -value	χ^2/ndf	p -value	χ^2/ndf	p -value
MG5_AMC + PYTHIA8	1.7/8	0.99	7.4/7	0.39	6.9/8	0.55	3.0/7	0.89	14.4/8	0.07
MG5_AMC + HERWIG7	2.0/8	0.98	7.4/7	0.39	6.6/8	0.58	3.1/7	0.88	14.4/8	0.07
MG5_AMC + PYTHIA8 (A14 Up)	1.6/8	0.99	8.4/7	0.30	7.4/8	0.49	3.4/7	0.85	14.0/8	0.08
MG5_AMC + PYTHIA8 (A14 Down)	1.6/8	0.99	7.9/7	0.34	7.5/8	0.48	3.2/7	0.87	14.4/8	0.07
POWHEG + PYTHIA8 $t\bar{t}$	20.1/8	0.01	10.8/7	0.15	8.6/8	0.38	4.5/7	0.72	9.8/8	0.28

ties are not constrained as in the case of fiducial cross-section measurement where a fit to ELD distribution is performed, and thus they have a much larger impact on the result.

The differences between the unfolded and the predicted distributions are quantified by the chi-squared per degree of freedom χ^2/ndf , where the χ^2 is

$$\chi^2 = \left(\sigma_{j,\text{data}}^{\text{norm}} - \sigma_{j,\text{pred.}}^{\text{norm}} \right) \cdot C_{jk}^{-1} \cdot \left(\sigma_{k,\text{data}}^{\text{norm}} - \sigma_{k,\text{pred.}}^{\text{norm}} \right),$$

where $\sigma_{\text{data}}^{\text{norm}}$ and $\sigma_{\text{pred.}}^{\text{norm}}$ are the unfolded and predicted normalized differential cross-sections, C_{jk} is the covariance

matrix of $\sigma_{\text{data}}^{\text{norm}}$, and j and k are the binning indices of the distribution. For normalized differential cross-sections, the last bin of the above formula is removed from the χ^2 calculation and ndf is reduced by one since this bin gives redundant information. The total correlation matrix is shown in Table 6, taking the $\Delta\phi(\ell, \ell)$ in the dilepton channel as an example. There is moderate correlation, either positive or negative, between different bins of the unfolded $\Delta\phi(\ell, \ell)$ distribution. The calculated χ^2/ndf values and their corresponding p -values are summarized in Tables 7 and 8, quantifying the compatibility between data and each of the predictions.

10 Conclusions

Fiducial cross-sections of top-quark pair production in association with a photon are measured in the single-lepton and dilepton decay channels of the top-quark pair using 36.1 fb^{-1} of 13 TeV pp collision data collected in 2015 and 2016 by the ATLAS detector at the LHC. The normalized differential cross-sections are measured as a function of the photon p_T and $|\eta|$, and the ΔR between the photon and the closest lepton for both channels, and the $|\Delta\eta|$ and $\Delta\phi$ between the two leptons for the dilepton channel.

In both channels, the measured fiducial cross-sections agree well with the NLO SM predictions within uncertainties. The measured normalized differential cross-sections also agree well with the LO $t\bar{t}\gamma$ prediction and the NLO $t\bar{t}$ prediction, where the photon comes from the parton shower. The largest disagreement between data and LO $t\bar{t}\gamma$ prediction is observed in the distribution of the azimuthal opening angle between the two leptons in the dilepton channel, which is sensitive to $t\bar{t}$ spin correlation, while the NLO $t\bar{t}$ sample provides an improved agreement with data in this variable.

Acknowledgements We thank CERN for the very successful operation of the LHC, as well as the support staff from our institutions without whom ATLAS could not be operated efficiently. We acknowledge the support of ANPCyT, Argentina; YerPhI, Armenia; ARC, Australia; BMWFW and FWF, Austria; ANAS, Azerbaijan; SSTC, Belarus; CNPq and FAPESP, Brazil; NSERC, NRC and CFI, Canada; CERN; CONICYT, Chile; CAS, MOST and NSFC, China; COLCIENCIAS, Colombia; MSMT CR, MPO CR and VSC CR, Czech Republic; DNRF and DNSRC, Denmark; IN2P3-CNRS, CEA-DRF/IRFU, France; SRNSFG, Georgia; BMBF, HGF, and MPG, Germany; GSRT, Greece; RGC, Hong Kong SAR, China; ISF and Benozziyo Center, Israel; INFN, Italy; MEXT and JSPS, Japan; CNRST, Morocco; NWO, Netherlands; RCN, Norway; MNiSW and NCN, Poland; FCT, Portugal; MNE/IFA, Romania; MES of Russia and NRC KI, Russian Federation; JINR; MESTD, Serbia; MSSR, Slovakia; ARRS and MIZŠ, Slovenia; DST/NRF, South Africa; MINECO, Spain; SRC and Wallenberg Foundation, Sweden; SERI, SNSF and Cantons of Bern and Geneva, Switzerland; MOST, Taiwan; TAEK, Turkey; STFC, United Kingdom; DOE and NSF, United States of America. In addition, individual groups and members have received support from BCKDF, CANARIE, CRC and Compute Canada, Canada; COST, ERC, ERDF, Horizon 2020, and Marie Skłodowska-Curie Actions, European Union; Investissements d' Avenir Labex and Idex, ANR, France; DFG and AvH Foundation, Germany; Herakleitos, Thales and Aristeia programmes co-financed by EU-ESF and the Greek NSRF, Greece; BSF-NSF and GIF, Israel; CERCA Programme Generalitat de Catalunya, Spain; The Royal Society and Leverhulme Trust, United Kingdom. The crucial computing support from all WLCG partners is acknowledged gratefully, in particular from CERN, the ATLAS Tier-1 facilities at TRIUMF (Canada), NDGF

(Denmark, Norway, Sweden), CC-IN2P3 (France), KIT/GridKA (Germany), INFN-CNAF (Italy), NL-T1 (Netherlands), PIC (Spain), ASGC (Taiwan), RAL (UK) and BNL (USA), the Tier-2 facilities worldwide and large non-WLCG resource providers. Major contributors of computing resources are listed in Ref. [64].

Data Availability Statement This manuscript has no associated data or the data will not be deposited. [Authors' comment: All ATLAS scientific output is published in journals, and preliminary results are made available in Conference Notes. All are openly available, without restriction on use by external parties beyond copyright law and the standard conditions agreed by CERN. Data associated with journal publications are also made available: tables and data from plots (e.g. cross section values, likelihood profiles, selection efficiencies, cross section limits, ...) are stored in appropriate repositories such as HEPDATA (<http://hepdata.cedar.ac.uk/>). ATLAS also strives to make additional material related to the paper available that allows a reinterpretation of the data in the context of new theoretical models. For example, an extended encapsulation of the analysis is often provided for measurements in the framework of RIVET (<http://rivet.hepforge.org/>). This information is taken from the ATLAS Data Access Policy, which is a public document that can be downloaded from <http://opendata.cern.ch/record/413> [opendata.cern.ch].]

Open Access This article is distributed under the terms of the Creative Commons Attribution 4.0 International License (<http://creativecommons.org/licenses/by/4.0/>), which permits unrestricted use, distribution, and reproduction in any medium, provided you give appropriate credit to the original author(s) and the source, provide a link to the Creative Commons license, and indicate if changes were made. Funded by SCOAP³.

Appendix

The definitions of the discriminating variables used in ATLAS photon identification are given in Table 9.

The shapes of the PPT of the prompt, hadronic-fake, and electron-fake photons are compared in Fig. 13.

Figure 14 shows the post-fit distributions of four important variables for the training of the ELD in the single-lepton channel.

Figure 15 shows the post-fit distributions of four important variables for the training of the ELD in the dilepton channel.

Figure 16 shows the distributions of the ELD and H_T in the hadronic-fake control region B, as defined in Sect. 6.1.

Figure 17 shows the distributions of the efficiency, outside fraction, and migration matrix for the dilepton azimuthal angle in the dilepton channel, which are the inputs for unfolding, as described in Sect. 7.3.

Table 9 Definitions of photon discriminating variables

Name	Description
Hadronic leakage	
R_{had} or R_{had1}	Transverse energy leakage in the hadronic calorimeter normalized to transverse energy of the photon candidate in the ECAL. In the region $0.8 \leq \eta \leq 1.37$, the entire energy of the photon candidate in the HCAL is used (R_{had}), while in the region $ \eta < 0.8$ and $ \eta > 1.37$ the energy of the first layer of the HCAL is used (R_{had1})
Energy ratios and width in the second layer of ECAL	
R_η	Energy ratio of 3×7 to 7×7 cells in the $\eta \times \phi$ plane
R_ϕ	Energy ratio of 3×3 to 3×7 cells in the $\eta \times \phi$ plane
$w_{\eta 2}$	Lateral width of the shower, using a window of $\eta \times \phi = 3 \times 5$ cells
Energy ratios and widths in the first (strip) layer of ECAL	
w_{s3}	Shower width along η , using 3 strips around the largest energy deposit
$w_{s \text{ tot}}$	Shower width along η , using 20×2 strip cells in the $\eta \times \phi$ plane
F_{side}	Energy outside the 3 central strips but within 7 strips, normalized to the energy within the 3 central strips
E_{ratio}	Ratio between difference of the first and second energy maximum divided by their sum ($E_{\text{ratio}} = 1$ if there is no second maximum)
ΔE	Difference between the second energy maximum and the minimum found between first and second maximum ($\Delta E = 0$ if there is no second maximum)

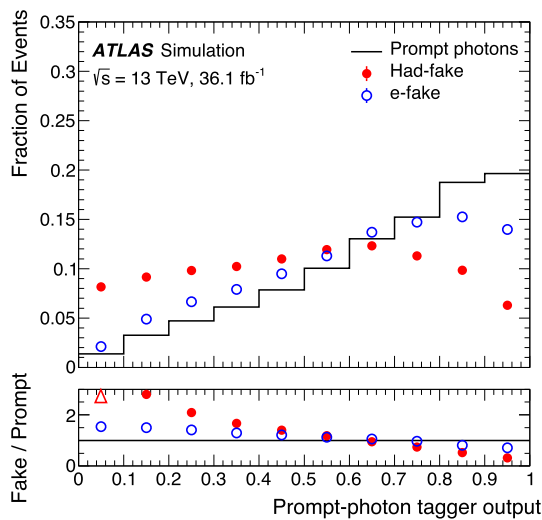


Fig. 13 The simulated shapes of the output of the prompt-photon tagger for the prompt, hadronic-fake, and electron-fake photons after applying Tight identification and isolation criteria

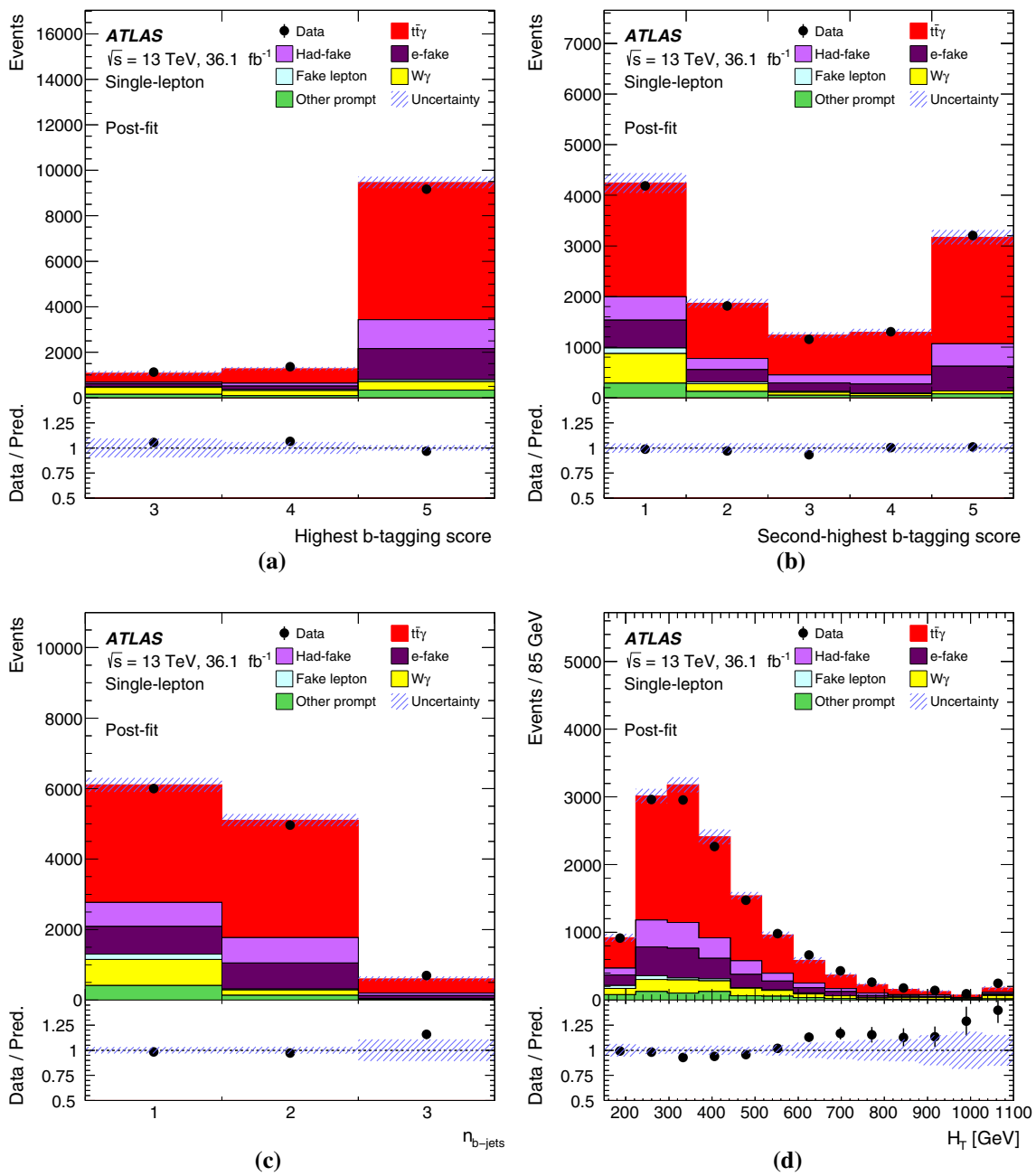


Fig. 14 Distributions of the **a** highest and **b** second highest *b*-tagging scores for all jets, **c** total number of *b*-tagged jets (at a 77% efficiency), and **d** scalar sum of the transverse energies of all the selected physical objects in the single-lepton channel after event selection and likelihood

fit. Each bin of **a** and **b**, from one to five, represents the *b*-tagging efficiencies of > 85%, 77–85%, 70–77%, 60–70%, and < 60%. All data-driven corrections and systematic uncertainties are included

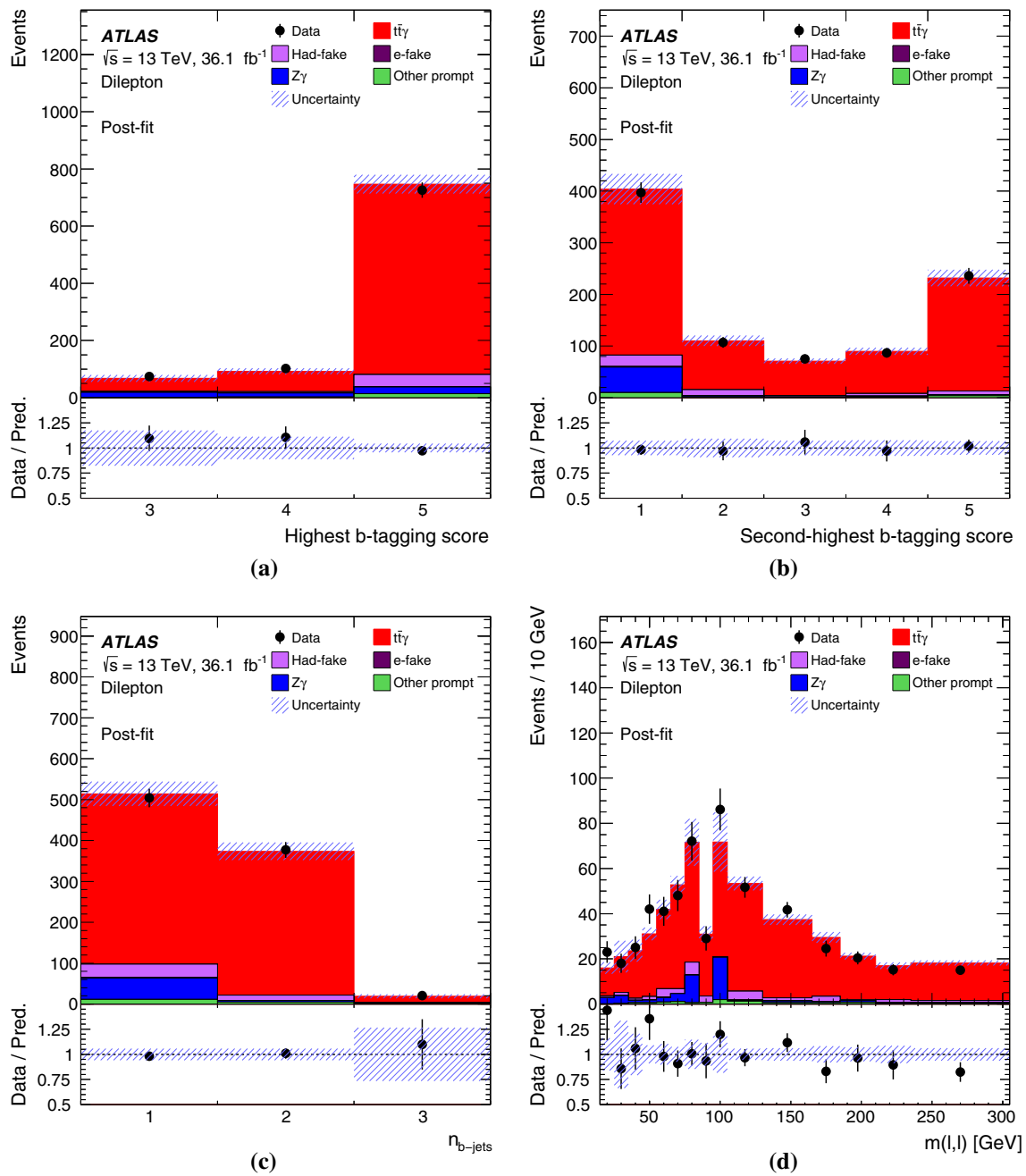


Fig. 15 Distributions of the **a** highest and **b** second highest b -tagging scores for all jets, **c** total number of b -tagged jets (at a 77% efficiency), and **d** invariant mass between the two leptons in the dilepton channel after event selection and likelihood fit. Each bin of **a** and **b**, from one

to five, represents the b -tagging efficiencies of $> 85\%$, $77\text{--}85\%$, $70\text{--}77\%$, $60\text{--}70\%$, and $< 60\%$. All data-driven corrections and systematic uncertainties are included

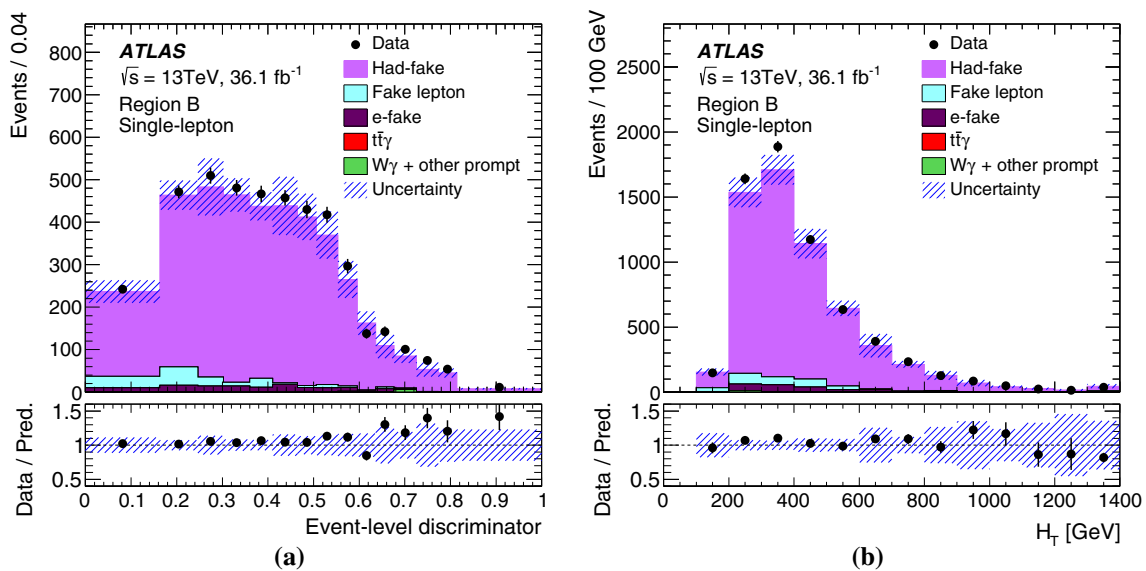


Fig. 16 Distributions of the **a** ELD and **b** H_T in the hadronic-fake control region B of the single-lepton channel. Data-driven correction to the electron-fake background and all systematic uncertainties are included.

The contributions from $t\bar{t}\gamma$ and $W\gamma$ + other prompts are very small (0.2% and 0.3%, respectively), therefore not visible

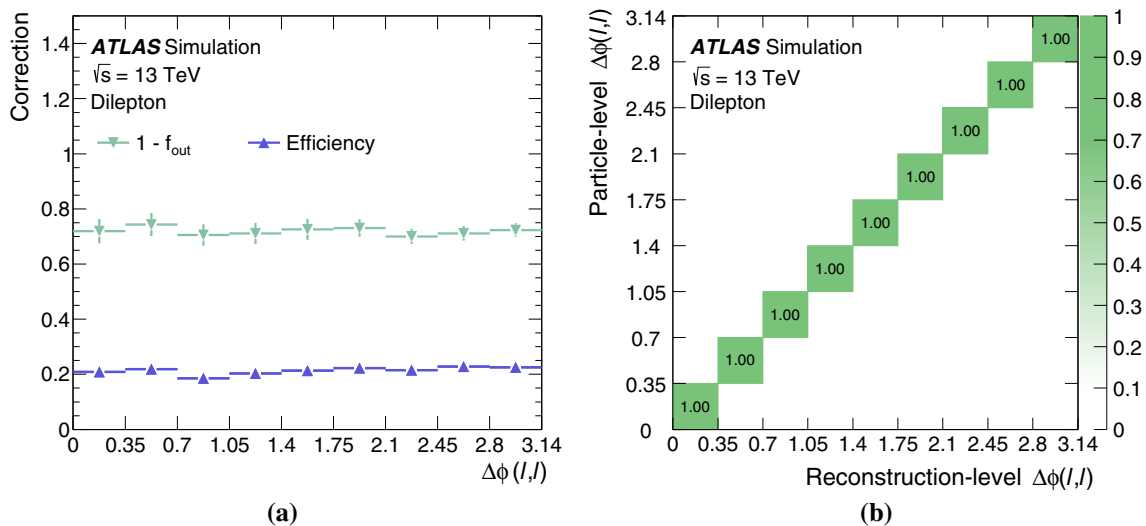


Fig. 17 The **a** efficiency and outside fraction and **b** migration matrix for the dilepton azimuthal angle in the dilepton channel

References

1. U. Baur, A. Juste, L.H. Orr, D. Rainwater, Probing electroweak top quark couplings at hadron colliders. *Phys. Rev. D* **71**, 054013 (2005). [arXiv:hep-ph/0412021](#)
2. A.O. Bouzas, F. Larios, Electromagnetic dipole moments of the top quark. *Phys. Rev. D* **87**, 074015 (2013). [arXiv:1212.6575](#) [hep-ph]
3. M. Schulze, Y. Soreq, Pinning down electroweak dipole operators of the top quark. *Eur. Phys. J. C* **76**, 466 (2016). [arXiv:1603.08911](#) [hep-ph]
4. O. Bessidskaia Bylund, F. Maltoni, I. Tsinikos, E. Vryonidou, C. Zhang, Probing top quark neutral couplings in the Standard Model Effective Field Theory at NLO in QCD. *JHEP* **05**, 052 (2016). [arXiv:1601.08193](#) [hep-ph]
5. J.A. Aguilar-Saavedra, E. Álvarez, A. Juste, F. Rubbo, Shedding light on the $t\bar{t}$ asymmetry: the photon handle. *JHEP* **04**, 188 (2014). [arXiv:1402.3598](#) [hep-ph]
6. CDF Collaboration, Evidence for $t\bar{t}\gamma$ production and measurement of $\sigma_{t\bar{t}\gamma}/\sigma_{t\bar{t}}$. *Phys. Rev. D* **84**, 031104(R) (2011). [arXiv:1106.3970](#) [hep-ex]
7. ATLAS Collaboration, Observation of top-quark pair production in association with a photon and measurement of the $t\bar{t}\gamma$ production cross section in pp collisions at $\sqrt{s} = 7\text{ TeV}$ using the ATLAS detector. *Phys. Rev. D* **91**, 072007 (2015). [arXiv:1502.00586](#) [hep-ex]

8. ATLAS Collaboration, Measurement of the $t\bar{t}\gamma$ production cross section in proton-proton collisions at $\sqrt{s} = 8\text{ TeV}$ with the ATLAS detector. *JHEP* **11**, 086 (2017). [arXiv:1706.03046](https://arxiv.org/abs/1706.03046) [hep-ex]
9. CMS Collaboration, Measurement of the semileptonic $t\bar{t} + \gamma$ production cross section in pp collisions at $\sqrt{s} = 8\text{ TeV}$. *JHEP* **10**, 006 (2017). [arXiv:1706.08128](https://arxiv.org/abs/1706.08128) [hep-ex]
10. K. Melnikov, M. Schulze, A. Scharf, QCD corrections to top quark pair production in association with a photon at hadron colliders. *Phys. Rev. D* **83**, 074013 (2011). [arXiv:1102.1967](https://arxiv.org/abs/1102.1967) [hep-ph]
11. ATLAS Collaboration, The ATLAS Experiment at the CERN Large Hadron Collider. *JINST* **3**, S08003 (2008)
12. ATLAS Collaboration, ATLAS Insertable B-Layer Technical Design Report, ATLAS-TDR-19, 2010. <https://cds.cern.ch/record/1291633>, ATLAS Insertable B-Layer Technical Design Report Addendum. ATLAS-TDR-19-ADD-1 (2012). <https://cds.cern.ch/record/1451888>
13. B. Abbott et al., Production and Integration of the ATLAS Insertable B-Layer. *JINST* **13**, T05008 (2018). [arXiv:1803.00844](https://arxiv.org/abs/1803.00844) [physics.ins-det]
14. ATLAS Collaboration, Performance of the ATLAS trigger system in 2015. *Eur. Phys. J. C* **77**, 317 (2017). [arXiv:1611.09661](https://arxiv.org/abs/1611.09661) [hep-ex]
15. S. Agostinelli et al., GEANT4—a simulation toolkit. *Nucl. Instrum. Meth. A* **506**, 250 (2003)
16. ATLAS Collaboration, The ATLAS Simulation Infrastructure. *Eur. Phys. J. C* **70**, 823 (2010). [arXiv:1005.4568](https://arxiv.org/abs/1005.4568) [physics.ins-det]
17. T. Sjöstrand, S. Mrenna, P.Z. Skands, A brief introduction to PYTHIA 8.1. *Comput. Phys. Commun.* **178**, 852 (2008). [arXiv:0710.3820](https://arxiv.org/abs/0710.3820) [hep-ph]
18. ATLAS Collaboration, Summary of ATLAS Pythia 8 tunes. *ATL-PHYS-PUB-2012-003* (2012). <https://cds.cern.ch/record/1474107>
19. A.D. Martin, W.J. Stirling, R.S. Thorne, G. Watt, Parton distributions for the LHC. *Eur. Phys. J. C* **63**, 189 (2009). [arXiv:0901.0002](https://arxiv.org/abs/0901.0002) [hep-ph]
20. J. Alwall et al., The automated computation of tree-level and next-to-leading order differential cross sections, and their matching to parton shower simulations. *JHEP* **07**, 079 (2014). [arXiv:1405.0301](https://arxiv.org/abs/1405.0301) [hep-ph]
21. T. Sjöstrand et al., An introduction to PYTHIA 8.2. *Comput. Phys. Commun.* **191**, 159 (2015). [arXiv:1410.3012](https://arxiv.org/abs/1410.3012) [hep-ph]
22. ATLAS Collaboration, ATLAS Pythia 8 tunes to 7 TeV data. *ATL-PHYS-PUB-2014-021* (2014). <https://cds.cern.ch/record/1966419>
23. J. Pumplin et al., New Generation of Parton Distributions with Uncertainties from Global QCD Analysis. *JHEP* **07**, 012 (2002). [arXiv:hep-ph/0201195](https://arxiv.org/abs/hep-ph/0201195) [hep-ph]
24. ATLAS Collaboration, Simulation of top-quark production for the ATLAS experiment at $\sqrt{s} = 13\text{ TeV}$. *ATL-PHYS-PUB-2016-004* (2016). <https://cds.cern.ch/record/2120417>
25. S. Frixione, P. Nason, C. Oleari, Matching NLO QCD computations with parton shower simulations: the POWHEG method. *JHEP* **11**, 070 (2007). [arXiv:0709.2092](https://arxiv.org/abs/0709.2092) [hep-ph]
26. R.D. Ball et al., Parton distributions for the LHC Run II. *JHEP* **04**, 040 (2015). [arXiv:1410.8849](https://arxiv.org/abs/1410.8849) [hep-ph]
27. T. Gleisberg et al., Event generation with SHERPA 1.1. *JHEP* **02**, 007 (2009). [arXiv:0811.4622](https://arxiv.org/abs/0811.4622) [hep-ph]
28. ATLAS Collaboration, Monte Carlo Generators for the Production of a W or Z/γ^* Boson in Association with Jets at ATLAS in Run 2. *ATL-PHYS-PUB-2016-003* (2016). <https://cds.cern.ch/record/2120133>
29. H.-L. Lai et al., New parton distributions for collider physics. *Phys. Rev. D* **82**, 074024 (2010). [arXiv:1007.2241](https://arxiv.org/abs/1007.2241) [hep-ph]
30. P.Z. Skands, Tuning Monte Carlo generators: The Perugia tunes. *Phys. Rev. D* **82**, 074018 (2010). [arXiv:1005.3457](https://arxiv.org/abs/1005.3457) [hep-ph]
31. ATLAS Collaboration, Multi-boson simulation for 13 TeV ATLAS analyses. *ATL-PHYS-PUB-2016-002* (2016). <https://cds.cern.ch/record/2119986>
32. ATLAS Collaboration, Modelling of the $t\bar{t}\bar{H}$ and $t\bar{t}V$ ($V = W, Z$) processes for $\sqrt{s} = 13\text{ TeV}$ ATLAS analyses. *ATL-PHYS-PUB-2016-005* (2016). <https://cds.cern.ch/record/2120826>
33. D.J. Lange, The EvtGen particle decay simulation package. *Nucl. Instrum. Meth. A* **462**, 152 (2001). ISSN: 0168-9002
34. J. Bellm et al., Herwig 7.0/Herwig++ 3.0 release note. *Eur. Phys. J. C* **76**, 196 (2016). [arXiv:1512.01178](https://arxiv.org/abs/1512.01178) [hep-ph]
35. P.-F. Duan et al., QCD corrections to associated production of $t\bar{t}\gamma$ at hadron colliders. *Phys. Rev. D* **80**, 014022 (2009). [arXiv:0907.1324](https://arxiv.org/abs/0907.1324) [hep-ph]
36. M. Cacciari, G.P. Salam, G. Soyez, The anti- k_r jet clustering algorithm. *JHEP* **04**, 063 (2008). [arXiv:0802.1189](https://arxiv.org/abs/0802.1189) [hep-ph]
37. ATLAS Collaboration, Electron reconstruction and identification in the ATLAS experiment using the 2015 and 2016 LHC proton-proton collision data at $\sqrt{s} = 13\text{ TeV}$. Submitted to: *Eur. Phys. J.* (2019). [arXiv:1902.04655](https://arxiv.org/abs/1902.04655) [hep-ex]
38. ATLAS Collaboration, Muon reconstruction performance of the ATLAS detector in proton-proton collision data at $\sqrt{s} = 13\text{ TeV}$. *Eur. Phys. J. C* **76**, 292 (2016). [arXiv:1603.05598](https://arxiv.org/abs/1603.05598) [hep-ex]
39. ATLAS Collaboration, Measurement of the photon identification efficiencies with the ATLAS detector using LHC Run 2 data collected in 2015 and 2016. *Eur. Phys. J.* (2018). [arXiv:1810.05087](https://arxiv.org/abs/1810.05087) [hep-ex]
40. ATLAS Collaboration, Properties of jets and inputs to jet reconstruction and calibration with the ATLAS detector using proton-proton collisions at $\sqrt{s} = 13\text{ TeV}$. *ATL-PHYS-PUB-2015-036* (2015). <https://cds.cern.ch/record/2044564>
41. ATLAS Collaboration, Jet energy scale measurements and their systematic uncertainties in proton-proton collisions at $\sqrt{s} = 13\text{ TeV}$ with the ATLAS detector. *Phys. Rev. D* **96**, 072002 (2017). [arXiv:1703.09665](https://arxiv.org/abs/1703.09665) [hep-ex]
42. ATLAS Collaboration, Tagging and suppression of pileup jets with the ATLAS detector. *ATLAS-CONF-2014-018* (2014). <https://cds.cern.ch/record/1700870>
43. ATLAS Collaboration, Measurements of b-jet tagging efficiency with the ATLAS detector using $t\bar{t}$ events at $\sqrt{s} = 13\text{ TeV}$. *JHEP* **08**, 089 (2018). [arXiv:1805.01845](https://arxiv.org/abs/1805.01845) [hep-ex]
44. ATLAS Collaboration, Optimisation of the ATLAS b-tagging performance for the 2016 LHC Run. *ATL-PHYS-PUB-2016-012* (2016). <https://cds.cern.ch/record/2160731>
45. ATLAS Collaboration, Performance of missing transverse momentum reconstruction with the ATLAS detector using proton-proton collisions $\sqrt{s} = 13\text{ TeV}$. *Eur. Phys. J. C* **78**, 903 (2018). [arXiv:1802.08168](https://arxiv.org/abs/1802.08168) [hep-ex]
46. F. Chollet et al., Keras. (2015). <https://github.com/fchollet/keras>
47. D. H. Guest, M. Paganini, M. Kagan, J. W. Smith, M. Lanfermann, lwttnn: Release for Athena v21, (2017). <https://doi.org/10.5281/zenodo.290682>
48. R. Al-Rfou et al., Theano: A Python framework for fast computation of mathematical expressions. *CoRR* (2016). [arXiv:1605.02688](https://arxiv.org/abs/1605.02688)
49. N. Srivastava, G. Hinton, A. Krizhevsky, I. Sutskever, R. Salakhutdinov, Dropout: a simple way to prevent neural networks from overfitting. *J. Mach. Learn. Res.* **15**, 1929 (2014). <http://jmlr.org/papers/v15/srivastava14a.html>
50. S. Ioffe, C. Szegedy, Batch normalization: accelerating deep network training by reducing internal covariate shift. *CoRR* (2015). [arXiv:1502.03167](https://arxiv.org/abs/1502.03167)
51. ATLAS Collaboration, Estimation of non-prompt and fake lepton backgrounds in final states with top quarks produced in proton-proton collisions at $\sqrt{s} = 8\text{ TeV}$ with the ATLAS Detector. *ATLAS-CONF-2014-058* (2014). <https://cds.cern.ch/record/1951336>
52. M. Cacciari, G.P. Salam, G. Soyez, The catchment area of jets. *JHEP* **04**, 005 (2008). [arXiv:0802.1188](https://arxiv.org/abs/0802.1188) [hep-ph]
53. G. D' Agostini, A multidimensional unfolding method based on Bayes' theorem. *Nucl. Instrum. Meth. A* **362**, 487 (1995)

54. T. Adye, Unfolding algorithms and tests using RooUnfold, Proceedings of PHYSTAT 2011 Workshop on Statistical Issues Related to Discovery Claims in Search Experiments and Unfolding, CERN, Geneva 313 (2011). [arXiv:1105.1160](https://arxiv.org/abs/1105.1160)
55. ATLAS Collaboration, Electron and photon energy calibration with the ATLAS detector using 2015–2016 LHC proton-proton collision data. JINST (2018). [arXiv:1812.03848](https://arxiv.org/abs/1812.03848) [hep-ex]
56. ATLAS Collaboration, Jet energy measurement and its systematic uncertainty in proton–proton collisions at $\sqrt{s} = 7\text{ TeV}$ with the ATLAS detector. Eur. Phys. J. C **75**, 17 (2015). [arXiv:1406.0076](https://arxiv.org/abs/1406.0076) [hep-ex]
57. ATLAS Collaboration, Jet energy measurement with the ATLAS detector in proton-proton collisions at $\sqrt{s} = 7\text{ TeV}$. Eur. Phys. J. C **73**, 2304 (2013). [arXiv:1112.6426](https://arxiv.org/abs/1112.6426) [hep-ex]
58. ATLAS Collaboration, Single hadron response measurement and calorimeter jet energy scale uncertainty with the ATLAS detector at the LHC. Eur. Phys. J. C **73**, 2305 (2013). [arXiv:1203.1302](https://arxiv.org/abs/1203.1302) [hep-ex]
59. ATLAS Collaboration, Jet energy resolution in proton-proton collisions at $\sqrt{s} = 7\text{ TeV}$ recorded in 2010 with the ATLAS detector. Eur. Phys. J. C **73**, 2306 (2013). [arXiv:1210.6210](https://arxiv.org/abs/1210.6210) [hep-ex]
60. ATLAS Collaboration, Expected performance of the ATLAS b-tagging algorithms in Run-2, ATL-PHYS-PUB-2015-022 (2015). <https://cds.cern.ch/record/2037697>
61. ATLAS Collaboration, Performance of Missing Transverse Momentum Reconstruction in ATLAS studied in Proton–Proton Collisions recorded in 2012 at $\sqrt{s} = 8\text{ TeV}$, ATLAS-CONF-2013-082 (2013). <https://cds.cern.ch/record/1570993>
62. ATLAS Collaboration, Luminosity determination in pp collisions at $\sqrt{s} = 8\text{ TeV}$ using the ATLAS detector at the LHC. Eur. Phys. J. C **76**, 653 (2016). [arXiv:1608.03953](https://arxiv.org/abs/1608.03953) [hep-ex]
63. G. Avoni et al., The new LUCID-2 detector for luminosity measurement and monitoring in ATLAS. JINST **13**, P07017 (2018)
64. ATLAS Collaboration, ATLAS Computing Acknowledgements. ATL-GEN-PUB-2016-002. <https://cds.cern.ch/record/2202407>

ATLAS Collaboration

M. Aaboud^{35d}, G. Aad¹⁰⁰, B. Abbott¹²⁷, D. C. Abbott¹⁰¹, O. Abdinov^{13,*}, B. Abeloos¹³¹, D. K. Abhayasinghe⁹², S. H. Abidi¹⁶⁶, O. S. AbouZeid⁴⁰, N. L. Abraham¹⁵⁵, H. Abramowicz¹⁶⁰, H. Abreu¹⁵⁹, Y. Abulaiti⁶, B. S. Acharya^{65a,65b,n}, S. Adachi¹⁶², L. Adam⁹⁸, L. Adamczyk^{82a}, L. Adamek¹⁶⁶, J. Adelman¹²⁰, M. Adersberger¹¹³, A. Adiguzel^{12c,ah}, T. Adye¹⁴³, A. A. Affolder¹⁴⁵, Y. Afik¹⁵⁹, C. Agheorghiesei^{27c}, J. A. Aguilar-Saavedra^{139a,139f}, F. Ahmadov^{78,af}, G. Aielli^{72a,72b}, S. Akatsuka⁸⁴, T. P. A. Åkesson⁹⁵, E. Akilli⁵³, A. V. Akimov¹⁰⁹, G. L. Alberghi^{23a,23b}, J. Albert¹⁷⁵, P. Albicocco⁵⁰, M. J. Alconada Verzini⁸⁷, S. Alderweireldt¹¹⁸, M. Aleksa³⁶, I. N. Aleksandrov⁷⁸, C. Alexa^{27b}, D. Alexandre¹⁹, T. Alexopoulos¹⁰, M. Alhroob¹²⁷, B. Ali¹⁴¹, G. Alimonti^{67a}, J. Alison³⁷, S. P. Alkire¹⁴⁷, C. Allaire¹³¹, B. M. M. Allbrooke¹⁵⁵, B. W. Allen¹³⁰, P. P. Allport²¹, A. Aloisio^{68a,68b}, A. Alonso⁴⁰, F. Alonso⁸⁷, C. Alpigiani¹⁴⁷, A. A. Alshehri⁵⁶, M. I. Alstady¹⁰⁰, B. Alvarez Gonzalez³⁶, D. Álvarez Piqueras¹⁷³, M. G. Alvigi^{68a,68b}, B. T. Amadio¹⁸, Y. Amaral Coutinho^{79b}, A. Ambler¹⁰², L. Ambroz¹³⁴, C. Amelung²⁶, D. Amidei¹⁰⁴, S. P. Amor Dos Santos^{139a,139c}, S. Amoroso⁴⁵, C. S. Amrouche⁵³, F. An⁷⁷, C. Anastopoulos¹⁴⁸, L. S. Ancu⁵³, N. Andari¹⁴⁴, T. Andeen¹¹, C. F. Anders^{60b}, J. K. Anders²⁰, K. J. Anderson³⁷, A. Andreazza^{67a,67b}, V. Andrei^{60a}, C. R. Anelli¹⁷⁵, S. Angelidakis³⁸, I. Angelozzi¹¹⁹, A. Angerami³⁹, A. V. Anisenkov^{121a,121b}, A. Annovi^{70a}, C. Antel^{60a}, M. T. Anthony¹⁴⁸, M. Antonelli⁵⁰, D. J. A. Antrim¹⁷⁰, F. Anulli^{71a}, M. Aoki⁸⁰, J. A. Aparisi Pozo¹⁷³, L. Aperio Bella³⁶, G. Arabidze¹⁰⁵, J. P. Araque^{139a}, V. Araujo Ferraz^{79b}, R. Araujo Pereira^{79b}, A. T. H. Arce⁴⁸, R. E. Ardell⁹², F. A. Arduh⁸⁷, J.-F. Arguin¹⁰⁸, S. Argyropoulos⁷⁶, J.-H. Arling⁴⁵, A. J. Armbruster³⁶, L. J. Armitage⁹¹, A. Armstrong¹⁷⁰, O. Arnaez¹⁶⁶, H. Arnold¹¹⁹, M. Arratia³², O. Arslan²⁴, A. Artamonov^{110,*}, G. Artoni¹³⁴, S. Artz⁹⁸, S. Asai¹⁶², N. Asbah⁵⁸, E. M. Asimakopoulou¹⁷¹, L. Asquith¹⁵⁵, K. Assamagan²⁹, R. Astalos^{28a}, R. J. Atkin^{33a}, M. Atkinson¹⁷², N. B. Atlay¹⁵⁰, K. Augsten¹⁴¹, G. Avolio³⁶, R. Avramidou^{59a}, M. K. Ayoub^{15a}, A. M. Azoulay^{167b}, G. Azuelos^{108,au}, A. E. Baas^{60a}, M. J. Baca²¹, H. Bachacou¹⁴⁴, K. Bachas^{66a,66b}, M. Backes¹³⁴, P. Bagnaia^{71a,71b}, M. Bahmani⁸³, H. Bahrasemani¹⁵¹, A. J. Bailey¹⁷³, V. R. Bailey¹⁷², J. T. Baines¹⁴³, M. Bajic⁴⁰, C. Bakalis¹⁰, O. K. Baker¹⁸², P. J. Bakker¹¹⁹, D. Bakshi Gupta⁸, S. Balaji¹⁵⁶, E. M. Baldin^{121a,121b}, P. Balek¹⁷⁹, F. Balli¹⁴⁴, W. K. Balunas¹³⁶, J. Balz⁹⁸, E. Banas⁸³, A. Bandyopadhyay²⁴, S. Banerjee^{180,i}, A. A. E. Bannoura¹⁸¹, L. Barak¹⁶⁰, W. M. Barbe³⁸, E. L. Barberio¹⁰³, D. Barberis^{54a,54b}, M. Barbero¹⁰⁰, T. Barillari¹¹⁴, M.-S. Barisits³⁶, J. Barkeloo¹³⁰, T. Barklow¹⁵², R. Barnea¹⁵⁹, S. L. Barnes^{59c}, B. M. Barnett¹⁴³, R. M. Barnett¹⁸, Z. Barnovska-Blenessy^{59a}, A. Baroncelli^{73a}, G. Barone²⁹, A. J. Barr¹³⁴, L. Barranco Navarro¹⁷³, F. Barreiro⁹⁷, J. Barreiro Guimarães da Costa^{15a}, R. Bartoldus¹⁵², A. E. Barton⁸⁸, P. Bartos^{28a}, A. Basalae¹³⁷, A. Bassalat¹³¹, R. L. Bates⁵⁶, S. J. Batista¹⁶⁶, S. Batlamous^{35e}, J. R. Batley³², M. Battaglia¹⁴⁵, M. Bauge^{71a,71b}, F. Bauer¹⁴⁴, K. T. Bauer¹⁷⁰, H. S. Bawa^{31,1}, J. B. Beacham¹²⁵, T. Beau¹³⁵, P. H. Beauchemin¹⁶⁹, P. Bechtel²⁴, H. C. Beck⁵², H. P. Beck^{20,q}, K. Becker⁵¹, M. Becker⁹⁸, C. Becot⁴⁵, A. Beddall^{12d}, A. J. Beddall^{12a}, V. A. Bednyakov⁷⁸, M. Bedognetti¹¹⁹, C. P. Bee¹⁵⁴, T. A. Beermann⁷⁵, M. Begalli^{79b}, M. Begel²⁹, A. Behera¹⁵⁴, J. K. Behr⁴⁵, F. Beisiegel²⁴, A. S. Bell⁹³, G. Bella¹⁶⁰, L. Bellagamba^{23b}, A. Bellerive³⁴, M. Bellomo¹⁵⁹, P. Bellos⁹, K. Belotskiy¹¹¹, N. L. Belyaev¹¹¹, O. Benary^{160,*}, D. Bencheikroun^{35a}, M. Bender¹¹³, N. Benekos¹⁰, Y. Benhammou¹⁶⁰, E. Benhar Nocchioli¹⁸², J. Benitez⁷⁶, D. P. Benjamin⁶, M. Benoit⁵³, J. R. Bensinger²⁶, S. Bentvelsen¹¹⁹, L. Beresford¹³⁴, M. Beretta⁵⁰, D. Berge⁴⁵, E. Bergeas Kuutmann¹⁷¹, N. Berger⁵, B. Bergmann¹⁴¹, L. J. Bergsten²⁶, J. Beringer¹⁸, S. Berlendis⁷, N. R. Bernard¹⁰¹,

G. Bernardi¹³⁵, C. Bernius¹⁵², F. U. Bernlochner²⁴, T. Berry⁹², P. Berta⁹⁸, C. Bertella^{15a}, G. Bertoli^{44a,44b}, I. A. Bertram⁸⁸, G. J. Besjes⁴⁰, O. Bessidskaia Bylund¹⁸¹, M. Bessner⁴⁵, N. Besson¹⁴⁴, A. Bethani⁹⁹, S. Bethke¹¹⁴, A. Betti²⁴, A. J. Bevan⁹¹, J. Beyer¹¹⁴, R. Bi¹³⁸, R. M. Bianchi¹³⁸, O. Biebel¹¹³, D. Biedermann¹⁹, R. Bielski³⁶, K. Bierwagen⁹⁸, N. V. Biesuz^{70a,70b}, M. Biglietti^{73a}, T. R. V. Billoud¹⁰⁸, M. Bindi⁵², A. Bingul^{12d}, C. Bini^{71a,71b}, S. Biondi^{23a,23b}, M. Birman¹⁷⁹, T. Bisanz⁵², J. P. Biswal¹⁶⁰, C. Bittrich⁴⁷, D. M. Bjerggaard⁴⁸, J. E. Black¹⁵², K. M. Black²⁵, T. Blazek^{28a}, I. Bloch⁴⁵, C. Blocker²⁶, A. Blue⁵⁶, U. Blumenschein⁹¹, Dr. Blunier^{146a}, G. J. Bobbink¹¹⁹, V. S. Bobrovnikov^{121a,121b}, S. S. Bocchetta⁹⁵, A. Bocci⁴⁸, D. Boerner¹⁸¹, D. Bogavac¹¹³, A. G. Bogdanchikov^{121a,121b}, C. Bohm^{44a}, V. Boisvert⁹², P. Bokan^{52,171}, T. Bold^{82a}, A. S. Boldyrev¹¹², A. E. Bolz^{60b}, M. Bomben¹³⁵, M. Bona⁹¹, J. S. Bonilla¹³⁰, M. Boonekamp¹⁴⁴, H. M. Borecka-Bielska⁸⁹, A. Borisov¹²², G. Borissov⁸⁸, J. Bortfeldt³⁶, D. Bortoletto¹³⁴, V. Bortolotto^{72a,72b}, D. Boscherini^{23b}, M. Bosman¹⁴, J. D. Bossio Sola³⁰, K. Bouaouda^{35a}, J. Boudreau¹³⁸, E. V. Bouhova-Thacker⁸⁸, D. Boumediene³⁸, C. Bourdarios¹³¹, S. K. Boutle⁵⁶, A. Boveia¹²⁵, J. Boyd³⁶, D. Boye^{33b}, I. R. Boyko⁷⁸, A. J. Bozson⁹², J. Bracinik²¹, N. Brahimi¹⁰⁰, A. Brandt⁸, G. Brandt¹⁸¹, O. Brandt^{60a}, F. Braren⁴⁵, U. Bratzler¹⁶³, B. Brau¹⁰¹, J. E. Brau¹³⁰, W. D. Breaden Madden⁵⁶, K. Brendlinger⁴⁵, L. Brenner⁴⁵, R. Brenner¹⁷¹, S. Bressler¹⁷⁹, B. Brickwedde⁹⁸, D. L. Briglin²¹, D. Britton⁵⁶, D. Britzger¹¹⁴, I. Brock²⁴, R. Brock¹⁰⁵, G. Brooijmans³⁹, T. Brooks⁹², W. K. Brooks^{146b}, E. Brost¹²⁰, J. H. Broughton²¹, P. A. Bruckman de Renstrom⁸³, D. Bruncko^{28b}, A. Bruni^{23b}, G. Bruni^{23b}, L. S. Bruni¹¹⁹, S. Bruno^{72a,72b}, B.H. Brunt³², M. Bruschi^{23b}, N. Brusino¹³⁸, P. Bryant³⁷, L. Bryngemark⁹⁵, T. Buanes¹⁷, Q. Buat³⁶, P. Buchholz¹⁵⁰, A. G. Buckley⁵⁶, I. A. Budagov⁷⁸, M. K. Bugge¹³³, F. Bühner⁵¹, O. Bulekov¹¹¹, D. Bullock⁸, T. J. Burch¹²⁰, S. Burdin⁸⁹, C. D. Burgard¹¹⁹, A. M. Burger⁵, B. Burghgrave⁸, K. Burka⁸³, S. Burke¹⁴³, I. Burmeister⁴⁶, J. T. P. Burr¹³⁴, V. Büscher⁹⁸, E. Buschmann⁵², P. J. Bussey⁵⁶, J. M. Butler²⁵, C. M. Buttar⁵⁶, J. M. Butterworth⁹³, P. Butti³⁶, W. Buttinger³⁶, A. Buzatu¹⁵⁷, A. R. Buzykaev^{121a,121b}, G. Cabras^{23a,23b}, S. Cabrera Urbán¹⁷³, D. Caforio¹⁴¹, H. Cai¹⁷², V. M. M. Cairo², O. Cakir^{4a}, N. Calace³⁶, P. Calafiura¹⁸, A. Calandri¹⁰⁰, G. Calderini¹³⁵, P. Calfayan⁶⁴, G. Callea⁵⁶, L. P. Caloba^{79b}, S. Calvente Lopez⁹⁷, D. Calvet³⁸, S. Calvet³⁸, T. P. Calvet¹⁵⁴, M. Calvetti^{70a,70b}, R. Camacho Toro¹³⁵, S. Camarda³⁶, D. Camarero Munoz⁹⁷, P. Camarri^{72a,72b}, D. Cameron¹³³, R. Caminal Armadans¹⁰¹, C. Camincher³⁶, S. Campana³⁶, M. Campanelli⁹³, A. Camplani⁴⁰, A. Campoverde¹⁵⁰, V. Canale^{68a,68b}, M. Cano Bret^{59c}, J. Cantero¹²⁸, T. Cao¹⁶⁰, Y. Cao¹⁵⁰, M. D. M. Capeans Garrido³⁶, I. Caprini^{27b}, M. Caprini^{27b}, M. Capua^{41a,41b}, R. M. Carbone³⁹, R. Cardarelli^{72a}, F. C. Cardillo¹⁴⁸, I. Carli¹⁴², T. Carli³⁶, G. Carlino^{68a}, B. T. Carlson¹³⁸, L. Carminati^{67a,67b}, R. M. D. Carney^{44a,44b}, S. Caron¹¹⁸, E. Carquin^{146b}, S. Carrá^{67a,67b}, J. W. S. Carter¹⁶⁶, D. Casadei^{33b}, M. P. Casado^{14,f}, A. F. Casha¹⁶⁶, D. W. Casper¹⁷⁰, R. Castelijin¹¹⁹, F. L. Castillo¹⁷³, V. Castillo Gimenez¹⁷³, N. F. Castro^{139a,139e}, A. Catinaccio³⁶, J. R. Catmore¹³³, A. Cattai³⁶, J. Caudron²⁴, V. Cavaliere²⁹, E. Cavallaro¹⁴, D. Cavalli^{67a}, M. Cavalli-Sforza¹⁴, V. Cavasinni^{70a,70b}, E. Celebi^{12b}, F. Ceradini^{73a,73b}, L. Cerda Alberich¹⁷³, A. S. Cerqueira^{79a}, A. Cerri¹⁵⁵, L. Cerrito^{72a,72b}, F. Cerutti¹⁸, A. Cervelli^{23a,23b}, S. A. Cetin^{12b}, A. Chafaq^{35a}, D. Chakraborty¹²⁰, S. K. Chan⁵⁸, W. S. Chan¹¹⁹, Y. L. Chan⁸⁹, J. D. Chapman³², B. Chargeishvili^{158b}, D. G. Charlton²¹, C. C. Chau³⁴, C. A. Chavez Barajas¹⁵⁵, S. Che¹²⁵, A. Chegwidan¹⁰⁵, S. Chekanov⁶, S. V. Chekulaev^{167a}, G. A. Chelkov^{78,at}, M. A. Chelstowska³⁶, C. Chen^{59a}, C. H. Chen⁷⁷, H. Chen²⁹, J. Chen^{59a}, J. Chen³⁹, S. Chen¹³⁶, S. J. Chen^{15c}, X. Chen^{15b,as}, Y. Chen⁸¹, Y.-H. Chen⁴⁵, H. C. Cheng^{62a}, H. J. Cheng^{15a,15d}, A. Cheplakov⁷⁸, E. Cheremushkina¹²², R. Cherkaoui El Moursli^{35e}, E. Cheu⁷, K. Cheung⁶³, T. J. A. Chevalérias¹⁴⁴, L. Chevalier¹⁴⁴, V. Chiarella⁵⁰, G. Chiarelli^{70a}, G. Chiodini^{66a}, A. S. Chisholm^{21,36}, A. Chitan^{27b}, I. Chiu¹⁶², Y. H. Chiu¹⁷⁵, M. V. Chizhov⁷⁸, K. Choi⁶⁴, A. R. Chomont¹³¹, S. Chouridou¹⁶¹, Y. S. Chow¹¹⁹, V. Christodoulou⁹³, M. C. Chu^{62a}, J. Chudoba¹⁴⁰, A. J. Chuinard¹⁰², J. J. Chwastowski⁸³, L. Chytka¹²⁹, D. Cinca⁴⁶, V. Cindro⁹⁰, I. A. Cioară²⁴, A. Ciocio¹⁸, F. Ciroto^{68a,68b}, Z. H. Citron¹⁷⁹, M. Citterio^{67a}, A. Clark⁵³, M. R. Clark³⁹, P. J. Clark⁴⁹, C. Clement^{44a,44b}, Y. Coadou¹⁰⁰, M. Cobal^{65a,65c}, A. Coccaro^{54b}, J. Cochran⁷⁷, H. Cohen¹⁶⁰, A. E. C. Coimbra¹⁷⁹, L. Colasurdo¹¹⁸, B. Cole³⁹, A. P. Colijn¹¹⁹, J. Collot⁵⁷, P. Conde Muiño^{139a}, E. Coniavitis⁵¹, S. H. Connell^{33b}, I. A. Connelly⁹⁹, S. Constantinescu^{27b}, F. Conventi^{68a,aw}, A. M. Cooper-Sarkar¹³⁴, F. Cormier¹⁷⁴, K. J. R. Cormier¹⁶⁶, L. D. Corpe⁹³, M. Corradi^{71a,71b}, E. E. Corrigan⁹⁵, F. Corriveau^{102,ad}, A. Cortes-Gonzalez³⁶, M. J. Costa¹⁷³, F. Costanza⁵, D. Costanzo¹⁴⁸, G. Cottin³², G. Cowan⁹², J. W. Cowley³², B. E. Cox⁹⁹, J. Crane⁹⁹, K. Cranmer¹²³, S. J. Crawley⁵⁶, R. A. Creager¹³⁶, G. Cree³⁴, S. Crépe-Renaudin⁵⁷, F. Crescioli¹³⁵, M. Cristinziani²⁴, V. Croft¹²³, G. Crosetti^{41a,41b}, A. Cueto⁹⁷, T. Cuhadar Donszelmann¹⁴⁸, A. R. Cukierman¹⁵², S. Czekierda⁸³, P. Czodrowski³⁶, M. J. Da Cunha Sargedas De Sousa^{59b}, C. Da Via⁹⁹, W. Dabrowski^{82a}, T. Dado^{28a,x}, S. Dahbi^{35e}, T. Dai¹⁰⁴, F. Dallaire¹⁰⁸, C. Dallapiccola¹⁰¹, M. Dam⁴⁰, G. D'amen^{23a,23b}, J. Damp⁹⁸, J. R. Dandoy¹³⁶, M. F. Daneri³⁰, N. P. Dang^{180,i}, N. D. Dann⁹⁹, M. Danninger¹⁷⁴, V. Dao³⁶, G. Darbo^{54b}, S. Darmora⁸, O. Dartsis⁵, A. Dattagupta¹³⁰, T. Daubney⁴⁵, S. D'Auria^{67a,67b}, W. Davey²⁴, C. David⁴⁵, T. Davidek¹⁴², D. R. Davis⁴⁸, E. Dawe¹⁰³, I. Dawson¹⁴⁸, K. De⁸, R. De Asmundis^{68a}, A. De Benedetti¹²⁷, M. De Beurs¹¹⁹, S. De Castro^{23a,23b}, S. De Cecco^{71a,71b}, N. De Groot¹¹⁸, P. de Jong¹¹⁹, H. De la Torre¹⁰⁵, F. De Lorenzi⁷⁷, A. De Maria^{70a,70b}, D. De Pedis^{71a}, A. De Salvo^{71a}, U. De Sanctis^{72a,72b}, M. De Santis^{72a,72b}, A. De Santo¹⁵⁵, K. De Vasconcelos Corga¹⁰⁰, J. B. De Vivie De Regie¹³¹, C. Debenedetti¹⁴⁵

D. V. Dedovich⁷⁸, N. Dehghanian³, A. M. Deiana⁴², M. Del Gaudio^{41a,41b}, J. Del Peso⁹⁷, Y. Delabat Diaz⁴⁵, D. Delgove¹³¹, F. Deliot¹⁴⁴, C. M. Delitzsch⁷, M. Della Pietra^{68a,68b}, D. Della Volpe⁵³, A. Dell'Acqua³⁶, L. Dell'Asta²⁵, M. Delmastro⁵, C. Delporte¹³¹, P. A. Delsart⁵⁷, D. A. DeMarco¹⁶⁶, S. Demers¹⁸², M. Demichev⁷⁸, S. P. Denisov¹²², D. Denysiuk¹¹⁹, L. D'Eramo¹³⁵, D. Derendarz⁸³, J. E. Derkaoui^{35d}, F. Derue¹³⁵, P. Dervan⁸⁹, K. Desch²⁴, C. Deterre⁴⁵, K. Dette¹⁶⁶, M. R. Devesa³⁰, P. O. Deviveiros³⁶, A. Dewhurst¹⁴³, S. Dhaliwal²⁶, F. A. Di Bello⁵³, A. Di Ciaccio^{72a,72b}, L. Di Ciaccio⁵, W. K. Di Clemente¹³⁶, C. Di Donato^{68a,68b}, A. Di Girolamo³⁶, G. Di Gregorio^{70a,70b}, B. Di Micco^{73a,73b}, R. Di Nardo¹⁰¹, K. F. Di Petrillo⁵⁸, R. Di Sipio¹⁶⁶, D. Di Valentino³⁴, C. Diaconu¹⁰⁰, M. Diamond¹⁶⁶, F. A. Dias⁴⁰, T. Dias Do Vale^{139a}, M. A. Diaz^{146a}, J. Dickinson¹⁸, E. B. Diehl¹⁰⁴, J. Dietrich¹⁹, S. Díez Cornell⁴⁵, A. Dimitrievska¹⁸, J. Dingfelder²⁴, F. Dittus³⁶, F. Djama¹⁰⁰, T. Djobava^{158b}, J. I. Djuvsland¹⁷, M. A. B. Do Vale^{79c}, M. Dobre^{27b}, D. Dodsworth²⁶, C. Doglioni⁹⁵, J. Dolejsi¹⁴², Z. Dolezal¹⁴², M. Donadelli^{79d}, J. Donini³⁸, A. D'onofrio⁹¹, M. D'Onofrio⁸⁹, J. Dopke¹⁴³, A. Doria^{68a}, M. T. Dova⁸⁷, A. T. Doyle⁵⁶, E. Drechsler¹⁵¹, E. Dreyer¹⁵¹, T. Dreyer⁵², Y. Du^{59b}, F. Dubinin¹⁰⁹, M. Dubovsky^{28a}, A. Dubreuil⁵³, E. Duchovni¹⁷⁹, G. Duckeck¹¹³, A. Ducourthial¹³⁵, O. A. Ducu^{108,w}, D. Duda¹¹⁴, A. Dudarev³⁶, A. C. Dudder⁹⁸, E. M. Duffield¹⁸, L. Duflot¹³¹, M. Dührssen³⁶, C. Dülsen¹⁸¹, M. Dumancic¹⁷⁹, A. E. Dumitriu^{27b,d}, A. K. Duncan⁵⁶, M. Dunford^{60a}, A. Duperrin¹⁰⁰, H. Duran Yildiz^{4a}, M. Düren⁵⁵, A. Durglishvili^{158b}, D. Duschinger⁴⁷, B. Dutta⁴⁵, D. Duvnjak¹, G. I. Dyckes¹³⁶, M. Dyndal⁴⁵, S. Dysch⁹⁹, B. S. Dziedzic⁸³, K. M. Ecker¹¹⁴, R. C. Edgar¹⁰⁴, T. Eifert³⁶, G. Eigen¹⁷, K. Einsweiler¹⁸, T. Ekelof¹⁷¹, M. El Kacimi^{35c}, R. El Kosseifi¹⁰⁰, V. Ellajosyula¹⁰⁰, M. Ellert¹⁷¹, F. Ellinghaus¹⁸¹, A. A. Elliot⁹¹, N. Ellis³⁶, J. Elmsheuser²⁹, M. Elsing³⁶, D. Emelianov¹⁴³, A. Emerman³⁹, Y. Enari¹⁶², J. S. Ennis¹⁷⁷, M. B. Epland⁴⁸, J. Erdmann⁴⁶, A. Ereditato²⁰, S. Errede¹⁷², M. Escalier¹³¹, C. Escobar¹⁷³, O. Estrada Pastor¹⁷³, A. I. Etienne¹⁴⁴, E. Etzion¹⁶⁰, H. Evans⁶⁴, A. Ezhilov¹³⁷, M. Ezzi^{35e}, F. Fabbri⁵⁶, L. Fabbri^{23a,23b}, V. Fabiani¹¹⁸, G. Facini⁹³, R. M. Faisca Rodrigues Pereira^{139a}, R. M. Fakhruddinov¹²², S. Falciano^{71a}, P. J. Falke⁵, S. Falke⁵, J. Faltova¹⁴², Y. Fang^{15a}, M. Fanti^{67a,67b}, A. Farbin⁸, A. Farilla^{73a}, E. M. Farina^{69a,69b}, T. Farooque¹⁰⁵, S. Farrell¹⁸, S. M. Farrington¹⁷⁷, P. Farthouat³⁶, F. Fassi^{35e}, P. Fassnacht³⁶, D. Fassouliotis⁹, M. Fauci Giannelli⁴⁹, W. J. Fawcett³², L. Fayard¹³¹, O. L. Fedin^{137,o}, W. Fedorko¹⁷⁴, M. Feickert⁴², S. Feigl¹³³, L. Feligioni¹⁰⁰, C. Feng^{59b}, E. J. Feng³⁶, M. Feng⁴⁸, M. J. Fenton⁵⁶, A. B. Fenyuk¹²², J. Ferrando⁴⁵, A. Ferrari¹⁷¹, P. Ferrari¹¹⁹, R. Ferrari^{69a}, D. E. Ferreira de Lima^{60b}, A. Ferrer¹⁷³, D. Ferrere⁵³, C. Ferretti¹⁰⁴, F. Fiedler⁹⁸, A. Filipčić⁹⁰, F. Filthaut¹¹⁸, K. D. Finelli²⁵, M. C. N. Fiolhais^{139a,139c,a}, L. Fiorini¹⁷³, C. Fischer¹⁴, W. C. Fisher¹⁰⁵, N. Flaschel⁴⁵, I. Fleck¹⁵⁰, P. Fleischmann¹⁰⁴, R. R. M. Fletcher¹³⁶, T. Flick¹⁸¹, B. M. Flierl¹¹³, L. M. Flores¹³⁶, L. R. Flores Castillo^{62a}, F. M. Follega^{74a,74b}, N. Fomin¹⁷, G. T. Forcolin^{74a,74b}, A. Formica¹⁴⁴, F. A. Förster¹⁴, A. C. Forti⁹⁹, A. G. Foster²¹, D. Fournier¹³¹, H. Fox⁸⁸, S. Fracchia¹⁴⁸, P. Francavilla^{70a,70b}, M. Franchini^{23a,23b}, S. Franchino^{60a}, D. Francis³⁶, L. Franconi¹⁴⁵, M. Franklin⁵⁸, M. Frate¹⁷⁰, A. N. Fray⁹¹, D. Freeborn⁹³, B. Freund¹⁰⁸, W. S. Freund^{79b}, E. M. Freundlich⁴⁶, D. C. Frizzell¹²⁷, D. Froidevaux³⁶, J. A. Frost¹³⁴, C. Fukunaga¹⁶³, E. Fullana Torregrosa¹⁷³, E. Fumagalli^{54a,54b}, T. Fusayasu¹¹⁵, J. Fuster¹⁷³, O. Gabizon¹⁵⁹, A. Gabrielli^{23a,23b}, A. Gabrielli¹⁸, G. P. Gach^{82a}, S. Gadatsch⁵³, P. Gadow¹¹⁴, G. Gagliardi^{54a,54b}, L. G. Gagnon¹⁰⁸, C. Galea^{27b}, B. Galhardo^{139a,139c}, E. J. Gallas¹³⁴, B. J. Gallop¹⁴³, P. Gallus¹⁴¹, G. Galster⁴⁰, R. Gamboa Goni⁹¹, K. K. Gan¹²⁵, S. Ganguly¹⁷⁹, J. Gao^{59a}, Y. Gao⁸⁹, Y. S. Gao^{31,1}, C. García¹⁷³, J. E. García Navarro¹⁷³, J. A. García Pascual^{15a}, C. Garcia-Argos⁵¹, M. Garcia-Sciveres¹⁸, R. W. Gardner³⁷, N. Garelli¹⁵², S. Gargiulo⁵¹, V. Garonne¹³³, K. Gasnikova⁴⁵, A. Gaudiello^{54a,54b}, G. Gaudio^{69a}, I. L. Gavrilenko¹⁰⁹, A. Gavrilyuk¹¹⁰, C. Gay¹⁷⁴, G. Gaycken²⁴, E. N. Gazis¹⁰, C. N. P. Gee¹⁴³, J. Geisen⁵², M. Geisen⁹⁸, M. P. Geisler^{60a}, C. Gemme^{54b}, M. H. Genest⁵⁷, C. Geng¹⁰⁴, S. Gentile^{71a,71b}, S. George⁹², D. Gerbaudo¹⁴, G. Gessner⁴⁶, S. Ghasemi¹⁵⁰, M. Ghasemi Bostanabad¹⁷⁵, M. Ghneimat²⁴, B. Giacobbe^{23b}, S. Giagu^{71a,71b}, N. Giangiacomi^{23a,23b}, P. Giannetti^{70a}, A. Giannini^{68a,68b}, S. M. Gibson⁹², M. Gignac¹⁴⁵, D. Gillberg³⁴, G. Gilles¹⁸¹, D. M. Gingrich^{3,au}, M. P. Giordani^{65a,65c}, F. M. Giorgi^{23b}, P. F. Giraud¹⁴⁴, P. Giromini⁵⁸, G. Giugliarelli^{65a,65c}, D. Giugni^{67a}, F. Giulì¹³⁴, M. Giulini^{60b}, S. Gkaitatzis¹⁶¹, I. Gkialas^{9,h}, E. L. Gkougkousis¹⁴, P. Gkoutoumis¹⁰, L. K. Gladilin¹¹², C. Glasman⁹⁷, J. Glatzer¹⁴, P. C. F. Glaysher⁴⁵, A. Glazov⁴⁵, M. Goblirsch-Kolb²⁶, J. Godlewski⁸³, S. Goldfarb¹⁰³, T. Golling⁵³, D. Golubkov¹²², A. Gomes^{139a,139b}, R. Goncalves Gama⁵², R. Gonçalo^{139a}, G. Gonella⁵¹, L. Gonella²¹, A. Gongadze⁷⁸, F. Gonnella²¹, J. L. Gonski⁵⁸, S. González de la Hoz¹⁷³, S. Gonzalez-Sevilla⁵³, L. Goossens³⁶, P. A. Gorbounov¹¹⁰, H. A. Gordon²⁹, B. Gorini³⁶, E. Gorini^{66a,66b}, A. Gorišek⁹⁰, A. T. Goshaw⁴⁸, C. Gössling⁴⁶, M. I. Gostkin⁷⁸, C. A. Gottardo²⁴, C. R. Goudet¹³¹, D. Goujdami^{35c}, A. G. Goussiou¹⁴⁷, N. Govender^{33b,c}, C. Goy⁵, E. Gozani¹⁵⁹, I. Grabowska-Bold^{82a}, P. O. J. Gradin¹⁷¹, E. C. Graham⁸⁹, J. Gramling¹⁷⁰, E. Gramstad¹³³, S. Grancagnolo¹⁹, V. Gratchev¹³⁷, P. M. Gravila^{27f}, F. G. Gravili^{66a,66b}, C. Gray⁵⁶, H. M. Gray¹⁸, Z. D. Greenwood⁹⁴, C. Grefe²⁴, K. Gregersen⁹⁵, I. M. Gregor⁴⁵, P. Grenier¹⁵², K. Grevtsov⁴⁵, N. A. Grieser¹²⁷, J. Griffiths⁸, A. A. Grillo¹⁴⁵, K. Grimm^{31,k}, S. Grinstein^{14,y}, Ph. Gris³⁸, J.-F. Grivaz¹³¹, S. Groh⁹⁸, E. Gross¹⁷⁹, J. Grosse-Knetter⁵², G. C. Grossi⁹⁴, Z. J. Grout⁹³, C. Grud¹⁰⁴, A. Grummer¹¹⁷, L. Guan¹⁰⁴, W. Guan¹⁸⁰, J. Guenther³⁶, A. Guerguichon¹³¹, F. Guescini^{167a}, D. Guest¹⁷⁰, R. Gugel⁵¹, B. Gui¹²⁵, T. Guillemin⁵, S. Guindon³⁶, U. Gul⁵⁶, J. Guo^{59c}, W. Guo¹⁰⁴, Y. Guo^{59a,r}, Z. Guo¹⁰⁰, R. Gupta⁴⁵, S. Gurbuz^{12c}, G. Gustavino¹²⁷,

P. Gutierrez¹²⁷, C. Gutsche⁹³, C. Guyot¹⁴⁴, M. P. Guzik^{82a}, C. Gwenlan¹³⁴, C. B. Gwilliam⁸⁹, A. Haas¹²³, C. Haber¹⁸, H. K. Hadavand⁸, N. Haddad^{35c}, A. Hadeef^{59a}, S. Hageböck²⁴, M. Hagihara¹⁶⁸, M. Haleem¹⁷⁶, J. Haley¹²⁸, G. Halladjian¹⁰⁵, G. D. Hallewell¹⁰⁰, K. Hamacher¹⁸¹, P. Hamal¹²⁹, K. Hamano¹⁷⁵, A. Hamilton^{33a}, G. N. Hamity¹⁴⁸, K. Han^{59a,aj}, L. Han^{59a}, S. Han^{15a,15d}, K. Hanagaki^{80,u}, M. Hance¹⁴⁵, D. M. Handl¹¹³, B. Haney¹³⁶, R. Hankache¹³⁵, P. Hanke^{60a}, E. Hansen⁹⁵, J. B. Hansen⁴⁰, J. D. Hansen⁴⁰, M. C. Hansen²⁴, P. H. Hansen⁴⁰, E. C. Hanson⁹⁹, K. Hara¹⁶⁸, A. S. Hard¹⁸⁰, T. Harenberg¹⁸¹, S. Harkusha¹⁰⁶, P. F. Harrison¹⁷⁷, N. M. Hartmann¹¹³, Y. Hasegawa¹⁴⁹, A. Hasib⁴⁹, S. Hassani¹⁴⁴, S. Haug²⁰, R. Hauser¹⁰⁴, L. Hauswald⁴⁷, L. B. Havener³⁹, M. Havranek¹⁴¹, C. M. Hawkes²¹, R. J. Hawkings³⁶, D. Hayden¹⁰⁵, C. Hayes¹⁵⁴, C. P. Hays¹³⁴, J. M. Hays⁹¹, H. S. Hayward⁸⁹, S. J. Haywood¹⁴³, F. He^{59a}, M. P. Heath⁴⁹, V. Hedberg⁹⁵, L. Heelan⁸, S. Heer²⁴, K. K. Heidegger⁵¹, J. Heilman³⁴, S. Heim⁴⁵, T. Heim¹⁸, B. Heinemann^{45,ap}, J. J. Heinrich¹¹³, L. Heinrich¹²³, C. Heinz⁵⁵, J. Hejbal¹⁴⁰, L. Helary³⁶, A. Held¹⁷⁴, S. Hellesund¹³³, C. M. Helling¹⁴⁵, S. Hellman^{44a,44b}, C. Helsens³⁶, R. C. W. Henderson⁸⁸, Y. Heng¹⁸⁰, S. Henkelmann¹⁷⁴, A. M. Henriques Correia³⁶, G. H. Herbert¹⁹, H. Herde²⁶, V. Herget¹⁷⁶, Y. Hernández Jiménez^{33c}, H. Herr⁹⁸, M. G. Herrmann¹¹³, T. Herrmann⁴⁷, G. Herten⁵¹, R. Hertenberger¹¹³, L. Hervas³⁶, T. C. Herwig¹³⁶, G. G. Hesketh⁹³, N. P. Hessey^{167a}, A. Higashida¹⁶², S. Higashino⁸⁰, E. Higón-Rodríguez¹⁷³, K. Hildebrand³⁷, E. Hill¹⁷⁵, J. C. Hill³², K. K. Hill²⁹, K. H. Hiller⁴⁵, S. J. Hillier²¹, M. Hils⁴⁷, I. Hinchliffe¹⁸, F. Hinterkeuser²⁴, M. Hirose¹³², D. Hirschbuehl¹⁸¹, B. Hiti⁹⁰, O. Hladik¹⁴⁰, D. R. Hlaluku^{33c}, X. Hoad⁴⁹, J. Hobbs¹⁵⁴, N. Hod^{167a}, M. C. Hodgkinson¹⁴⁸, A. Hoecker³⁶, M. R. Hoefkamp¹¹⁷, F. Hoenig¹¹³, D. Hohn⁵¹, D. Hohov¹³¹, T. R. Holmes³⁷, M. Holzbock¹¹³, M. Homann⁴⁶, L. B. A. H. Hommels³², S. Honda¹⁶⁸, T. Honda⁸⁰, T. M. Hong¹³⁸, A. Höhle¹¹⁴, B. H. Hooberman¹⁷², W. H. Hopkins¹³⁰, Y. Horii¹¹⁶, P. Horn⁴⁷, A. J. Horton¹⁵¹, L. A. Horyn³⁷, J.-Y. Hostachy⁵⁷, A. Hostiuc¹⁴⁷, S. Hou¹⁵⁷, A. Houmada^{35a}, J. Howarth⁹⁹, J. Hoya⁸⁷, M. Hrabovsky¹²⁹, J. Hrdinka³⁶, I. Hristova¹⁹, J. Hrivnac¹³¹, A. Hrynevich¹⁰⁷, T. Hryn'ova⁵, P. J. Hsu⁶³, S.-C. Hsu¹⁴⁷, Q. Hu²⁹, S. Hu^{59c}, Y. Huang^{15a}, Z. Hubacek¹⁴¹, F. Hubaut¹⁰⁰, M. Huebner²⁴, F. Huegging²⁴, T. B. Huffman¹³⁴, M. Huhtinen³⁶, R. F. H. Hunter³⁴, P. Huo¹⁵⁴, A. M. Hupe³⁴, N. Huseynov^{78,af}, J. Huston¹⁰⁵, J. Huth⁵⁸, R. Hyneman¹⁰⁴, G. Iacobucci⁵³, G. Iakovidis²⁹, I. Ibragimov¹⁵⁰, L. Iconomidou-Fayard¹³¹, Z. Idrissi^{35e}, P. I. Iengo³⁶, R. Ignazzi⁴⁰, O. Igonkina^{119,aa}, R. Iguchi¹⁶², T. Iizawa⁵³, Y. Ikegami⁸⁰, M. Ikeno⁸⁰, D. Iliadis¹⁶¹, N. Ilic¹¹⁸, F. Iltzsche⁴⁷, G. Introzzi^{69a,69b}, M. Iodice^{73a}, K. Iordanidou³⁹, V. Ippolito^{71a,71b}, M. F. Isacson¹⁷¹, N. Ishijima¹³², M. Ishino¹⁶², M. Ishitsuka¹⁶⁴, W. Islam¹²⁸, C. Issever¹³⁴, S. Istin¹⁵⁹, F. Ito¹⁶⁸, J. M. Iturbe Ponce^{62a}, R. Iuppa^{74a,74b}, A. Ivina¹⁷⁹, H. Iwasaki⁸⁰, J. M. Izen⁴³, V. Izzo^{68a}, P. Jacka¹⁴⁰, P. Jackson¹, R. M. Jacobs²⁴, V. Jain², G. Jäkel¹⁸¹, K. B. Jakobi⁹⁸, K. Jakobs⁵¹, S. Jakobsen⁷⁵, T. Jakoubek¹⁴⁰, D. O. Jamin¹²⁸, R. Jansky⁵³, J. Janssen²⁴, M. Janus⁵², P. A. Janus^{82a}, G. Jarlskog⁹⁵, N. Javadov^{78,af}, T. Javůrek³⁶, M. Javurkova⁵¹, F. Jeanneau¹⁴⁴, L. Jeanty¹⁸, J. Jeljela^{158a,ag}, A. Jelinskas¹⁷⁷, P. Jenni^{51,c}, J. Jeong⁴⁵, N. Jeong⁴⁵, S. Jézéquel⁵, H. Ji¹⁸⁰, J. Jia¹⁵⁴, H. Jiang⁷⁷, Y. Jiang^{59a}, Z. Jiang^{152,p}, S. Jiggins⁵¹, F. A. Jimenez Morales³⁸, J. Jimenez Pena¹⁷³, S. Jin^{15c}, A. Jinaru^{27b}, O. Jinnouchi¹⁶⁴, H. Jivan^{33c}, P. Johansson¹⁴⁸, K. A. Johns⁷, C. A. Johnson⁶⁴, K. Jon-And^{44a,44b}, R. W. L. Jones⁸⁸, S. D. Jones¹⁵⁵, S. Jones⁷, T. J. Jones⁸⁹, J. Jongmanns^{60a}, P. M. Jorge^{139a,139b}, J. Jovicevic^{167a}, X. Ju¹⁸, J. J. Junggeburth¹¹⁴, A. Juste Rozas^{14,y}, A. Kaczmarska⁸², M. Kado¹³¹, H. Kagan¹²⁵, M. Kagan¹⁵², T. Kaji¹⁷⁸, E. Kajomovitz¹⁵⁹, C. W. Kalderon⁹⁵, A. Kaluza⁹⁸, S. Kama⁴², A. Kamenshchikov¹²², L. Kanjir⁹⁰, Y. Kano¹⁶², V. A. Kantserov¹¹¹, J. Kanzaki⁸⁰, L. S. Kaplan¹⁸⁰, D. Kar^{33c}, M. J. Kareem^{167b}, E. Karentzos¹⁰, S. N. Karpov⁷⁸, Z. M. Karpova⁷⁸, V. Kartvelishvili⁸⁸, A. N. Karyukhin¹²², L. Kashif¹⁸⁰, R. D. Kass¹²⁵, A. Kastanas^{44a,44b}, Y. Kataoka¹⁶², C. Kato^{59c,59d}, J. Katzy⁴⁵, K. Kawade⁸¹, K. Kawagoe⁸⁶, T. Kawaguchi¹¹⁶, T. Kawamoto¹⁶², G. Kawamura⁵², E. F. Kay⁸⁹, V. F. Kazanin^{121a,121b}, R. Keeler¹⁷⁵, R. Kehoe⁴², J. S. Keller³⁴, E. Kellermann⁹⁵, J. J. Kempster²¹, J. Kendrick²¹, O. Kepka¹⁴⁰, S. Kersten¹⁸¹, B. P. Kerševan⁹⁰, S. Ketabchi Haghighat¹⁶⁶, R. A. Keyes¹⁰², M. Khader¹⁷², F. Khalil-Zada¹³, A. Khanov¹²⁸, A. G. Kharlamov^{121a,121b}, T. Kharlamova^{121a,121b}, E. E. Khoda¹⁷⁴, A. Khodinov¹⁶⁵, T. J. Khoo⁵³, E. Khramov⁷⁸, J. Khubua^{158b}, S. Kido⁸¹, M. Kiehn⁵³, C. R. Kilby⁹², Y. K. Kim³⁷, N. Kimura^{65a,65c}, O. M. Kind¹⁹, B. T. King^{89,*}, D. Kirchmeier⁴⁷, J. Kirk¹⁴³, A. E. Kiryunin¹¹⁴, T. Kishimoto¹⁶², D. Kisielewska^{82a}, V. Kitali⁴⁵, O. Kivernyk⁵, E. Kladiva^{28b,*}, T. Klapdor-Kleingrothaus⁵¹, M. H. Klein¹⁰⁴, M. Klein⁸⁹, U. Klein⁸⁹, K. Kleinknecht⁹⁸, P. Klimek¹²⁰, A. Klimentov²⁹, T. Klingl²⁴, T. Klioutchnikova³⁶, F. F. Klitzner¹¹³, P. Kluit¹¹⁹, S. Kluth¹¹⁴, E. Kneringer⁷⁵, E. B. F. G. Knoop¹⁰⁰, A. Knue⁵¹, A. Kobayashi¹⁶², D. Kobayashi⁸⁶, T. Kobayashi¹⁶², M. Kobel⁴⁷, M. Kocian¹⁵², P. Kodys¹⁴², P. T. Koenig²⁴, T. Koffas³⁴, E. Koffeman¹¹⁹, N. M. Köhler¹¹⁴, T. Koi¹⁵², M. Kolb^{60b}, I. Koletsou⁵, T. Kondo⁸⁰, N. Kondrashova^{59c}, K. Köneke⁵¹, A. C. König¹¹⁸, T. Kono¹²⁴, R. Konoplich^{123,am}, V. Konstantinides⁹³, N. Konstantinidis⁹³, B. Konya⁹⁵, R. Kopeliansky⁶⁴, S. Koperny^{82a}, K. Korcyl⁸³, K. Kordas¹⁶¹, G. Koren¹⁶⁰, A. Korn⁹³, I. Korolkov¹⁴, E. V. Korolkova¹⁴⁸, N. Korotkova¹¹², O. Kortner¹¹⁴, S. Kortner¹¹⁴, T. Kosek¹⁴², V. V. Kostyukhin²⁴, A. Kotwal⁴⁸, A. Koulouris¹⁰, A. Kourkoumeli-Charalampidi^{69a,69b}, C. Kourkoumelis⁹, E. Kourlitis¹⁴⁸, V. Kouskoura²⁹, A. B. Kowalewska⁸³, R. Kowalewski¹⁷⁵, T. Z. Kowalski^{82a}, C. Kozakai¹⁶², W. Kozanecki¹⁴⁴, A. S. Kozhin¹²², V. A. Kramarenko¹¹², G. Kramberger⁹⁰, D. Krasnopevtsev^{59a}, M. W. Krasny¹³⁵, A. Krasznahorkay³⁶, D. Krauss¹¹⁴, J. A. Kremer^{82a}, J. Kretzschmar⁸⁹, P. Krieger¹⁶⁶, K. Krizka¹⁸, K. Kroeninger⁴⁶, H. Kroha¹¹⁴, J. Kroll¹⁴⁰, J. Kroll¹³⁶,

J. Krstic¹⁶, U. Kruchonak⁷⁸, H. Krüger²⁴, N. Krumnack⁷⁷, M. C. Kruse⁴⁸, T. Kubota¹⁰³, S. Kudah^{4b}, J. T. Kuechler¹⁸¹, S. Kuehn³⁶, A. Kugel^{60a}, T. Kuhl⁴⁵, V. Kukhtin⁷⁸, R. Kukla¹⁰⁰, Y. Kulchitsky^{106,ai}, S. Kuleshov^{146b}, Y. P. Kulinich¹⁷², M. Kuna⁵⁷, T. Kunigo⁸⁴, A. Kupco¹⁴⁰, T. Kupfer⁴⁶, O. Kuprash¹⁶⁰, H. Kurashige⁸¹, L. L. Kurchaninov^{167a}, Y. A. Kurochkin¹⁰⁶, A. Kurova¹¹¹, M. G. Kurth^{15a,15d}, E. S. Kuwertz³⁶, M. Kuze¹⁶⁴, J. Kvita¹²⁹, T. Kwan¹⁰², A. La Rosa¹¹⁴, J. L. La Rosa Navarro^{79d}, L. La Rotonda^{41a,41b}, F. La Ruffa^{41a,41b}, C. Lacasta¹⁷³, F. Lacava^{71a,71b}, J. Lacey⁴⁵, D. P. J. Lack⁹⁹, H. Lacker¹⁹, D. Lacour¹³⁵, E. Ladygin⁷⁸, R. Lafaye⁵, B. Laforge¹³⁵, T. Lagouri^{33c}, S. Lai⁵², S. Lammers⁶⁴, W. Lampl⁷, E. Lançon²⁹, U. Landgraf⁵¹, M. P. J. Landon⁹¹, M. C. Lanfermann⁵³, V. S. Lang⁴⁵, J. C. Lange⁵², R. J. Langenberg³⁶, A. J. Lankford¹⁷⁰, F. Lanni²⁹, K. Lantsch²⁴, A. Lanza^{69a}, A. Lapertosa^{54a,54b}, S. Laplace¹³⁵, J. F. Laporte¹⁴⁴, T. Lari^{67a}, F. Lasagni Manghi^{23a,23b}, M. Lassnig³⁶, T. S. Lau^{62a}, A. Laudrain¹³¹, M. Lavorgna^{68a,68b}, M. Lazzaroni^{67a,67b}, B. Le¹⁰³, O. Le Dortz¹³⁵, E. Le Guirriec¹⁰⁰, E. P. Le Quilleuc¹⁴⁴, M. LeBlanc⁷, T. LeCompte⁶, F. Ledroit-Guillon⁵⁷, C. A. Lee²⁹, G. R. Lee^{146a}, L. Lee⁵⁸, S. C. Lee¹⁵⁷, B. Lefebvre¹⁰², M. Lefebvre¹⁷⁵, F. Legger¹¹³, C. Leggett¹⁸, K. Lehmann¹⁵¹, N. Lehmann¹⁸¹, G. Lehmann Miotto³⁶, W. A. Leight⁴⁵, A. Leisos^{161,v}, M. A. L. Leite^{79d}, R. Leitner¹⁴², D. Lellouch^{179,*}, K. J. C. Leney⁹³, T. Lenz²⁴, B. Lenzi³⁶, R. Leone⁷, S. Leone^{70a}, C. Leonidopoulos⁴⁹, G. Lerner¹⁵⁵, C. Leroy¹⁰⁸, R. Les¹⁶⁶, A. A. J. Lesage¹⁴⁴, C. G. Lester³², M. Levchenko¹³⁷, J. Levêque⁵, D. Levin¹⁰⁴, L. J. Levinson¹⁷⁹, D. Lewis⁹¹, B. Li^{15b}, B. Li¹⁰⁴, C.-Q. Li^{59a,al}, H. Li^{59a}, H. Li^{59b}, K. Li¹⁵², L. Li^{59c}, M. Li^{15a}, Q. Li^{15a,15d}, Q. Y. Li^{59a}, S. Li^{59c,59d}, X. Li^{59c}, Y. Li¹⁵⁰, Z. Liang^{15a}, B. Liberti^{72a}, A. Liblong¹⁶⁶, K. Lie^{62c}, S. Liem¹¹⁹, A. Limosani¹⁵⁶, C. Y. Lin³², K. Lin¹⁰⁵, T. H. Lin⁹⁸, R. A. Linck⁶⁴, J. H. Lindon²¹, B. E. Lindquist¹⁵⁴, A. L. Lioni⁵³, E. Lipeles¹³⁶, A. Lipniacka¹⁷, M. Lisovyi^{60b}, T. M. Liss^{172,ar}, A. Lister¹⁷⁴, A. M. Litke¹⁴⁵, J. D. Little⁸, B. Liu⁷⁷, B. L. Liu⁶, H. B. Liu²⁹, H. Liu¹⁰⁴, J. B. Liu^{59a}, J. K. K. Liu¹³⁴, K. Liu¹³⁵, M. Liu^{59a}, P. Liu¹⁸, Y. Liu^{15a,15d}, Y. L. Liu^{59a}, Y. W. Liu^{59a}, M. Livan^{69a,69b}, A. Lleres⁵⁷, J. Llorente Merino^{15a}, S. L. Lloyd⁹¹, C. Y. Lo^{62b}, F. Lo Sterzo⁴², E. M. Lobodzinska⁴⁵, P. Loch⁷, T. Lohse¹⁹, K. Lohwasser¹⁴⁸, M. Lokajicek¹⁴⁰, J. D. Long¹⁷², R. E. Long⁸⁸, L. Longo^{66a,66b}, K. A. Looper¹²⁵, J. A. Lopez^{146b}, I. Lopez Paz⁹⁹, A. Lopez Solis¹⁴⁸, J. Lorenz¹¹³, N. Lorenzo Martinez⁵, M. Losada²², P. J. Lösel¹¹³, A. Lösle⁵¹, X. Lou⁴⁵, X. Lou^{15a}, A. Lounis¹³¹, J. Love⁶, P. A. Love⁸⁸, J. J. Lozano Bahilo¹⁷³, H. Lu^{62a}, M. Lu^{59a}, Y. J. Lu⁶³, H. J. Lubatti¹⁴⁷, C. Luci^{71a,71b}, A. Lucotte⁵⁷, C. Luedtke⁵¹, F. Luehring⁶⁴, I. Luise¹³⁵, L. Luminari^{71a}, B. Lund-Jensen¹⁵³, M. S. Lutz¹⁰¹, P. M. Luzzi¹³⁵, D. Lynn²⁹, R. Lysak¹⁴⁰, E. Lytken⁹⁵, F. Lyu^{15a}, V. Lyubushkin⁷⁸, T. Lyubushkina⁷⁸, H. Ma²⁹, L. L. Ma^{59b}, Y. Ma^{59b}, G. Maccarrone⁵⁰, A. Macchiolo¹¹⁴, C. M. Macdonald¹⁴⁸, J. Machado Miguens^{136,139b}, D. Madaffari¹⁷³, R. Madar³⁸, W. F. Mader⁴⁷, N. Madysa⁴⁷, J. Maeda⁸¹, K. Maekawa¹⁶², S. Maeland¹⁷, T. Maeno²⁹, M. Maerker⁴⁷, A. S. Maevskiy¹¹², V. Magerl⁵¹, D. J. Mahon³⁹, C. Maidantchik^{79b}, T. Maier¹¹³, A. Maio^{139a,139b,139d}, O. Majersky^{28a}, S. Majewski¹³⁰, Y. Makida⁸⁰, N. Makovec¹³¹, B. Malaescu¹³⁵, Pa. Malecki⁸³, V. P. Maleev¹³⁷, F. Malek⁵⁷, U. Mallik⁷⁶, D. Malon⁶, C. Malone³², S. Maltezos¹⁰, S. Malyukov³⁶, J. Mamuzic¹⁷³, G. Mancini⁵⁰, I. Mandić⁹⁰, J. Maneira^{139a}, L. Manhaes de Andrade Filho^{79a}, J. Manjarres Ramos⁴⁷, K. H. Mankinen⁹⁵, A. Mann¹¹³, A. Manousos⁷⁵, B. Mansoulie¹⁴⁴, S. Manzoni^{67a,67b}, A. Marantis¹⁶¹, G. Marceca³⁰, L. March⁵³, L. Marchese¹³⁴, G. Marchiori¹³⁵, M. Marcisovsky¹⁴⁰, C. Marcon⁹⁵, C. A. Marin Tobon³⁶, M. Marjanovic³⁸, F. Marroquim^{79b}, Z. Marshall¹⁸, M. U. F. Martensson¹⁷¹, S. Marti-Garcia¹⁷³, C. B. Martin¹²⁵, T. A. Martin¹⁷⁷, V. J. Martin⁴⁹, B. Martin dit Latour¹⁷, M. Martinez^{14,y}, V. I. Martinez Outschoorn¹⁰¹, S. Martin-Haugh¹⁴³, V. S. Martoiu^{27b}, A. C. Martyniuk⁹³, A. Marzin³⁶, L. Masetti⁹⁸, T. Mashimo¹⁶², R. Mashinistov¹⁰⁹, J. Masik⁹⁹, A. L. Maslennikov^{121a,121b}, L. H. Mason¹⁰³, L. Massa^{72a,72b}, P. Massarotti^{68a,68b}, P. Mastrandrea¹⁵⁴, A. Mastroberardino^{41a,41b}, T. Masubuchi¹⁶², P. Mättig²⁴, J. Maurer^{27b}, B. Maček⁹⁰, S. J. Maxfield⁸⁹, D. A. Maximov^{121a,121b}, R. Mazini¹⁵⁷, I. Maznas¹⁶¹, S. M. Mazza¹⁴⁵, S. P. Mc Kee¹⁰⁴, T. G. McCarthy¹¹⁴, L. I. McClymont⁹³, W. P. McCormack¹⁸, E. F. McDonald¹⁰³, J. A. McFayden³⁶, G. Mchedlidze⁵², M. A. McKay⁴², K. D. McLean¹⁷⁵, S. J. McMahan¹⁴³, P. C. McNamara¹⁰³, C. J. McNicol¹⁷⁷, R. A. McPherson^{175,ad}, J. E. Mdhului^{33c}, Z. A. Meadows¹⁰¹, S. Meehan¹⁴⁷, T. Megy⁵¹, S. Mehlhase¹¹³, A. Mehta⁸⁹, T. Meideck⁵⁷, B. Meirose⁴³, D. Melini^{173,av}, B. R. Mellado Garcia^{33c}, J. D. Mellenthin⁵², M. Melo^{28a}, F. Meloni⁴⁵, A. Melzer²⁴, S. B. Menary⁹⁹, E. D. Mendes Gouveia^{139a}, L. Meng⁸⁹, X. T. Meng¹⁰⁴, S. Menke¹¹⁴, E. Meoni^{41a,41b}, S. Mergelmeyer¹⁹, S. A. M. Merkt¹³⁸, C. Merlassino²⁰, P. Mermod⁵³, L. Merola^{68a,68b}, C. Meroni^{67a}, F. S. Merritt³⁷, A. Messina^{71a,71b}, J. Metcalfe⁶, A. S. Mete¹⁷⁰, C. Meyer⁶⁴, J. Meyer¹⁵⁹, J.-P. Meyer¹⁴⁴, H. Meyer Zu Theenhausen^{60a}, F. Miano¹⁵⁵, R. P. Middleton¹⁴³, L. Mijović⁴⁹, G. Mikenberg¹⁷⁹, M. Mikesikova¹⁴⁰, M. Mikuz⁹⁰, M. Milesi¹⁰³, A. Milic¹⁶⁶, D. A. Millar⁹¹, D. W. Miller³⁷, A. Milov¹⁷⁹, D. A. Milstead^{44a,44b}, R. A. Mina^{152,p}, A. A. Minaenko¹²², M. Miñano Moya¹⁷³, I. A. Minashvili^{158b}, A. I. Mincer¹²³, B. Mindur^{82a}, M. Mineev⁷⁸, Y. Minegishi¹⁶², Y. Ming¹⁸⁰, L. M. Mir¹⁴, A. Mirto^{66a,66b}, K. P. Mistry¹³⁶, T. Mitani¹⁷⁸, J. Mitrevski¹¹³, V. A. Mitsou¹⁷³, M. Mittal^{59c}, A. Miucci²⁰, P. S. Miyagawa¹⁴⁸, A. Mizukami⁸⁰, J. U. Mjörnmark⁹⁵, T. Mkrtychyan¹⁸³, M. Mlynarikova¹⁴², T. Moa^{44a,44b}, K. Mochizuki¹⁰⁸, P. Mogg⁵¹, S. Mohapatra³⁹, S. Molander^{44a,44b}, R. Moles-Valls²⁴, M. C. Mondragon¹⁰⁵, K. Mönig⁴⁵, J. Monk⁴⁰, E. Monnier¹⁰⁰, A. Montalbano¹⁵¹, J. Montejo Berlingen³⁶, F. Monticelli⁸⁷, S. Monzani^{67a}, N. Morange¹³¹, D. Moreno²², M. Moreno Llacer³⁶, P. Morettini^{54b}, M. Morgenstern¹¹⁹, S. Morgenstern⁴⁷, D. Mori¹⁵¹, M. Morii⁵⁸, M. Morinaga¹⁷⁸, V. Morisbak¹³³, A. K. Morley³⁶

G. Mornacchi³⁶, A. P. Morris⁹³, J. D. Morris⁹¹, L. Morvaj¹⁵⁴, P. Moschovakos¹⁰, M. Mosidze^{158b}, H. J. Moss¹⁴⁸, J. Moss^{31,m}, K. Motohashi¹⁶⁴, R. Mount¹⁵², E. Mountricha³⁶, E. J. W. Moyses¹⁰¹, S. Muanza¹⁰⁰, F. Mueller¹¹⁴, J. Mueller¹³⁸, R. S. P. Mueller¹¹³, D. Muenstermann⁸⁸, G. A. Mullier⁹⁵, F. J. Munoz Sanchez⁹⁹, P. Murin^{28b}, W. J. Murray^{143,177}, A. Murrone^{67a,67b}, M. Muškinja⁹⁰, C. Mwewa^{33a}, A. G. Myagkov^{122,an}, J. Myers¹³⁰, M. Myska¹⁴¹, B. P. Nachman¹⁸, O. Nackenhorst⁴⁶, K. Nagai¹³⁴, K. Nagano⁸⁰, Y. Nagasaka⁶¹, M. Nagel⁵¹, E. Nagy¹⁰⁰, A. M. Nairz³⁶, Y. Nakahama¹¹⁶, K. Nakamura⁸⁰, T. Nakamura¹⁶², I. Nakano¹²⁶, H. Nanjo¹³², F. Napolitano^{60a}, R. F. Naranjo Garcia⁴⁵, R. Narayan¹¹, D. I. Narrias Villar^{60a}, I. Naryshkin¹³⁷, T. Naumann⁴⁵, G. Navarro²², R. Nayyar⁷, H. A. Neal^{104,*}, P. Y. Nechaeva¹⁰⁹, T. J. Neep¹⁴⁴, A. Negri^{69a,69b}, M. Negrini^{23b}, S. Nektarijevic¹¹⁸, C. Nellist⁵², M. E. Nelson¹³⁴, S. Nemecek¹⁴⁰, P. Nemethy¹²³, M. Nessi^{36,e}, M. S. Neubauer¹⁷², M. Neumann¹⁸¹, P. R. Newman²¹, T. Y. Ng^{62c}, Y. S. Ng¹⁹, Y. W. Y. Ng¹⁷⁰, H. D. N. Nguyen¹⁰⁰, T. Nguyen Manh¹⁰⁸, E. Nibigira³⁸, R. B. Nickerson¹³⁴, R. Nicolaidou¹⁴⁴, D. S. Nielsen⁴⁰, J. Nielsen¹⁴⁵, N. Nikiforou¹¹, V. Nikolaenko^{122,an}, I. Nikolic-Audit¹³⁵, K. Nikolopoulos²¹, P. Nilsson²⁹, H. R. Nindhito⁵³, Y. Ninomiya⁸⁰, A. Nisati^{71a}, N. Nishu^{59c}, R. Nisius¹¹⁴, I. Nitsche⁴⁶, T. Nitta¹⁷⁸, T. Nobe¹⁶², Y. Noguchi⁸⁴, M. Nomachi¹³², I. Nomidis¹³⁵, M. A. Nomura²⁹, T. Nooney⁹¹, M. Nordberg³⁶, N. Norjoharuddeen¹³⁴, T. Novak⁹⁰, O. Novgorodova⁴⁷, R. Novotny¹⁴¹, L. Nozka¹²⁹, K. Ntekas¹⁷⁰, E. Nurse⁹³, F. Nuti¹⁰³, F. G. Oakham^{34,au}, H. Oberlack¹¹⁴, J. Ocariz¹³⁵, A. Ochi⁸¹, I. Ochoa³⁹, J. P. Ochoa-Ricoux^{146a}, K. O'Connor²⁶, S. Oda⁸⁶, S. Odaka⁸⁰, S. Oerdek⁵², A. Oh⁹⁹, S. H. Oh⁴⁸, C. C. Ohm¹⁵³, H. Oide^{54a,54b}, M. L. Ojeda¹⁶⁶, H. Okawa¹⁶⁸, Y. Okazaki⁸⁴, Y. Okumura¹⁶², T. Okuyama⁸⁰, A. Olariu^{27b}, L. F. Oleiro Seabra^{139a}, S. A. Olivares Pino^{146a}, D. Oliveira Damazio²⁹, J. L. Oliver¹, M. J. R. Olsson³⁷, A. Olszewski⁸³, J. Olszowska⁸³, D. C. O'Neil¹⁵¹, A. Onofre^{139a,139e}, K. Onogi¹¹⁶, P. U. E. Onyisi¹¹, H. Oppen¹³³, M. J. Oreglia³⁷, G. E. Orellana⁸⁷, Y. Oren¹⁶⁰, D. Orestano^{73a,73b}, N. Orlando^{62b}, A. A. O'Rourke⁴⁵, R. S. Orr¹⁶⁶, B. Osculati^{54a,54b,*}, V. O'Shea⁵⁶, R. Ospanov^{59a}, G. Otero y Garzon³⁰, H. Otono⁸⁶, M. Ouchrif^{35d}, F. Ould-Saada¹³³, A. Ouraou¹⁴⁴, Q. Ouyang^{15a}, M. Owen⁵⁶, R. E. Owen²¹, V. E. Ozcan^{12c}, N. Ozturk⁸, J. Pacalt¹²⁹, H. A. Pacey³², K. Pachal¹⁵¹, A. Pacheco Pages¹⁴, L. Pacheco Rodriguez¹⁴⁴, C. Padilla Aranda¹⁴, S. Pagan Griso¹⁸, M. Paganini¹⁸², G. Palacino⁶⁴, S. Palazzo⁴⁹, S. Palestini³⁶, M. Palka^{82b}, D. Pallin³⁸, I. Panagoulas¹⁰, C. E. Pandini³⁶, J. G. Panduro Vazquez⁹², P. Pani³⁶, G. Panizzo^{65a,65c}, L. Paolozzi⁵³, T. D. Papadopoulou¹⁰, K. Papageorgiou^{9,h}, A. Paramonov⁶, D. Paredes Hernandez^{62b}, S. R. Paredes Saenz¹³⁴, B. Parida¹⁶⁵, T. H. Park³⁴, A. J. Parker⁸⁸, K. A. Parker⁴⁵, M. A. Parker³², F. Parodi^{54a,54b}, J. A. Parsons³⁹, U. Parzefall⁵¹, V. R. Pascuzzi¹⁶⁶, J. M. P. Pasner¹⁴⁵, E. Pasqualucci^{71a}, S. Passaggio^{54b}, F. Pastore⁹², P. Pasuwan^{44a,44b}, S. Pataraja⁹⁸, J. R. Pater⁹⁹, A. Pathak^{180,i}, T. Pauly³⁶, B. Pearson¹¹⁴, M. Pedersen¹³³, L. Pedraza Diaz¹¹⁸, R. Pedro^{139a,139b}, S. V. Peleganchuk^{121a,121b}, O. Penc¹⁴⁰, C. Peng^{15a}, H. Peng^{59a}, B. S. Peralva^{79a}, M. M. Perego¹³¹, A. P. Pereira Peixoto^{139a}, D. V. Perepelitsa²⁹, F. Peri¹⁹, L. Perini^{67a,67b}, H. Pernegger³⁶, S. Perrella^{68a,68b}, V. D. Peshekhonov^{78,*}, K. Peters⁴⁵, R. F. Y. Peters⁹⁹, B. A. Petersen³⁶, T. C. Petersen⁴⁰, E. Petit⁵⁷, A. Petridis¹, C. Petridou¹⁶¹, P. Petroff¹³¹, M. Petrov¹³⁴, F. Petrucci^{73a,73b}, M. Pettee¹⁸², N. E. Pettersson¹⁰¹, A. Peyaud¹⁴⁴, R. Pezoa^{146b}, T. Pham¹⁰³, F. H. Phillips¹⁰⁵, P. W. Phillips¹⁴³, M. W. Phipps¹⁷², G. Piacquadio¹⁵⁴, E. Pianori¹⁸, A. Picazio¹⁰¹, R. H. Pickles⁹⁹, R. Piegai³⁰, J. E. Pilcher³⁷, A. D. Pilkington⁹⁹, M. Pinamonti^{72a,72b}, J. L. Pinfold³, M. Pitt¹⁷⁹, L. Pizzimento^{72a,72b}, M.-A. Pleier²⁹, V. Pleskot¹⁴², E. Plotnikova⁷⁸, D. Pluth⁷⁷, P. Podberczko^{121a,121b}, R. Poettgen⁹⁵, R. Poggi⁵³, L. Poggioli¹³¹, I. Pogrebnyak¹⁰⁵, D. Pohl²⁴, I. Pokharel⁵², G. Polesello^{69a}, A. Poley¹⁸, A. Policicchio^{71a,71b}, R. Polifka³⁶, A. Polini^{23b}, C. S. Pollard⁴⁵, V. Polychronakos²⁹, D. Ponomarenko¹¹¹, L. Pontecorvo³⁶, G. A. Popeneciu^{27d}, D. M. Portillo Quintero¹³⁵, S. Pospisil¹⁴¹, K. Potamianos⁴⁵, I. N. Potrap⁷⁸, C. J. Potter³², H. Potti¹¹, T. Poulsen⁹⁵, J. Poveda³⁶, T. D. Powell¹⁴⁸, M. E. Pozo Astigarraga³⁶, P. Pralavorio¹⁰⁰, S. Prell⁷⁷, D. Price⁹⁹, M. Primavera^{66a}, S. Prince¹⁰², M. L. Proffitt¹⁴⁷, N. Proklova¹¹¹, K. Prokofiev^{62c}, F. Prokoshin^{146b}, S. Protopopescu²⁹, J. Proudfoot⁶, M. Przybycien^{82a}, A. Puri¹⁷², P. Puzo¹³¹, J. Qian¹⁰⁴, Y. Qin⁹⁹, A. Quadt⁵², M. Queitsch-Maitland⁴⁵, A. Qureshi¹, P. Rados¹⁰³, F. Ragusa^{67a,67b}, G. Rahal⁹⁶, J. A. Raine⁵³, S. Rajagopalan²⁹, A. Ramirez Morales⁹¹, K. Ran^{15a,15b}, T. Rashid¹³¹, S. Raspopov⁵, M. G. Ratti^{67a,67b}, D. M. Rauch⁴⁵, F. Rauscher¹¹³, S. Rave⁹⁸, B. Ravina¹⁴⁸, I. Ravinovich¹⁷⁹, J. H. Rawling⁹⁹, M. Raymond³⁶, A. L. Read¹³³, N. P. Readioff⁵⁷, M. Reale^{66a,66b}, D. M. Rebuffi^{69a,69b}, A. Redelbach¹⁷⁶, G. Redlinger²⁹, R. Reece¹⁴⁵, R. G. Reed^{33c}, K. Reeves⁴³, L. Rehnisch¹⁹, J. Reichert¹³⁶, D. Reikher¹⁶⁰, A. Reiss⁹⁸, A. Rej¹⁵⁰, C. Rembser³⁶, H. Ren^{15a}, M. Rescigno^{71a}, S. Resconi^{67a}, E. D. Resseguie¹³⁶, S. Rettie¹⁷⁴, E. Reynolds²¹, O. L. Rezanova^{121a,121b}, P. Reznicek¹⁴², E. Ricci^{74a,74b}, R. Richter¹¹⁴, S. Richter⁴⁵, E. Richter-Was^{82b}, O. Ricken²⁴, M. Ridel¹³⁵, P. Rieck¹¹⁴, C. J. Riegel¹⁸¹, O. Rifki⁴⁵, M. Rijssenbeek¹⁵⁴, A. Rimoldi^{69a,69b}, M. Rimoldi²⁰, L. Rinaldi^{23b}, G. Ripellino¹⁵³, B. Ristic⁸⁸, E. Ritsch³⁶, I. Riu¹⁴, J. C. Rivera Vergara^{146a}, F. Rizatdinova¹²⁸, E. Rizvi⁹¹, C. Rizzi¹⁴, R. T. Roberts⁹⁹, S. H. Robertson^{102,ad}, D. Robinson³², J. E. M. Robinson⁴⁵, A. Robson⁵⁶, E. Rocco⁹⁸, C. Roda^{70a,70b}, Y. Rodina¹⁰⁰, S. Rodriguez Bosca¹⁷³, A. Rodriguez Perez¹⁴, D. Rodriguez Rodriguez¹⁷³, A. M. Rodriguez Vera^{167b}, S. Roe³⁶, C. S. Rogan⁵⁸, O. Røhne¹³³, R. Röhrig¹¹⁴, C. P. A. Roland⁶⁴, J. Roloff⁵⁸, A. Romaniouk¹¹¹, M. Romano^{23a,23b}, N. Rompotis⁸⁹, M. Ronzani¹²³, L. Roos¹³⁵, S. Rosati^{71a}, K. Rosbach⁵¹, N.-A. Rosien⁵², B. J. Rosser¹³⁶, E. Rossi⁴⁵, E. Rossi^{73a,73b}, E. Rossi^{68a,68b},

L. P. Rossi^{54b}, L. Rossini^{67a,67b}, J. H. N. Rosten³², R. Rosten¹⁴, M. Rotaru^{27b}, J. Rothberg¹⁴⁷, D. Rousseau¹³¹, D. Roy^{33c}, A. Rozanov¹⁰⁰, Y. Rozen¹⁵⁹, X. Ruan^{33c}, F. Rubbo¹⁵², F. Rühr⁵¹, A. Ruiz-Martinez¹⁷³, Z. Rurikova⁵¹, N. A. Rusakovich⁷⁸, H. L. Russell¹⁰², J. P. Rutherford⁷, E. M. Rüttinger^{45,j}, Y. F. Ryabov¹³⁷, M. Rybar³⁹, G. Rybkin¹³¹, S. Ryu⁶, A. Ryzhov¹²², G. F. Rzehorz⁵², P. Sabatini⁵², G. Sabato¹¹⁹, S. Sacerdoti¹³¹, H. F.-W. Sadrozinski¹⁴⁵, R. Sadykov⁷⁸, F. Safai Tehrani^{71a}, P. Saha¹²⁰, M. Sahinsoy^{60a}, A. Sahu¹⁸¹, M. Saimpert⁴⁵, M. Saito¹⁶², T. Saito¹⁶², H. Sakamoto¹⁶², A. Sakharov^{123,am}, D. Salamani⁵³, G. Salamanna^{73a,73b}, J. E. Salazar Loyola^{146b}, P. H. Sales De Bruin¹⁷¹, D. Salihagic^{114,*}, A. Salnikov¹⁵², J. Salt¹⁷³, D. Salvatore^{41a,41b}, F. Salvatore¹⁵⁵, A. Salvucci^{62a,62b,62c}, A. Salzburger³⁶, J. Samarati³⁶, D. Sammel⁵¹, D. Sampsonidis¹⁶¹, D. Sampsonidou¹⁶¹, J. Sánchez¹⁷³, A. Sanchez Pineda^{65a,65c}, H. Sandaker¹³³, C. O. Sander⁴⁵, M. Sandhoff¹⁸¹, C. Sandoval²², D. P. C. Sankey¹⁴³, M. Sannino^{54a,54b}, Y. Sano¹¹⁶, A. Sansoni⁵⁰, C. Santoni³⁸, H. Santos^{139a}, I. Santoyo Castillo¹⁵⁵, A. Santra¹⁷³, A. Sapronov⁷⁸, J. G. Saraiva^{139a,139d}, O. Sasaki⁸⁰, K. Sato¹⁶⁸, E. Sauvan⁵, P. Savard^{166,au}, N. Savic¹¹⁴, R. Sawada¹⁶², C. Sawyer¹⁴³, L. Sawyer^{94,ak}, C. Sbarra^{23b}, A. Sbrizzi^{23a}, T. Scanlon⁹³, J. Schaarschmidt¹⁴⁷, P. Schacht¹¹⁴, B. M. Schachtner¹¹³, D. Schaefer³⁷, L. Schaefer¹³⁶, J. Schaeffer⁹⁸, S. Schaepe³⁶, U. Schäfer⁹⁸, A. C. Schaffer¹³¹, D. Schaile¹¹³, R. D. Schamberger¹⁵⁴, N. Scharmberg⁹⁹, V. A. Schegelsky¹³⁷, D. Scheirich¹⁴², F. Schenck¹⁹, M. Schernau¹⁷⁰, C. Schiavi^{54a,54b}, S. Schier¹⁴⁵, L. K. Schildgen²⁴, Z. M. Schillaci²⁶, E. J. Schioppa³⁶, M. Schioppa^{41a,41b}, K. E. Schleicher⁵¹, S. Schlenker³⁶, K. R. Schmidt-Sommerfeld¹¹⁴, K. Schmieden³⁶, C. Schmitt⁹⁸, S. Schmitt⁴⁵, S. Schmitz⁹⁸, J. C. Schmoekel⁴⁵, U. Schnoor⁵¹, L. Schoeffel¹⁴⁴, A. Schoening^{60b}, E. Schopf¹³⁴, M. Schott⁹⁸, J. F. P. Schouwenberg¹¹⁸, J. Schovancova³⁶, S. Schramm⁵³, A. Schulte⁹⁸, H.-C. Schultz-Coulon^{60a}, M. Schumacher⁵¹, B. A. Schumm¹⁴⁵, Ph. Schune¹⁴⁴, A. Schwartzman¹⁵², T. A. Schwarz¹⁰⁴, Ph. Schwemling¹⁴⁴, R. Schwienhorst¹⁰⁵, A. Sciandra²⁴, G. Sciolla²⁶, M. Scornajenghi^{41a,41b}, F. Scuri^{70a}, F. Scutti¹⁰³, L. M. Scyboz¹¹⁴, C. D. Sebastiani^{71a,71b}, P. Seema¹⁹, S. C. Seidel¹¹⁷, A. Seiden¹⁴⁵, T. Seiss³⁷, J. M. Seixas^{79b}, G. Sekhniaidze^{68a}, K. Sekhon¹⁰⁴, S. J. Sekula⁴², N. Semprini-Cesari^{23a,23b}, S. Sen⁴⁸, S. Senkin³⁸, C. Serfon¹³³, L. Serin¹³¹, L. Serkin^{65a,65b}, M. Sessa^{59a}, H. Severini¹²⁷, F. Sforza¹⁶⁹, A. Sfyrta⁵³, E. Shabalina⁵², J. D. Shahinian¹⁴⁵, N. W. Shaikh^{44a,44b}, D. Shaked Renous¹⁷⁹, L. Y. Shan^{15a}, R. Shang¹⁷², J. T. Shank²⁵, M. Shapiro¹⁸, A. S. Sharma¹, A. Sharma¹³⁴, P. B. Shatalov¹¹⁰, K. Shaw¹⁵⁵, S. M. Shaw⁹⁹, A. Shcherbakova¹³⁷, Y. Shen¹²⁷, N. Sherafati³⁴, A. D. Sherman²⁵, P. Sherwood⁹³, L. Shi^{157,aq}, S. Shimizu⁸⁰, C. O. Shimmin¹⁸², Y. Shimogama¹⁷⁸, M. Shimojima¹¹⁵, I. P. J. Shipsey¹³⁴, S. Shirabe⁸⁶, M. Shiyakova^{78,ab}, J. Shlomi¹⁷⁹, A. Shmeleva¹⁰⁹, D. Shoaleh Saadi¹⁰⁸, M. J. Shochet³⁷, S. Shojaii¹⁰³, D. R. Shope¹²⁷, S. Shrestha¹²⁵, E. Shulga¹¹¹, P. Sicho¹⁴⁰, A. M. Sickles¹⁷², P. E. Sidebo¹⁵³, E. Sideras Haddad^{33c}, O. Sidiropoulou³⁶, A. Sidoti^{23a,23b}, F. Siegert⁴⁷, Dj. Sijacki¹⁶, J. Silva^{139a}, M. Silva Jr.¹⁸⁰, M. V. Silva Oliveira^{79a}, S. B. Silverstein^{44a}, S. Simion¹³¹, E. Simioni⁹⁸, M. Simon⁹⁸, R. Simoniello⁹⁸, P. Sinervo¹⁶⁶, N. B. Sinev¹³⁰, M. Sioli^{23a,23b}, I. Siral¹⁰⁴, S. Yu. Sivoklov¹¹², J. Sjölin^{44a,44b}, P. Skubic¹²⁷, M. Slater²¹, T. Slavicek¹⁴¹, M. Slawinska⁸³, K. Sliwa¹⁶⁹, R. Slovak¹⁴², V. Smakhtin¹⁷⁹, B. H. Smart⁵, J. Smiesko^{28a}, N. Smirnov¹¹¹, S. Yu. Smirnov¹¹¹, Y. Smirnov¹¹¹, L. N. Smirnova^{112,s}, O. Smirnova⁹⁵, J. W. Smith⁵², M. Smizanska⁸⁸, K. Smolek¹⁴¹, A. Smykiewicz⁸³, A. A. Snesarev¹⁰⁹, I. M. Snyder¹³⁰, S. Snyder²⁹, R. Sobie^{175,ad}, A. M. Soffa¹⁷⁰, A. Soffer¹⁶⁰, A. Sogaard⁴⁹, F. Sohns⁵², G. Sokhrannyi⁹⁰, C. A. Solans Sanchez³⁶, M. Solar¹⁴¹, E. Yu. Soldatov¹¹¹, U. Soldevila¹⁷³, A. A. Solodkov¹²², A. Soloshenko⁷⁸, O. V. Solovyanov¹²², V. Solovye¹³⁷, P. Sommer¹⁴⁸, H. Son¹⁶⁹, W. Song¹⁴³, W. Y. Song^{167b}, A. Sopczak¹⁴¹, F. Sopkova^{28b}, C. L. Sotiropoulou^{70a,70b}, S. Sottocornola^{69a,69b}, R. Soualah^{65a,65c,g}, A. M. Soukharev^{121a,121b}, D. South⁴⁵, S. Spagnolo^{66a,66b}, M. Spalla¹¹⁴, M. Spangenberg¹⁷⁷, F. Spano⁹², D. Sperlich¹⁹, T. M. Spieker^{60a}, R. Spighi^{23b}, G. Spigo³⁶, L. A. Spiller¹⁰³, D. P. Spiteri⁵⁶, M. Spousta¹⁴², A. Stabile^{67a,67b}, R. Stamen^{60a}, S. Stamm¹⁹, E. Stanecka⁸³, R. W. Stanek⁶, C. Stancu^{73a}, B. Stanislaus¹³⁴, M. M. Stanitzki⁴⁵, B. Stapf¹¹⁹, E. A. Starchenko¹²², G. H. Stark¹⁴⁵, J. Stark⁵⁷, S. H. Stark⁴⁰, P. Staroba¹⁴⁰, P. Starovoitov^{60a}, S. Stärz¹⁰², R. Staszewski⁸³, M. Stegler⁴⁵, P. Steinberg²⁹, B. Stelzer¹⁵¹, H. J. Stelzer³⁶, O. Stelzer-Chilton^{167a}, H. Stenzel⁵⁵, T. J. Stevenson¹⁵⁵, G. A. Stewart³⁶, M. C. Stockton³⁶, G. Stoica^{27b}, P. Stolte⁵², S. Stonjek¹¹⁴, A. Straessner⁴⁷, J. Strandberg¹⁵³, S. Strandberg^{44a,44b}, M. Strauss¹²⁷, P. Strizenec^{28b}, R. Ströhmer¹⁷⁶, D. M. Strom¹³⁰, R. Stroynowski⁴², A. Strubig⁴⁹, S. A. Stucci²⁹, B. Stugu¹⁷, J. Stupak¹²⁷, N. A. Styles⁴⁵, D. Su¹⁵², J. Su¹³⁸, S. Suček^{60a}, Y. Sugaya¹³², M. Suk¹⁴¹, V. V. Sulin¹⁰⁹, M. J. Sullivan⁸⁹, D. M. S. Sultan⁵³, S. Sultansoy^{4c}, T. Sumida⁸⁴, S. Sun¹⁰⁴, X. Sun³, K. Suruliz¹⁵⁵, C. J. E. Suster¹⁵⁶, M. R. Sutton¹⁵⁵, S. Suzuki⁸⁰, M. Svatos¹⁴⁰, M. Swiatlowski³⁷, S. P. Swift², A. Sydorenko⁹⁸, I. Sykora^{28a}, M. Sykora¹⁴², T. Sykora¹⁴², D. Ta⁹⁸, K. Tackmann^{45,z}, J. Taenzer¹⁶⁰, A. Taffard¹⁷⁰, R. Tafirout^{167a}, E. Tahirovic⁹¹, N. Taiblum¹⁶⁰, H. Takai²⁹, R. Takashima⁸⁵, E. H. Takasugi¹¹⁴, K. Takeda⁸¹, T. Takeshita¹⁴⁹, Y. Takubo⁸⁰, M. Talby¹⁰⁰, A. A. Talyshev^{121a,121b}, J. Tanaka¹⁶², M. Tanaka¹⁶⁴, R. Tanaka¹³¹, B. B. Tannenwald¹²⁵, S. Tapia Araya¹⁷², S. Tapprogge⁹⁸, A. Tarek Abouelfadl Mohamed¹³⁵, S. Tarem¹⁵⁹, G. Tarna^{27b,d}, G. F. Tartarelli^{67a}, P. Tas¹⁴², M. Tasevsky¹⁴⁰, T. Tashiro⁸⁴, E. Tassi^{41a,41b}, A. Tavares Delgado^{139a,139b}, Y. Tayalati^{35e}, A. J. Taylor⁴⁹, G. N. Taylor¹⁰³, P. T. E. Taylor¹⁰³, W. Taylor^{167b}, A. S. Tee⁸⁸, R. Teixeira De Lima¹⁵², P. Teixeira-Dias⁹², H. Ten Kate³⁶, J. J. Teoh¹¹⁹, S. Terada⁸⁰, K. Terashi¹⁶², J. Terron⁹⁷, S. Terzo¹⁴, M. Testa⁵⁰, R. J. Teuscher^{166,ad}, S. J. Thais¹⁸², T. Thevenaux-Pelzer⁴⁵, F. Thiele⁴⁰, D. W. Thomas⁹², J. P. Thomas²¹, A. S. Thompson⁵⁶, P. D. Thompson²¹

L. A. Thomsen¹⁸², E. Thomson¹³⁶, Y. Tian³⁹, R. E. Ticse Torres⁵², V. O. Tikhomirov^{109,ao}, Yu. A. Tikhonov^{121a,121b}, S. Timoshenko¹¹¹, P. Tipton¹⁸², S. Tisserant¹⁰⁰, K. Todome¹⁶⁴, S. Todorova-Nova⁵, S. Todt⁴⁷, J. Tojo⁸⁶, S. Tokár^{28a}, K. Tokushuku⁸⁰, E. Tolley¹²⁵, K. G. Tomiwa^{33c}, M. Tomoto¹¹⁶, L. Tompkins^{152,p}, K. Toms¹¹⁷, B. Tong⁵⁸, P. Tornambe⁵¹, E. Torrence¹³⁰, H. Torres⁴⁷, E. Torró Pastor¹⁴⁷, C. Tosciri¹³⁴, J. Toth^{100,ac}, F. Touchard¹⁰⁰, D. R. Tovey¹⁴⁸, C. J. Treado¹²³, T. Trefzger¹⁷⁶, F. Tresoldi¹⁵⁵, A. Tricoli²⁹, I. M. Trigger^{167a}, S. Trincaz-Duvoid¹³⁵, W. Trischuk¹⁶⁶, B. Trocme⁵⁷, A. Trofymov¹³¹, C. Troncon^{67a}, M. Trovatelli¹⁷⁵, F. Trovato¹⁵⁵, L. Truong^{33b}, M. Trzebinski⁸³, A. Trzupek⁸³, F. Tsai⁴⁵, J. C.-L. Tseng¹³⁴, P. V. Tsiarshka^{106,ai}, A. Tsigotis¹⁶¹, N. Tsirintanis⁹, V. Tsiskaridze¹⁵⁴, E. G. Tskhadadze^{158a}, I. I. Tsukerman¹¹⁰, V. Tsulaia¹⁸, S. Tsuno⁸⁰, D. Tsybychev¹⁵⁴, Y. Tu^{62b}, A. Tudorache^{27b}, V. Tudorache^{27b}, T. T. Tulbure^{27a}, A. N. Tuna⁵⁸, S. Turchikhin⁷⁸, D. Turgeman¹⁷⁹, I. Turk Cakir^{4b,t}, R. J. Turner²¹, R. T. Turra^{67a}, P. M. Tuts³⁹, S. Tzamarias¹⁶¹, E. Tzovara⁹⁸, G. Uccielli⁴⁶, I. Ueda⁸⁰, M. Ughetto^{44a,44b}, F. Ukegawa¹⁶⁸, G. Unal³⁶, A. Undrus²⁹, G. Unel¹⁷⁰, F. C. Ungaro¹⁰³, Y. Unno⁸⁰, K. Uno¹⁶², J. Urban^{28b}, P. Urquijo¹⁰³, G. Usai⁸, J. Usui⁸⁰, L. Vacavant¹⁰⁰, V. Vacek¹⁴¹, B. Vachon¹⁰², K. O. H. Vadla¹³³, A. Vaidya⁹³, C. Valderanis¹¹³, E. Valdes Santurio^{44a,44b}, M. Valente⁵³, S. Valentinetti^{23a,23b}, A. Valero¹⁷³, L. Valéry⁴⁵, R. A. Vallance²¹, A. Vallier⁵, J. A. Valls Ferrer¹⁷³, T. R. Van Daalen¹⁴, H. Van der Graaf¹¹⁹, P. Van Gemmeren⁶, I. Van Vulpen¹¹⁹, M. Vanadia^{72a,72b}, W. Vandelli³⁶, A. Vaniachine¹⁶⁵, P. Vankov¹¹⁹, R. Vari^{71a}, E. W. Varnes⁷, C. Varni^{54a,54b}, T. Varol⁴², D. Varouchas¹³¹, K. E. Varvell¹⁵⁶, G. A. Vasquez^{146b}, J. G. Vasquez¹⁸², F. Vazeille³⁸, D. Vazquez Furelos¹⁴, T. Vazquez Schroeder³⁶, J. Veatch⁵², V. Vecchio^{73a,73b}, L. M. Veloce¹⁶⁶, F. Veloso^{139a,139c}, S. Veneziano^{71a}, A. Ventura^{66a,66b}, N. Venturi³⁶, V. Vercesi^{69a}, M. Verducci^{73a,73b}, C. M. Vergel Infante⁷⁷, C. Vergis²⁴, W. Verkerke¹¹⁹, A. T. Vermeulen¹¹⁹, J. C. Vermeulen¹¹⁹, M. C. Vetterli^{151,au}, N. Viaux Maira^{146b}, M. Vicente Barreto Pinto⁵³, I. Vichou^{172,*}, T. Vickey¹⁴⁸, O. E. Vickey Boeriu¹⁴⁸, G. H. A. Viehhauser¹³⁴, S. Viel¹⁸, L. Vigani¹³⁴, M. Villa^{23a,23b}, M. Villaplana Perez^{67a,67b}, E. Vilucchi⁵⁰, M. G. Vincter³⁴, V. B. Vinogradov⁷⁸, A. Vishwakarma⁴⁵, C. Vittori^{23a,23b}, I. Vivarelli¹⁵⁵, S. Vlachos¹⁰, M. Vogel¹⁸¹, P. Vokac¹⁴¹, B. Volkel⁵², G. Volpi¹⁴, S. E. Von Buddenbrock^{33c}, E. von Toerne²⁴, V. Vorobel¹⁴², K. Vorobev¹¹¹, M. Vos¹⁷³, J. H. Vossebeld⁸⁹, N. Vranjes¹⁶, M. Vranjes Milosavljevic¹⁶, V. Vrba¹⁴¹, M. Vreeswijk¹¹⁹, T. Šfiligoj⁹⁰, R. Vuillemet³⁶, I. Vukotic³⁷, T. Ženiš^{28a}, L. Živković¹⁶, P. Wagner²⁴, W. Wagner¹⁸¹, J. Wagner-Kuhr¹¹³, H. Wahlberg⁸⁷, S. Wahrenmund⁴⁷, K. Wakamiya⁸¹, V. M. Walbrecht¹¹⁴, J. Walder⁸⁸, R. Walker¹¹³, S. D. Walker⁹², W. Walkowiak¹⁵⁰, V. Wallangen^{44a,44b}, A. M. Wang⁵⁸, C. Wang^{59b}, F. Wang¹⁸⁰, H. Wang¹⁸, H. Wang³, J. Wang¹⁵⁶, J. Wang^{60b}, P. Wang⁴², Q. Wang¹²⁷, R.-J. Wang¹³⁵, R. Wang^{59a}, R. Wang⁶, S. M. Wang¹⁵⁷, W. T. Wang^{59a}, W. Wang^{15c,ae}, W. X. Wang^{59a,ae}, Y. Wang^{59a,al}, Z. Wang^{59c}, C. Wanotayaroj⁴⁵, A. Warburton¹⁰², C. P. Ward³², D. R. Wardrope⁹³, A. Washbrook⁴⁹, P. M. Watkins²¹, A. T. Watson²¹, M. F. Watson²¹, G. Watts¹⁴⁷, S. Watts⁹⁹, B. M. Waugh⁹³, A. F. Webb¹¹, S. Webb⁹⁸, C. Weber¹⁸², M. S. Weber²⁰, S. A. Weber³⁴, S. M. Weber^{60a}, A. R. Weidberg¹³⁴, J. Weingarten⁴⁶, M. Weirich⁹⁸, C. Weiser⁵¹, P. S. Wells³⁶, T. Wenaus²⁹, T. Wengler³⁶, S. Wenig³⁶, N. Vermes²⁴, M. D. Werner⁷⁷, P. Werner³⁶, M. Wessels^{60a}, T. D. Weston²⁰, K. Whalen¹³⁰, N. L. Whallon¹⁴⁷, A. M. Wharton⁸⁸, A. S. White¹⁰⁴, A. White⁸, M. J. White¹, R. White^{146b}, D. Whiteson¹⁷⁰, B. W. Whitmore⁸⁸, F. J. Wickens¹⁴³, W. Wiedenmann¹⁸⁰, M. Wielers¹⁴³, C. Wiglesworth⁴⁰, L. A. M. Wiik-Fuchs⁵¹, F. Wilk⁹⁹, H. G. Wilkens³⁶, L. J. Wilkins⁹², H. H. Williams¹³⁶, S. Williams³², C. Willis¹⁰⁵, S. Willocq¹⁰¹, J. A. Wilson²¹, I. Wingerter-Seetz⁵, E. Winkels¹⁵⁵, F. Winklmeier¹³⁰, O. J. Winston¹⁵⁵, B. T. Winter⁵¹, M. Wittgen¹⁵², M. Wobisch⁹⁴, A. Wolf⁹⁸, T. M. H. Wolf¹¹⁹, R. Wolff¹⁰⁰, J. Wollrath⁵¹, M. W. Wolter⁸³, H. Wolters^{139a,139c}, V. W. S. Wong¹⁷⁴, N. L. Woods¹⁴⁵, S. D. Worm²¹, B. K. Wosiek⁸³, K. W. Woźniak⁸³, K. Wraight⁵⁶, M. Wu³⁷, S. L. Wu¹⁸⁰, X. Wu⁵³, Y. Wu^{59a}, T. R. Wyatt⁹⁹, B. M. Wynne⁴⁹, S. Xella⁴⁰, Z. Xi¹⁰⁴, L. Xia¹⁷⁷, D. Xu^{15a}, H. Xu^{59a,d}, L. Xu²⁹, T. Xu¹⁴⁴, W. Xu¹⁰⁴, Z. Xu¹⁵², B. Yabsley¹⁵⁶, S. Yacoob^{33a}, K. Yajima¹³², D. P. Yallup⁹³, D. Yamaguchi¹⁶⁴, Y. Yamaguchi¹⁶⁴, A. Yamamoto⁸⁰, T. Yamanaka¹⁶², F. Yamane⁸¹, M. Yamatani¹⁶², T. Yamazaki¹⁶², Y. Yamazaki⁸¹, Z. Yan²⁵, H. J. Yang^{59c,59d}, H. T. Yang¹⁸, S. Yang⁷⁶, Y. Yang¹⁶², Z. Yang¹⁷, W.-M. Yao¹⁸, Y. C. Yap⁴⁵, Y. Yasu⁸⁰, E. Yatsenko^{59c,59d}, J. Ye⁴², S. Ye²⁹, I. Yeletsikh⁷⁸, E. Yigitbasi²⁵, E. Yildirim⁹⁸, K. Yorita¹⁷⁸, K. Yoshihara¹³⁶, C. J. S. Young³⁶, C. Young¹⁵², J. Yu⁸, J. Yu⁷⁷, X. Yue^{60a}, S. P. Y. Yuen²⁴, B. Zabinski⁸³, G. Zacharis¹⁰, E. Zaffaroni⁵³, R. Zaidan¹⁴, A. M. Zaitsev^{122,an}, T. Zakareishvili^{158b}, N. Zakharchuk³⁴, S. Zambito⁵⁸, D. Zanzi³⁶, D. R. Zaripovas⁵⁶, S. V. Zeißner⁴⁶, C. Zeitnitz¹⁸¹, G. Zemaityte¹³⁴, J. C. Zeng¹⁷², Q. Zeng¹⁵², O. Zenin¹²², D. Zerwas¹³¹, M. Zgubič¹³⁴, D. F. Zhang^{59b}, D. Zhang¹⁰⁴, F. Zhang¹⁸⁰, G. Zhang^{59a}, G. Zhang^{15b}, H. Zhang^{15c}, J. Zhang⁶, L. Zhang^{15c}, L. Zhang^{59a}, M. Zhang¹⁷², P. Zhang^{15c}, R. Zhang^{59a}, R. Zhang²⁴, X. Zhang^{59b}, Y. Zhang^{15a,15d}, Z. Zhang¹³¹, P. Zhao⁴⁸, Y. Zhao^{59b,131,aj}, Z. Zhao^{59a}, A. Zhemchugov⁷⁸, Z. Zheng¹⁰⁴, D. Zhong¹⁷², B. Zhou¹⁰⁴, C. Zhou¹⁸⁰, M. S. Zhou^{15a,15d}, M. Zhou¹⁵⁴, N. Zhou^{59c}, Y. Zhou⁷, C. G. Zhu^{59b}, H. L. Zhu^{59a}, H. Zhu^{15a}, J. Zhu¹⁰⁴, Y. Zhu^{59a}, X. Zhuang^{15a}, K. Zhukov¹⁰⁹, V. Zhulanov^{121a,121b}, A. Zibell¹⁷⁶, D. Zieminska⁶⁴, N. I. Zimine⁷⁸, S. Zimmermann⁵¹, Z. Zinonos¹¹⁴, M. Ziolkowski¹⁵⁰, G. Zobernig¹⁸⁰, A. Zoccoli^{23a,23b}, K. Zoch⁵², T. G. Zorbas¹⁴⁸, R. Zou³⁷, M. Zur Nedden¹⁹, L. Zwalinski³⁶

¹ Department of Physics, University of Adelaide, Adelaide, Australia

- ² Physics Department, SUNY Albany, Albany, NY, USA
- ³ Department of Physics, University of Alberta, Edmonton, AB, Canada
- ⁴ (a) Department of Physics, Ankara University, Ankara, Turkey; (b) Istanbul Aydin University, Istanbul, Turkey; (c) Division of Physics, TOBB University of Economics and Technology, Ankara, Turkey
- ⁵ LAPP, Université Grenoble Alpes, Université Savoie Mont Blanc, CNRS/IN2P3, Annecy, France
- ⁶ High Energy Physics Division, Argonne National Laboratory, Argonne, IL, USA
- ⁷ Department of Physics, University of Arizona, Tucson, AZ, USA
- ⁸ Department of Physics, University of Texas at Arlington, Arlington, TX, USA
- ⁹ Physics Department, National and Kapodistrian University of Athens, Athens, Greece
- ¹⁰ Physics Department, National Technical University of Athens, Zografou, Greece
- ¹¹ Department of Physics, University of Texas at Austin, Austin, TX, USA
- ¹² (a) Faculty of Engineering and Natural Sciences, Bahcesehir University, Istanbul, Turkey; (b) Faculty of Engineering and Natural Sciences, Istanbul Bilgi University, Istanbul, Turkey; (c) Department of Physics, Bogazici University, Istanbul, Turkey; (d) Department of Physics Engineering, Gaziantep University, Gaziantep, Turkey
- ¹³ Institute of Physics, Azerbaijan Academy of Sciences, Baku, Azerbaijan
- ¹⁴ Institut de Física d'Altes Energies (IFAE), Barcelona Institute of Science and Technology, Barcelona, Spain
- ¹⁵ (a) Institute of High Energy Physics, Chinese Academy of Sciences, Beijing, China; (b) Physics Department, Tsinghua University, Beijing, China; (c) Department of Physics, Nanjing University, Nanjing, China; (d) University of Chinese Academy of Science (UCAS), Beijing, China
- ¹⁶ Institute of Physics, University of Belgrade, Belgrade, Serbia
- ¹⁷ Department for Physics and Technology, University of Bergen, Bergen, Norway
- ¹⁸ Physics Division, Lawrence Berkeley National Laboratory and University of California, Berkeley, CA, USA
- ¹⁹ Institut für Physik, Humboldt Universität zu Berlin, Berlin, Germany
- ²⁰ Albert Einstein Center for Fundamental Physics and Laboratory for High Energy Physics, University of Bern, Bern, Switzerland
- ²¹ School of Physics and Astronomy, University of Birmingham, Birmingham, UK
- ²² Facultad de Ciencias y Centro de Investigaciones, Universidad Antonio Nariño, Bogota, Colombia
- ²³ (a) Dipartimento di Fisica, INFN Bologna and Università di Bologna, Bologna, Italy; (b) INFN Sezione di Bologna, Bologna, Italy
- ²⁴ Physikalisches Institut, Universität Bonn, Bonn, Germany
- ²⁵ Department of Physics, Boston University, Boston, MA, USA
- ²⁶ Department of Physics, Brandeis University, Waltham, MA, USA
- ²⁷ (a) Transilvania University of Brasov, Brasov, Romania; (b) Horia Hulubei National Institute of Physics and Nuclear Engineering, Bucharest, Romania; (c) Department of Physics, Alexandru Ioan Cuza University of Iasi, Iasi, Romania; (d) Physics Department, National Institute for Research and Development of Isotopic and Molecular Technologies, Cluj-Napoca, Romania; (e) University Politehnica Bucharest, Bucharest, Romania; (f) West University in Timisoara, Timisoara, Romania
- ²⁸ (a) Faculty of Mathematics, Physics and Informatics, Comenius University, Bratislava, Slovakia; (b) Department of Subnuclear Physics, Institute of Experimental Physics of the Slovak Academy of Sciences, Kosice, Slovak Republic
- ²⁹ Physics Department, Brookhaven National Laboratory, Upton, NY, USA
- ³⁰ Departamento de Física, Universidad de Buenos Aires, Buenos Aires, Argentina
- ³¹ California State University, Long Beach, CA, USA
- ³² Cavendish Laboratory, University of Cambridge, Cambridge, UK
- ³³ (a) Department of Physics, University of Cape Town, Cape Town, South Africa; (b) Department of Mechanical Engineering Science, University of Johannesburg, Johannesburg, South Africa; (c) School of Physics, University of the Witwatersrand, Johannesburg, South Africa
- ³⁴ Department of Physics, Carleton University, Ottawa, ON, Canada
- ³⁵ (a) Faculté des Sciences Ain Chock, Réseau Universitaire de Physique des Hautes Energies - Université Hassan II, Casablanca, Morocco; (b) Faculté des Sciences, Université Ibn-Tofail, Kenitra, Morocco; (c) Faculté des Sciences Semlalia, Université Cadi Ayyad, LPHEA-Marrakech, Marrakech, Morocco; (d) Faculté des Sciences, Université Mohamed Premier and LTPM, Oujda, Morocco; (e) Faculté des sciences, Université Mohammed V, Rabat, Morocco
- ³⁶ CERN, Geneva, Switzerland
- ³⁷ Enrico Fermi Institute, University of Chicago, Chicago, IL, USA

- ³⁸ LPC, Université Clermont Auvergne, CNRS/IN2P3, Clermont-Ferrand, France
- ³⁹ Nevis Laboratory, Columbia University, Irvington, NY, USA
- ⁴⁰ Niels Bohr Institute, University of Copenhagen, Copenhagen, Denmark
- ⁴¹ ^(a)Dipartimento di Fisica, Università della Calabria, Rende, Italy; ^(b)INFN Gruppo Collegato di Cosenza, Laboratori Nazionali di Frascati, Frascati, Italy
- ⁴² Physics Department, Southern Methodist University, Dallas, TX, USA
- ⁴³ Physics Department, University of Texas at Dallas, Richardson, TX, USA
- ⁴⁴ ^(a)Department of Physics, Stockholm University, Stockholm, Sweden; ^(b)Oskar Klein Centre, Stockholm, Sweden
- ⁴⁵ Deutsches Elektronen-Synchrotron DESY, Hamburg and Zeuthen, Germany
- ⁴⁶ Lehrstuhl für Experimentelle Physik IV, Technische Universität Dortmund, Dortmund, Germany
- ⁴⁷ Institut für Kern- und Teilchenphysik, Technische Universität Dresden, Dresden, Germany
- ⁴⁸ Department of Physics, Duke University, Durham, NC, USA
- ⁴⁹ SUPA-School of Physics and Astronomy, University of Edinburgh, Edinburgh, UK
- ⁵⁰ INFN e Laboratori Nazionali di Frascati, Frascati, Italy
- ⁵¹ Physikalisches Institut, Albert-Ludwigs-Universität Freiburg, Freiburg, Germany
- ⁵² II. Physikalisches Institut, Georg-August-Universität Göttingen, Göttingen, Germany
- ⁵³ Département de Physique Nucléaire et Corpusculaire, Université de Genève, Geneva, Switzerland
- ⁵⁴ ^(a)Dipartimento di Fisica, Università di Genova, Genoa, Italy; ^(b)INFN Sezione di Genova, Genoa, Italy
- ⁵⁵ II. Physikalisches Institut, Justus-Liebig-Universität Giessen, Giessen, Germany
- ⁵⁶ SUPA-School of Physics and Astronomy, University of Glasgow, Glasgow, UK
- ⁵⁷ LPSC, Université Grenoble Alpes, CNRS/IN2P3, Grenoble INP, Grenoble, France
- ⁵⁸ Laboratory for Particle Physics and Cosmology, Harvard University, Cambridge, MA, USA
- ⁵⁹ ^(a)Department of Modern Physics and State Key Laboratory of Particle Detection and Electronics, University of Science and Technology of China, Hefei, China; ^(b)Institute of Frontier and Interdisciplinary Science and Key Laboratory of Particle Physics and Particle Irradiation (MOE), Shandong University, Qingdao, China; ^(c)School of Physics and Astronomy, Shanghai Jiao Tong University, KLPPAC-MoE, SKLPPC, Shanghai, China; ^(d)Tsung-Dao Lee Institute, Shanghai, China
- ⁶⁰ ^(a)Kirchhoff-Institut für Physik, Ruprecht-Karls-Universität Heidelberg, Heidelberg, Germany; ^(b)Physikalisches Institut, Ruprecht-Karls-Universität Heidelberg, Heidelberg, Germany
- ⁶¹ Faculty of Applied Information Science, Hiroshima Institute of Technology, Hiroshima, Japan
- ⁶² ^(a)Department of Physics, Chinese University of Hong Kong, Shatin, N.T., Hong Kong; ^(b)Department of Physics, University of Hong Kong, Hong Kong, China; ^(c)Department of Physics and Institute for Advanced Study, Hong Kong University of Science and Technology, Clear Water Bay, Kowloon, Hong Kong, China
- ⁶³ Department of Physics, National Tsing Hua University, Hsinchu, Taiwan
- ⁶⁴ Department of Physics, Indiana University, Bloomington, IN, USA
- ⁶⁵ ^(a)INFN Gruppo Collegato di Udine, Sezione di Trieste, Udine, Italy; ^(b)ICTP, Trieste, Italy; ^(c)Dipartimento Politecnico di Ingegneria e Architettura, Università di Udine, Udine, Italy
- ⁶⁶ ^(a)INFN Sezione di Lecce, Lecce, Italy; ^(b)Dipartimento di Matematica e Fisica, Università del Salento, Lecce, Italy
- ⁶⁷ ^(a)INFN Sezione di Milano, Milan, Italy; ^(b)Dipartimento di Fisica, Università di Milano, Milan, Italy
- ⁶⁸ ^(a)INFN Sezione di Napoli, Naples, Italy; ^(b)Dipartimento di Fisica, Università di Napoli, Naples, Italy
- ⁶⁹ ^(a)INFN Sezione di Pavia, Pavia, Italy; ^(b)Dipartimento di Fisica, Università di Pavia, Pavia, Italy
- ⁷⁰ ^(a)INFN Sezione di Pisa, Pisa, Italy; ^(b)Dipartimento di Fisica E. Fermi, Università di Pisa, Pisa, Italy
- ⁷¹ ^(a)INFN Sezione di Roma, Rome, Italy; ^(b)Dipartimento di Fisica, Sapienza Università di Roma, Rome, Italy
- ⁷² ^(a)INFN Sezione di Roma Tor Vergata, Rome, Italy; ^(b)Dipartimento di Fisica, Università di Roma Tor Vergata, Rome, Italy
- ⁷³ ^(a)INFN Sezione di Roma Tre, Rome, Italy; ^(b)Dipartimento di Matematica e Fisica, Università Roma Tre, Rome, Italy
- ⁷⁴ ^(a)INFN-TIFPA, Povo, Italy; ^(b)Università degli Studi di Trento, Trento, Italy
- ⁷⁵ Institut für Astro- und Teilchenphysik, Leopold-Franzens-Universität, Innsbruck, Austria
- ⁷⁶ University of Iowa, Iowa City, IA, USA
- ⁷⁷ Department of Physics and Astronomy, Iowa State University, Ames, IA, USA
- ⁷⁸ Joint Institute for Nuclear Research, Dubna, Russia
- ⁷⁹ ^(a)Departamento de Engenharia Elétrica, Universidade Federal de Juiz de Fora (UFJF), Juiz de Fora,

- Brazil; ^(b)Universidade Federal do Rio De Janeiro COPPE/EE/IF, Rio de Janeiro, Brazil; ^(c)Universidade Federal de São João del Rei (UFSJ), São João del Rei, Brazil; ^(d)Instituto de Física, Universidade de São Paulo, São Paulo, Brazil
- 80 KEK, High Energy Accelerator Research Organization, Tsukuba, Japan
- 81 Graduate School of Science, Kobe University, Kobe, Japan
- 82 ^(a)Faculty of Physics and Applied Computer Science, AGH University of Science and Technology, Krakow, Poland; ^(b)Marian Smoluchowski Institute of Physics, Jagiellonian University, Krakow, Poland
- 83 Institute of Nuclear Physics Polish Academy of Sciences, Krakow, Poland
- 84 Faculty of Science, Kyoto University, Kyoto, Japan
- 85 Kyoto University of Education, Kyoto, Japan
- 86 Research Center for Advanced Particle Physics and Department of Physics, Kyushu University, Fukuoka, Japan
- 87 Instituto de Física La Plata, Universidad Nacional de La Plata and CONICET, La Plata, Argentina
- 88 Physics Department, Lancaster University, Lancaster, UK
- 89 Oliver Lodge Laboratory, University of Liverpool, Liverpool, UK
- 90 Department of Experimental Particle Physics, Jožef Stefan Institute and Department of Physics, University of Ljubljana, Ljubljana, Slovenia
- 91 School of Physics and Astronomy, Queen Mary University of London, London, UK
- 92 Department of Physics, Royal Holloway University of London, Egham, UK
- 93 Department of Physics and Astronomy, University College London, London, UK
- 94 Louisiana Tech University, Ruston, LA, USA
- 95 Fysiska institutionen, Lunds universitet, Lund, Sweden
- 96 Centre de Calcul de l'Institut National de Physique Nucléaire et de Physique des Particules (IN2P3), Villeurbanne, France
- 97 Departamento de Física Teórica C-15 and CIAFF, Universidad Autónoma de Madrid, Madrid, Spain
- 98 Institut für Physik, Universität Mainz, Mainz, Germany
- 99 School of Physics and Astronomy, University of Manchester, Manchester, UK
- 100 CPPM, Aix-Marseille Université, CNRS/IN2P3, Marseille, France
- 101 Department of Physics, University of Massachusetts, Amherst, MA, USA
- 102 Department of Physics, McGill University, Montreal, QC, Canada
- 103 School of Physics, University of Melbourne, Victoria, Australia
- 104 Department of Physics, University of Michigan, Ann Arbor, MI, USA
- 105 Department of Physics and Astronomy, Michigan State University, East Lansing, MI, USA
- 106 B.I. Stepanov Institute of Physics, National Academy of Sciences of Belarus, Minsk, Belarus
- 107 Research Institute for Nuclear Problems of Byelorussian State University, Minsk, Belarus
- 108 Group of Particle Physics, University of Montreal, Montreal, QC, Canada
- 109 P.N. Lebedev Physical Institute of the Russian Academy of Sciences, Moscow, Russia
- 110 Institute for Theoretical and Experimental Physics of the National Research Centre Kurchatov Institute, Moscow, Russia
- 111 National Research Nuclear University MEPhI, Moscow, Russia
- 112 D.V. Skobel'syn Institute of Nuclear Physics, M.V. Lomonosov Moscow State University, Moscow, Russia
- 113 Fakultät für Physik, Ludwig-Maximilians-Universität München, Munich, Germany
- 114 Max-Planck-Institut für Physik (Werner-Heisenberg-Institut), Munich, Germany
- 115 Nagasaki Institute of Applied Science, Nagasaki, Japan
- 116 Graduate School of Science and Kobayashi-Maskawa Institute, Nagoya University, Nagoya, Japan
- 117 Department of Physics and Astronomy, University of New Mexico, Albuquerque, NM, USA
- 118 Institute for Mathematics, Astrophysics and Particle Physics, Radboud University Nijmegen/Nikhef, Nijmegen, The Netherlands
- 119 Nikhef National Institute for Subatomic Physics and University of Amsterdam, Amsterdam, The Netherlands
- 120 Department of Physics, Northern Illinois University, DeKalb, IL, USA
- 121 ^(a)Budker Institute of Nuclear Physics and NSU, SB RAS, Novosibirsk, Russia; ^(b)Novosibirsk State University, Novosibirsk, Russia
- 122 Institute for High Energy Physics of the National Research Centre Kurchatov Institute, Protvino, Russia
- 123 Department of Physics, New York University, New York, NY, USA
- 124 Ochanomizu University, Otsuka, Bunkyo-ku, Tokyo, Japan
- 125 Ohio State University, Columbus, OH, USA

- 126 Faculty of Science, Okayama University, Okayama, Japan
- 127 Homer L. Dodge Department of Physics and Astronomy, University of Oklahoma, Norman, OK, USA
- 128 Department of Physics, Oklahoma State University, Stillwater, OK, USA
- 129 Palacký University, RCPTM, Joint Laboratory of Optics, Olomouc, Czech Republic
- 130 Center for High Energy Physics, University of Oregon, Eugene, OR, USA
- 131 LAL, Université Paris-Sud, CNRS/IN2P3, Université Paris-Saclay, Orsay, France
- 132 Graduate School of Science, Osaka University, Osaka, Japan
- 133 Department of Physics, University of Oslo, Oslo, Norway
- 134 Department of Physics, Oxford University, Oxford, UK
- 135 LPNHE, Sorbonne Université, Paris Diderot Sorbonne Paris Cité, CNRS/IN2P3, Paris, France
- 136 Department of Physics, University of Pennsylvania, Philadelphia, PA, USA
- 137 Konstantinov Nuclear Physics Institute of National Research Centre “Kurchatov Institute”, PNPI, St. Petersburg, Russia
- 138 Department of Physics and Astronomy, University of Pittsburgh, Pittsburgh, PA, USA
- 139 ^(a)Laboratório de Instrumentação e Física Experimental de Partículas - LIP, Lisbon, Portugal; ^(b)Departamento de Física, Faculdade de Ciências, Universidade de Lisboa, Lisbon, Portugal; ^(c)Departamento de Física, Universidade de Coimbra, Coimbra, Portugal; ^(d)Centro de Física Nuclear da Universidade de Lisboa, Lisbon, Portugal; ^(e)Departamento de Física, Universidade do Minho, Braga, Portugal; ^(f)Universidad de Granada, Granada, Spain; ^(g)Dep Física and CEFITEC of Faculdade de Ciências e Tecnologia, Universidade Nova de Lisboa, Caparica, Portugal
- 140 Institute of Physics of the Czech Academy of Sciences, Prague, Czech Republic
- 141 Czech Technical University in Prague, Prague, Czech Republic
- 142 Faculty of Mathematics and Physics, Charles University, Prague, Czech Republic
- 143 Particle Physics Department, Rutherford Appleton Laboratory, Didcot, UK
- 144 IRFU, CEA, Université Paris-Saclay, Gif-sur-Yvette, France
- 145 Santa Cruz Institute for Particle Physics, University of California Santa Cruz, Santa Cruz, CA, USA
- 146 ^(a)Departamento de Física, Pontificia Universidad Católica de Chile, Santiago, Chile; ^(b)Departamento de Física, Universidad Técnica Federico Santa María, Valparaíso, Chile
- 147 Department of Physics, University of Washington, Seattle, WA, USA
- 148 Department of Physics and Astronomy, University of Sheffield, Sheffield, UK
- 149 Department of Physics, Shinshu University, Nagano, Japan
- 150 Department Physik, Universität Siegen, Siegen, Germany
- 151 Department of Physics, Simon Fraser University, Burnaby, BC, Canada
- 152 SLAC National Accelerator Laboratory, Stanford, CA, USA
- 153 Physics Department, Royal Institute of Technology, Stockholm, Sweden
- 154 Departments of Physics and Astronomy, Stony Brook University, Stony Brook, NY, USA
- 155 Department of Physics and Astronomy, University of Sussex, Brighton, UK
- 156 School of Physics, University of Sydney, Sydney, Australia
- 157 Institute of Physics, Academia Sinica, Taipei, Taiwan
- 158 ^(a)E. Andronikashvili Institute of Physics, Iv. Javakhishvili Tbilisi State University, Tbilisi, Georgia; ^(b)High Energy Physics Institute, Tbilisi State University, Tbilisi, Georgia
- 159 Department of Physics, Technion, Israel Institute of Technology, Haifa, Israel
- 160 Raymond and Beverly Sackler School of Physics and Astronomy, Tel Aviv University, Tel Aviv, Israel
- 161 Department of Physics, Aristotle University of Thessaloniki, Thessaloniki, Greece
- 162 International Center for Elementary Particle Physics and Department of Physics, University of Tokyo, Tokyo, Japan
- 163 Graduate School of Science and Technology, Tokyo Metropolitan University, Tokyo, Japan
- 164 Department of Physics, Tokyo Institute of Technology, Tokyo, Japan
- 165 Tomsk State University, Tomsk, Russia
- 166 Department of Physics, University of Toronto, Toronto, ON, Canada
- 167 ^(a)TRIUMF, Vancouver, BC, Canada; ^(b)Department of Physics and Astronomy, York University, Toronto, ON, Canada
- 168 Division of Physics and Tomonaga Center for the History of the Universe, Faculty of Pure and Applied Sciences, University of Tsukuba, Tsukuba, Japan
- 169 Department of Physics and Astronomy, Tufts University, Medford, MA, USA
- 170 Department of Physics and Astronomy, University of California Irvine, Irvine, CA, USA
- 171 Department of Physics and Astronomy, University of Uppsala, Uppsala, Sweden

- 172 Department of Physics, University of Illinois, Urbana, IL, USA
- 173 Instituto de Física Corpuscular (IFIC), Centro Mixto Universidad de Valencia - CSIC, Valencia, Spain
- 174 Department of Physics, University of British Columbia, Vancouver, BC, Canada
- 175 Department of Physics and Astronomy, University of Victoria, Victoria, BC, Canada
- 176 Fakultät für Physik und Astronomie, Julius-Maximilians-Universität Würzburg, Würzburg, Germany
- 177 Department of Physics, University of Warwick, Coventry, UK
- 178 Waseda University, Tokyo, Japan
- 179 Department of Particle Physics, Weizmann Institute of Science, Rehovot, Israel
- 180 Department of Physics, University of Wisconsin, Madison, WI, USA
- 181 Fakultät für Mathematik und Naturwissenschaften, Fachgruppe Physik, Bergische Universität Wuppertal, Wuppertal, Germany
- 182 Department of Physics, Yale University, New Haven, CT, USA
- 183 Yerevan Physics Institute, Yerevan, Armenia
- ^a Also at Borough of Manhattan Community College, City University of New York, New York, NY, USA
- ^b Also at Centre for High Performance Computing, CSIR Campus, Rosebank, Cape Town, South Africa
- ^c Also at CERN, Geneva, Switzerland
- ^d Also at CPPM, Aix-Marseille Université, CNRS/IN2P3, Marseille, France
- ^e Also at Département de Physique Nucléaire et Corpusculaire, Université de Genève, Geneva, Switzerland
- ^f Also at Departament de Física de la Universitat Autònoma de Barcelona, Barcelona, Spain
- ^g Also at Department of Applied Physics and Astronomy, University of Sharjah, Sharjah, United Arab Emirates
- ^h Also at Department of Financial and Management Engineering, University of the Aegean, Chios, Greece
- ⁱ Also at Department of Physics and Astronomy, University of Louisville, Louisville, KY, USA
- ^j Also at Department of Physics and Astronomy, University of Sheffield, Sheffield, UK
- ^k Also at Department of Physics, California State University, East Bay, USA.
- ^l Also at Department of Physics, California State University, Fresno, USA.
- ^m Also at Department of Physics, California State University, Sacramento, USA
- ⁿ Also at Department of Physics, King's College London, London, UK
- ^o Also at Department of Physics, St. Petersburg State Polytechnical University, St. Petersburg, Russia
- ^p Also at Department of Physics, Stanford University, Stanford CA, USA
- ^q Also at Department of Physics, University of Fribourg, Fribourg, Switzerland
- ^r Also at Department of Physics, University of Michigan, Ann Arbor, MI, USA
- ^s Also at Faculty of Physics, M.V. Lomonosov Moscow State University, Moscow, Russia.
- ^t Also at Giresun University, Faculty of Engineering, Giresun, Turkey
- ^u Also at Graduate School of Science, Osaka University, Osaka, Japan
- ^v Also at Hellenic Open University, Patras, Greece
- ^w Also at Horia Hulubei National Institute of Physics and Nuclear Engineering, Bucharest, Romania
- ^x Also at II Physikalisches Institut, Georg-August-Universität Göttingen, Göttingen, Germany
- ^y Also at Institutio Catalana de Recerca i Estudis Avancats, ICREA, Barcelona, Spain
- ^z Also at Institut für Experimentalphysik, Universität Hamburg, Hamburg, Germany
- ^{aa} Also at Institute for Mathematics, Astrophysics and Particle Physics, Radboud University Nijmegen/Nikhef, Nijmegen, The Netherlands
- ^{ab} Also at Institute for Nuclear Research and Nuclear Energy (INRNE) of the Bulgarian Academy of Sciences, Sofia, Bulgaria
- ^{ac} Also at Institute for Particle and Nuclear Physics, Wigner Research Centre for Physics, Budapest, Hungary
- ^{ad} Also at Institute of Particle Physics (IPP), Canada
- ^{ae} Also at Institute of Physics, Academia Sinica, Taipei, Taiwan
- ^{af} Also at Institute of Physics, Azerbaijan Academy of Sciences, Baku, Azerbaijan
- ^{ag} Also at Institute of Theoretical Physics, Ilia State University, Tbilisi, Georgia
- ^{ah} Also at Istanbul University, Dept. of Physics, Istanbul, Turkey
- ^{ai} Also at Joint Institute for Nuclear Research, Dubna, Russia
- ^{aj} Also at LAL, Université Paris-Sud, CNRS/IN2P3, Université Paris-Saclay, Orsay, France
- ^{ak} Also at Louisiana Tech University, Ruston, LA, USA

- ^{al} Also at LPNHE, Sorbonne Université, Paris Diderot Sorbonne Paris Cité, CNRS/IN2P3, Paris, France
- ^{am} Also at Manhattan College, New York, NY, USA
- ^{an} Also at Moscow Institute of Physics and Technology State University, Dolgoprudny, Russia
- ^{ao} Also at National Research Nuclear University MEPhI, Moscow, Russia
- ^{ap} Also at Physikalisches Institut, Albert-Ludwigs-Universität Freiburg, Freiburg, Germany
- ^{aq} Also at School of Physics, Sun Yat-sen University, Guangzhou, China
- ^{ar} Also at The City College of New York, New York, NY, USA
- ^{as} Also at The Collaborative Innovation Center of Quantum Matter (CICQM), Beijing, China
- ^{at} Also at Tomsk State University, Tomsk, and Moscow Institute of Physics and Technology State University, Dolgoprudny, Russia
- ^{au} Also at TRIUMF, Vancouver, BC, Canada
- ^{av} Also at Universidad de Granada, Granada (Spain), Spain
- ^{aw} Also at Università di Napoli Parthenope, Napoli, Italy
- * Deceased